University of Cincinnati

Date: 10/27/2021

I, Ahmad Yahya, hereby submit this original work as part of the requirements for the degree of Doctor of Philosophy in Chemical Engineering.

It is entitled:

The Viscous and Transport Properties of Aqueous Systems

Student's name: **Ahmad Yahya**

This work and its defense approved by:

Committee chair: Jonathan Nickels, Ph.D.

Committee member: Anastasios Angelopoulos, Ph.D.

Committee member: Gregory Beaucage, Ph.D.

Committee member: Xiaolin Cheng, Ph.D.

Committee member: Yoonjee Park, Ph.D.

41587

Viscoelastic and Transport Properties of Aqueous Systems

A dissertation submitted to the

Graduate School

Of the University of Cincinnati

In partial fulfillment of the

Requirements for the degree of

Doctor of Philosophy

in the Department of Chemical and Environmental Engineering

of the College of Engineering and Applied Sciences

By

Ahmad A. Yahya

M. Eng University of Cincinnati

October 2021

Committee Chair: Prof. Jonathan D. Nickels

Overview

This dissertation outlines a course of study to investigate changes in the molecular structure and dynamics of water near solute surfaces. The fundamental relaxations governing viscosity and solute diffusion occur on the nanosecond/picosecond timescale – and occur via a complex molecular rotation and translational motion that reset the local structure of liquid water. Solutes impose changes in the interactions and structure of water molecules, resulting in different rates of structural reorganization – and manifesting as changes in the viscosity and transport properties of aqueous materials. In this dissertation I specifically studied the mechanical properties of pure water, mechanical properties and polymer dynamics in fully hydrated PEG hydrogels, and transport properties in green fluorescent protein (GFP) solutions as three aqueous systems. The main experimental technique is neutron scattering along with supporting information from dynamic light scattering, and molecular dynamics simulation. These detailed studies provide new details about the water-solute interface and will lead into drug delivery, consumer product and many other applications.

Copyright

By

Ahmad A. Yahya

2021

Dissertation Acknowledgement

First and foremost, I would like to express my sincere gratitude to my supervisor Prof. Jonathan David Nickels for making this work possible. His guidance and advice carried me through all the stages of writing this dissertation. For the continuous support through all the years of my PhD study and research, for his patience, motivation, enthusiasm, and immense knowledge. I could not imagine having a better advisor and mentor for my PhD study.

Besides my advisor, I would like to thank the rest of my dissertation committee Prof. Anastasios Angelopoulos, Prof. Yoonjee Park, Prof. Gregory Beaucage and Prof. Xiaolin Cheng for their encouragement, insightful comments, and guidance. Thank you for being part of this dissertation committee and part of my PhD studies whether in instructing me in my degree courses or offering me valuable research and teaching assistant opportunities that lead to developing technical skills and self-confidence.

I must thank my beloved parents for always being with me since day one in all my academic and life endeavors and for believing in me and encouraging me to pursue my graduate studies. Much love and appreciation to my two siblings Yahya and Abdullah for all the love and support overseas. I would like to thank my cousin Dr. Zainab Al Ani for all her support and guidance.

I would also like to thank my fellow lab mates Jacob Hogg and Luoxi Tan at the University of Cincinnati for all the valuable discussions and work we all put together through out all the past years.

Finally, I would like to thank my friends for making Cincinnati my second home and supporting me and believing in me.

Table of Contents

List of Figures

List of Tables

Chapter 1 : Objectives and Approach

1.1 Abstract

This dissertation outlines a course of study to investigate changes in the molecular structure and dynamics of water near solute surfaces. Solutes impose changes in the interactions and structure of water molecules, resulting in different rates of structural reorganization – and manifesting as changes in the viscosity and transport properties of aqueous materials. The fundamental relaxations governing viscosity and solute diffusion occur on the nanosecond/picosecond timescale – and occur via a complex molecular rotation and translational motion that reset the local structure of liquid water. In this dissertation I will be specifically looking at (1) the mechanical properties of pure water, (2) viscous and transport properties and polymer dynamics in fully swollen PEG hydrogels, and (3) transport properties as a function of concentration in GFP solutions as three aqueous systems. The experimental technique is mainly neutron scattering along with supporting information from dynamic light scattering, and molecular dynamics simulation. These results will be beneficial in many applications, especially drug delivery and formulation stability.

1.2 Research Objectives

This dissertation has three main objectives, to be considered as three projects/publications.

1.2.1 Molecular Origins of Bulk Viscosity in Water (Published)

1.2.1.1 Theoretical Background

Water molecular structure which is dynamic explain the origin of the system's viscosity and molecular diffusion in the system and the properties of the liquid and the systems as an overall.

To be able to distinguish and see the changes in water dynamics in aqueous systems where a solute is dissolved in the hydrogen bond network, we first need to fully understand the dynamics and structure in neat or bulk water. The first part of this dissertation began with a consideration of the motions associated with bulk viscosity in neat water. The bulk viscosity is also known as the second viscosity coefficient, the dilational viscosity or the volume viscosity corresponds to the viscous (not elastic) response to volume change – compression or expansion. This project has already resulted in a peer-reviewed publication [1]. The main goal of the study was to connect equilibrium molecular motions to rheological timescales for bulk viscosity.

Viscosity emerges from the way molecules move and reorganize the local structure on the molecular scale and the rate of reorganization of the structure or in other words the structural relaxation rate of the water molecules defines different local viscosities in the system. The fact that there is a molecular scale relaxation time that determines the response to an external stress and defines viscosity has been long proposed by Maxwell[2]; recognizing a fundamental molecular relaxation time, τ_M, emerges as the ratio of shear viscosity, μ, to infinite shear modulus, G_∞. This relationship distinguishes the timescales at which the mechanical response of a liquid will be solid-like ($\tau < \tau_M$) or liquid-like ($\tau > \tau_M$). Borrowing this approach and using it to determine the molecular scale relaxation time governing the viscous response to a change in volume was the approach of this project where the bulk viscosity and the bulk modulus were determined experimentally using inelastic light scattering, and the molecular scale dynamics and atomic pair correlations associated with the response to the external stress were determined using neutron scattering.

1.2.1.2 Objectives

To use inelastic light scattering and neutron scattering techniques to find the molecular origin of bulk viscosity with an associated molecular relaxation time. Also, to understand neat or bulk water dynamics and structure to be used in the other two projects for observing changes in dynamics and structure due to the presence of solute.

1.2.1.3 Experimental Procedure and Analysis

We accomplish our goal using two experimental approaches – inelastic light scattering and inelastic neutron scattering. Inelastic light scattering – specifically Brillouin scattering – was used to experimentally illustrate the bulk viscosity timescale. While inelastic neutron scattering was used to directly measure molecular relaxation and associated structures.

➢ Inelastic light scattering (Brillouin Scattering)

Experiment:

- Brillouin scattering measurements were performed at the University of Cincinnati in a polarized, backscattering configuration using a Sandercock tandem Fabry-Perot interferometer with a 532 nm single-mode solid state laser.

- A spectral range of 24 GHz was accessed using a 6mm mirror separation.

- The temperature of the liquid was controlled using Linkam temperature control cell.

- Spectra were collected over approximately 60 minutes.

Analysis:

- A damped harmonic oscillator model was used to fit the longitudinal mode in the observed spectra or the Brillouin doublets.

- The fit parameters, which are the frequency shift Ω_L and the width at half max (also called attenuation factor) Γ_L are used to obtain the longitudinal sound velocity, c_L, the bulk viscosity, ζ_b, and the bulk modulus, K [3].

➢ Inelastic Neutron Scattering

Experiment and Analysis:

- The inelastic neutron scattering spectra of H_2O and D_2O were measured at same temperature range at Oak Ridge National Laboratory, using two instruments BASIS and CNCS at the spallation neutron source.

- The spectra of both the instruments are stitched together for a complete dynamical window.

- The dynamic structure factor $S(q,E$ is converted to the susceptibility formalism, $\chi''(q,\upsilon)$.

- H_2O spectra was fitted with two Debye function representing the rotational and translational motions of water.

- The coherent scattering from D_2O was analysed to obtain the atom pair lifetimes at the length scale of the first sharp diffraction peak.

- Similar treatment as in H_2O was used with an additional Debye function representing the coherent contribution.

1.2.2 Origin of Apparent Viscosity Effects and Nonergodicity of PEG Hydrogels

1.2.2.1 Theoretical Background

Solutes affect the water interaction, dynamics and structural reorganization [4]. This effect can range from immobilization of water molecules on the solute to momentary perturbation of the translational or rotational motions of water by the solute. Such perturbation to the water molecular dynamic will result in changes to the macroscopic physical properties of the system[5] [6]. Since the origin of such properties are the dynamics of water at the nanoscale. In this dissertation we focus on such perturbation effect on the viscoelastic and transport properties of aqueous systems by studying such observations in dilute Polyethylene glycol hydrogels.

1.2.2.2 Objectives

To access the physical parameters that describe PEG hydrogels performance along with the changes in dynamics of water near the polymer chains. The polymer chain dynamics itself can be accessed to using neutron spin echo. Our approach of explaining the degree and extent of perturbation to the water dynamics can identify the population of water that is perturbed and the degree by which it is perturbed or by what factor it is slowed down. This therefore translates in to the origin of local viscosities due to the change in rate of structural reorganization of the water molecules due the dynamic perturbation from interacting with the polymer chains. This understanding of the hydration water population and its dynamics is beneficial for models used in different fields such as drug deliver. Also, Hydrogels are stated in the literature to be nonergodic but to our knowledge there is no experimental prove of such statement and we believe our full structural and dynamical analysis using neutron scattering shows a prove of non-ergodicity of hydrogels.

1.2.2.3 Experimental Procedure and Analysis

We accomplish our goal using different inelastic neutron scattering techniques. Inelastic neutron scattering measurements will be used to look directly at the changes in water dynamics within PEG gels of differing volume fraction using BASIS/CNCS; and then attempt to understand the connection of the equilibrium water dynamics within PEG hydrogels to the polymer dynamics and macroscopic viscoelastic properties. For this we will use NSE to observe the polymer chain motions and SANS to understand the polymer network structure. Five different hydrogels with different initial polymer concentration and mechanical properties are used, those mechanical properties are estimated from models that depend mainly on the swelling experiments observations.

➢ Small Angle Neutron Scattering (SANS)

Experiment:

- SANS technique was used to characterize the structure of the hydrogel at the nanometer length scale.

- SANS data was collected on each bulk hydrogel mounted between windows of a Ti sample cell in D_2O at 280K.

- The measured quantity I(q) was analyzed though two different approaches one to estimate the mesh size in the hydrogel network, and the other to access the persistence length of the polymer chain between cross-links.

Analysis:

- Data were fitted by Ornstein-Zernike Model with an extra term to evaluate any inhomogeneities present in the gels, this model works well with hydrogels and was used in several SANS studies on polymer solutions[7] [8] [9].

- The same data was analyzed with the Kratky approach by normalizing the I(q) by multiplying it with q^2 which should give a linear dependence, due to the cross-over from a rigid rod like behavior to a flexible Gaussian chain behavior we observe a deviation from a linear dependence which reflects the persistence length.

➢ Neutron Spin Echo (NSE)

Experiment:

- NSE was used to measure polymer chain dynamics as a function of concentration in context to the degree of slowed water dynamics.

- It was performed on q range from 0.05 to 0.3 $Å^{-1}$ covering length scales where the mesh size, and polymer chain motions between cross-links dominate the scattering.

- NSE was performed on each of the hydrogel materials using a 100% D_2O background.

Analysis:

- The observed experimental quantity is the intermediate scattering function which reflects the fraction of pair correlations still in existence after a given time interval.

- The relaxation times are extracted then as a function of scattering wave vector using exponential decay fit.

- The data clearly showed cubic dependence on q which reflects Zimm dynamics of flexible polymers in water.

➢ Back Scattering (BASIS) and Cold Neutron Chopper Spectrometer (CNCS)

Experiment:

- To access the water dynamics directly, the techniques used are quasielastic neutron scattering (QENS) measurements using the Backscattering Silicon Spectrometer (BASIS), and inelastic neutron scattering using the Cold Neutron Chopper Spectrometer (CNCS).

- The scattering experiment was done on the gels samples and pure water in a temperature range 280-303K.

Analysis:

- The Spectra of water were fit with one Cole Davidson (CD) function for coupled translational-rotational motions of water and a damped harmonic oscillator for vibrations occurring at high frequency.

- The analysis of the hydrogels samples have an extra Cole Davidson function for the dynamics in the hydration population and the dynamics of bulk water are fixed as seen in pure water by another Cole Davidson function.

- Data analysis for gels follow the approach in Perticaroli et al. [10]. The result of this analysis will be two parameters used to explain the extent and magnitude of this perturbation; the hydration number, N_H, and the retardation factor, R_H.

- The hydration number describes the extent of perturbation in terms of the number of water molecules per monomer unit which are dynamically altered. It is calculated by the amplitude fraction of each population.

- The retardation factor describes the degree of the observed perturbation as defined by the ratio of characteristic relaxation times of hydration water to bulk water.

1.2.3 The Role of Hydrodynamics in the Self-Diffusion of Green Fluorescent Protein.

1.2.3.1 Theoretical Background

Explaining transport at higher concentration solutions is also another topic of interest in recent research. For biological solutions such as GFP, the question is whether diffusion can be understood based on concepts developed for nearly uncharged colloidal particles. For a colloid hydrodynamic interaction mediated by the solvent play an important role. Where basically particles immersed in a fluid excite long-ranged flows as they move and move in response to the solvent motion. By reaction to the solvent's dynamics, the colloidal particles experience hydrodynamic interaction with each other. Therefore, particles will experience solvent-mediated forces, apart from the other possible direct interactions such as steric, depletive, electrostatic, magnetic interactions. The flow velocity due to these hydrodynamic interactions decays in a fast rate proportional to the distance scale squared [11]. Hydrodynamic interactions are fundamental in the equilibrium dynamics of colloidal systems.

Crowded solutions especially protein solutions are of great interest in the design of pharmaceutical formulation and understanding the natural biological environment within a cell. The translational diffusion constant of proteins has been seen to be reduced by a factor of five

according to NMR experiments [12]. The reduced mobility has generally been attributed to excluded volume effects in crowded media.

1.2.3.2 Objectives

To observe experimentally the theory behind the weak dependence of the collective diffusion constant. Find other factors such as hydrodynamic interaction terms that are likely to be involved in reduced immobility of crowded solutions along with the excluded volume effect. Previous work [13] focused on the hydration water in GFP solutions. Where the structurally and dynamically perturbed water surrounding the protein was the main aspect of the study. As a continuation for this project, we are studying the protein dynamics as a function of concentration. Previous experimental observations showed that diffusion coefficients of hemoglobin, myoglobin decreases exponentially with concentration [14]. Such reduction in mobility is assigned to excluded volume effects in crowded media, However the collective or gradient diffusion coefficient of hemoglobin is only weakly dependent on concentration. This is due to the compensation of osmotic and friction forces. Our experimental procedures will have a tracer approach where contrast matched dGFP will be used as a crowder and the self-diffusion coefficient of hGFP will be estimated using NSE. The effective volume will be taken into consideration having a full set of data on the hydration population from previous work [10]. A full explanation of the dynamics and protein diffusion in concentrated solutions is the approach including hydrodynamics, excluded volume and thermal fluctuations.

1.2.3.3 Experimental Procedure and Analysis

The dynamic structure factor obtained by NSE can give information about inter-particle correlations and their time evolution. This way we can obtain the effective diffusion coefficient

by fitting an exponential function. SANS is also be used to access the structure of GFP solution and combine it with the NSE data to get a complete explanation of the reduced mobility origin. Neutron contrast is the enabling tool to make this experiment possible. a contrast matched crowded protein environment is created (this will be invisible to the neutrons) and allow us to observe hydrogenated population of the protein diffusing at several concentrations. We can then compare this to the dilute limit self-diffusion coefficient obtained from dynamic light scattering, and the diffusion of the hydrogenated protein at the same concentration using NSE. Also, Dynamic light scattering will be used to understand the Brownian motion of proteins in less concentrated solutions and then observe this reduced mobility when moving into higher concentrations using the above experimental techniques.

➢ Small Angle Neutron Scattering (SANS) and Neutron Spin Echo (NSE)

Experiment:

- The samples used to achieve the above observation are as follows

   1. 1, 5, 10, 17.5 and 25 mg/ml h-GFP in solution.

   2. 5 mg/ml h-GFP in solution / 5 mg/ml g-D_2O-matched GFP in solution.

   3. 5 mg/ml h-GFP in solution / 12.5 mg/ml g-D_2O-matched GFP in solution.

   4. 5 mg/ml h-GFP in solution / 20 mg/ml g-D_2O-matched GFP in solution.

- NSE and were performed as seen on different concentrations and a contrast variation is to be used to hide the crowding effects from being accessed by the neutrons.

Analysis:

- First the contrast matched dGFP was generated by utilizing SANS to measure the low q region for about 15 minutes only to get the I(0) quantity.

- The measurement was performed on the sample and the buffer at different volume fractions of the buffer to obtain the scattering from the protein.

- The null scattering was estimated using the I(0) approach and the Porod Invariant approach. This was used to determine the contrast matched GFP conditions.

- SANS was then used to confirm the contrast matched dGFP by measuring over the whole q range at the decided buffer conditions and also the structural information of GFP was obtained at a non-contrast matched condition.

- NSE was then performed to obtain the self-diffusion coefficient of GFP using a contrast matched crowder that was confirmed.

➤ Dynamic light scattering and molecular dynamics simulations

Experiment:

- The samples used in the dynamic light scattering were in the infinite dilute regime less than 0.6 mg/ml to observe the diffusion coefficient of GFP at the very dilute regime and compare it to the self-diffusion coefficient of GFP reduction with concentration.

Analysis:

- The excess polarizability by the concentration fluctuation, where the intensity fluctuation can be measured.

- The characteristic relaxation rate τ_C for the concentration fluctuation is related to the diffusion coefficient $\tau_c = K^2 D$ [15], where the scattering field amplitude is proportional to the concentration fluctuation.

References

1. Yahya, A., et al., *Molecular origins of bulk viscosity in liquid water.* Physical Chemistry Chemical Physics, 2020. **22**(17): p. 9494-9502.
2. Maxwell, J.C., *IV. On the dynamical theory of gases.* Philosophical transactions of the Royal Society of London, 1867. **157**: p. 49-88.
3. Berne, B.J. and R. Pecora, *Dynamic light scattering: with applications to chemistry, biology, and physics*. 2000: Courier Corporation.
4. Timasheff, S.N., *Protein-solvent preferential interactions, protein hydration, and the modulation of biochemical reactions by solvent components.* Proceedings of the National Academy of Sciences, 2002. **99**(15): p. 9721-9726.
5. Constantinides, G., et al., *Probing mechanical properties of fully hydrated gels and biological tissues.* Journal of biomechanics, 2008. **41**(15): p. 3285-3289.
6. Yakimets, I., et al., *Mechanical properties with respect to water content of gelatin films in glassy state.* Polymer, 2005. **46**(26): p. 12577-12585.
7. Matsunaga, T., et al., *SANS studies on Tetra-PEG Gel under uniaxial deformation.* Macromolecules, 2011. **44**(5): p. 1203-1210.
8. Horkay, F., et al., *Osmotic and SANS observations on sodium polyacrylate hydrogels in physiological salt solutions.* Macromolecules, 2000. **33**(22): p. 8329-8333.
9. Matsunaga, T., et al., *SANS and SLS studies on tetra-arm PEG gels in as-prepared and swollen states.* Macromolecules, 2009. **42**(16): p. 6245-6252.
10. Perticaroli, S., et al., *Description of Hydration Water in Protein (GFP) Solution.* Biophysical Journal, 2017. **112**(3): p. 201a.
11. Diamant, H., et al., *Hydrodynamic interaction in quasi-two-dimensional suspensions.* Journal of Physics: Condensed Matter, 2005. **17**(31): p. S2787.
12. Doster, W. and S. Longeville, *Microscopic diffusion and hydrodynamic interactions of hemoglobin in red blood cells.* Biophysical journal, 2007. **93**(4): p. 1360-1368.
13. Perticaroli, S., et al., *Description of hydration water in protein (green fluorescent protein) solution.* Journal of the American Chemical Society, 2017. **139**(3): p. 1098-1105.
14. Everhart, C.H. and C.S. Johnson Jr, *The determination of tracer diffusion coefficients for proteins by means of pulsed field gradient NMR with applications to hemoglobin.* Journal of Magnetic Resonance (1969), 1982. **48**(3): p. 466-474.
15. Langowski, J., W. Kremer, and U. Kapp, *[21] Dynamic light scattering for study of solution conformation and dynamics of superhelical DNA*, in *Methods in enzymology*. 1992, Elsevier. p. 430-448.

Chapter 2 : Introduction

2.1 Overview

My doctoral work focuses on the molecular scale dynamics and structure of aqueous solutions. I have studied in detail the molecular scale relaxations of water in three different systems: bulk neat water, Polyethylene glycol hydrogels and green fluorescent protein solutions. The rate of structural reorganization of the water population is the origin of different local viscosities. Such differences depend on the water-solute interactions where the water is divided into two populations with different dynamics. One being ideal like the neat bulk water and the other has perturbed dynamics due to the solute. My work uses neutron scattering as main tool in investigating these complex molecular scale dynamics. A powerful tool like neutron scattering allowed me to broaden my investigation to estimate important structural analysis of the aqueous systems I studied. This work resulted in three important studies with one successfully published, the second and the third are in the submission process at the time of this writing. The first discussed the molecular origins of bulk viscosity in liquid water[1] using neutron and light scattering techniques. The second is a full description study of the dynamics of water and the polymer in fully swollen Polyethylene hydrogels along with detailed structural analysis of the hydrogels system. The third is a project based on a previous study [2] where the water dynamics in green fluorescent protein solutions were studied in details and I continued by studying the protein's dynamics. While this has been my primary work, I have also participated in other projects. The first to mention is an experimental study on lipids rafts [3] where It was found that lipid rafts can stabilize the membrane physical properties over varying temperatures. The second [4] where it focused on the transition between different diffusion regimes and its relationship

with structural properties in Nafion. There are several ongoing projects that I am participating in which uses neutron and light scattering techniques where I can contribute. This dissertation will be composed of seven chapters; (1) Objectives and approach (2) an introduction, (3) the methods and techniques used, (4) molecular origins of bulk viscosity in liquid water, (5) detailed structure and dynamics studies of fully swollen polyethylene glycol hydrogels, and (6) the role of hydrodynamics in the self-diffusion coefficient of green fluorescent protein, and finally (7) other neutron scattering experiments that resulted in co-author publications, and my conclusions. Chapter 2 is to give the reader an idea of how work and theory is oriented to explain properties of aqueous systems using molecular scale dynamics and structural information. Also, it explains the theories behind polymer and protein solutions which is a background needed to understand the results obtained in this dissertation. The fourth chapter shows the molecular scale dynamics that are responsible for the volume resistance viscous property of neat water. The next chapter uses the bulk water dynamics from the previous chapter to investigate the perturbation to the dynamics caused by interactions with the polymer in fully swollen PEG hydrogels. The study explains macroscopic properties using structural parameters that define the structure of the gels. The sixth chapter is an experimental approach to model protein (in this case green fluorescent protein) using colloidal theories where hydrodynamic interactions are the reason behind the reduction in the self-diffusion coefficient with increasing volume fractions. The seventh chapter briefly goes through other work that I contributed to using neutron scattering experiments and finally it summarizes my conclusions.

2.2 Motivation

The long experience of my advisor Dr. Jonathan David Nickels in the neutron scattering world and its applications in chemical and biological applications and studies inspired me to use this powerful technique to pursue this study where I looked at the molecular scale structure and dynamics of aqueous solutions in details. This kind of study was done earlier on green fluorescent protein where the full description of the hydration shell dynamics was obtained [5]. It occurred to us that applying similar observation to hydrogels was unique and important since the properties of hydrogels are controlled or decided by its bulk structure which basically depends on the content of water in the system, in other words the swelling degree. I believed studying the perturbation to the water dynamics near the polymer surface will be beneficial for future applications where the diffusion of a solute in the hydrogel network is necessary. The work I have done is a foundation for future work with multi-arm PEG hydrogels where all information needed from structural and dynamical point of view is available for the reader to build his/her work on. Also, the way protein's diffusion is sensitive to concentration changes in the solution is studied where I studied the protein dynamics and specified the origin of diffusion coefficient reduction using neutron spin echo technique. This dissertation is believed to significantly contribute to advancing the knowledge of water population around solutes in biological solutions and how the dynamics and structure of both the media and the solute are related in such systems. Which then explains how the macroscopic properties such as viscoelastic properties for the hydrogels and the transport diffusional properties of proteins are sensitive. This will indeed be one of the main keys in developing new models for drug delivery, food industry preservatives and texture

enhancers, tissue engineering applications like cartilage implant and many biological applications.

In scientific field, this project explores the molecular dynamics and structure of polyethylene glycol hydrogels at different solute concentrations which have not been done in this detail before. The origins and the dynamical behavior of water in bulk and hydration layer is still an ongoing topic in the field. An interesting combination with protein dynamics in the system will be of a great impact to different biochemical and industrial applications. This project is believed to help in both industrial and education worlds.

The impact to society will be in providing a clearer understanding of molecular dynamics of macromolecules in an aqueous environment to ease the applications used to synthesis different products from medicine to self-care products. Our experienced research team and collaborators were strongly interested and had the abilities to carry out this project research and achieved its objectives. Similar studies have been done on describing hydration water in green fluorescent protein [6] [7].The required knowledge and experience with neutron scattering techniques including data analysis is available in our research group candidates.

2.3 Water as a Solvent

Water is the solvent of life, possessing great importance as the main solvent in biological systems and many chemical processes and industrial applications, driving the rapid molecular motions and structural configurations in biomolecules such as proteins. Despite this importance, the fundamental molecular relaxation mechanism(s) of water are still an active field of study, with many open questions to be addressed. Due to its ability to form intermolecular interactions

knows as hydrogen bonds[8], it has complex dynamical behavior and structure, leading to unique physical properties[9-11]. When water interacts with simple and complex molecules dissolved the local hydrogen bond network is effected, and a hydration shell forms, in which the water molecules have altered dynamics and structure [7, 12].The extent to which the water dynamics and structure are altered is vitally important for understanding the physical and transport properties of solutions and complex media like hydrogels[13, 14]. Improving this understanding is the goal of this dissertation. I begin by discussing the origin of the dynamics of water itself as a bulk material; before moving on to studying the role of water dynamics in determining the properties of simple PEG hydrogels; and concluding with an investigation of diffusion in protein solutions in which the water dynamics have been well studied [2].

Water acts as a solvent in biological systems, whether it is cytoplasm[15] or formulated protein solutions[6], extracellular spaces[16], or constructed hydrogels[17, 18]; the water can be broadly described in two classes; hydration water and free neat water. We can imagine that the two water populations are coexisting in an equilibrium which determines the thermodynamics of the system and defines the transport and mechanical properties of the macromolecular system[19]. The translational and rotational mobility of water molecules are lower in the bound population of water (around solutes)[20]. Therefore, by observing molecular dynamics of the water in the system we can directly investigate the effect of the hydration water on changes in transport properties within the system. The thermodynamics of the system is dominated via a two competing components; the enthalpy of tightly packed water molecules near the solute surface and the entropy-driven formation of water phase in the bulk[19]. This equilibrium will define the amount of water in each population whether bulk or bound. Studying those dynamics and

populations will lead to different useful models to predict properties such as viscoelastic properties and solute transport within the system. It is known that the more perturbed the water molecules are the slower the solute will diffuse within the system due to increased hydrodynamic drag experienced[21] due to increased local viscosity.

Water interfaces are important in a wide range disciplines beyond biology as well; including electrochemistry, catalysis [22], It is important to access knowledge of this interfacial population of water in these applications as well to aid in the development of many technologies. The main challenge facing experimental approaches of studying the interfacial water is isolating the molecules that make up the interface population from the bulk water population typically making up most of the sample. Not only are the dynamics of water molecules altered near surfaces, but the hydrogen bonding strength and distribution is different from that of bulk water; and differs according to the nature of the interface. The water-air interface for example the interfacial hydrogen bonding is very similar to that of bulk water; while for lipid-water interfaces hydrogen bonding can be substantially stronger, but with greater heterogeneity [23]. Another study showed that water molecules around small hydrophobic solutes have strengthened hydrogen bonds [24]. These stronger, longer lasting hydrogen bonds are interrelated with extensive structural ordering and restricted mobility. Simulations provide some insight about this phenomenon [24, 25], where a pair of water molecules form stronger hydrogen bond to each other if there are no intercalating water molecules surrounding them. This is provided by the excluded volume which ensures a comfort zone for those water molecules close to the solute and restricts the population of water molecules so that the hydrogen bonding is strengthened.

In other words, the solute ensures lower effect or disturbance on the neighboring water molecules which leads to stronger hydrogen bonds between them.

In the other chapters of this dissertation different dynamics and corresponding viscoelastic and transport properties are addressed in more details. Where, origins of mechanical properties of pure water such as viscosity are studied on molecular scale, the mechanical properties of Polyethylene glycol hydrogels are explained in context of water content and bulk structure. Finally, the dynamics and transport properties GFP solutions are studied using theories of colloidal solution and hydrodynamic interactions. Water molecular structure and dynamics explain the macroscopic viscoelastic and transport properties of mentioned aqueous biological materials, and it behooves us to first understand these connections in pure water.

2.4 Water Structure and Dynamics

The small size, tetrahedral geometry, and hydrogen bonding ability of water all play a role in determining the interactions water takes part in with itself as well as with polar and non-polar solutes. The properties of water in interfacial systems often exhibit notable thermal anomalies and these anomalies are interpreted as evidence of structural transitions. In general, water near surfaces is thought to be more ordered, leading to a common description of this water as 'ice-like'[26]. It might be further envisioned that this order decreases as a function of distance from the interface, though the extent of this perturbation remains as a current topic of research. Other thoughts are that the interfacial water is not exactly ice-like but may be preferably assuming cage-like structure or resemble the various high pressure ice polymorphs [27]. The significance of the structural modification of water around solutes upon the properties of solutions and

hydrated materials is extremely important and has driven the development of models based upon the structural changes.

Each water molecule forms almost less than four hydrogen bonds with neighboring water molecules. The molecular arrangement of the hydrogen bond network is dynamic, and the fluctuation of the hydrogen bond network happens on a picosecond time scale. Those structural dynamics are rapid where the shortest are the vibrational motions. On a timescale between several tens and several hundreds of femtoseconds, liberational or hindered rotational motions of water occurs. Models describing the dynamical fluctuations have appealed to a range of different mechanisms and are explained in the next section.

The key timescale of water motions is the nanosecond to picosecond timeline as fluctuations in the water position (translation) and orientation (rotation) occur [28], in concert with changes in the hydrogen bonding described above [29] [30], atom motions within the local cage [31], and finally very fast molecular vibration. This complex picture has been studied by many researchers and a large number of mechanisms have been suggested to explain how these motions occur and combine. Concepts such as flickering clusters [32] to ice-like orientational defects [33] to modeling it as Debye-small-step diffusion model [34] have all be suggested. A leading recent model of water dynamics [35] suggests a molecular jump mechanism for water reorientation, starting with breakage of an existing hydrogen bond between two water molecules, followed by the rotation of the trajectory on the central water molecule and finally forming a new hydrogen bond when a neighboring water molecule is within the required distance and angle range to form a new hydrogen bond. This model is supported by Laage and co-workers through molecular dynamic simulations which suggests a three-step model presented in Figure 2.1.

31
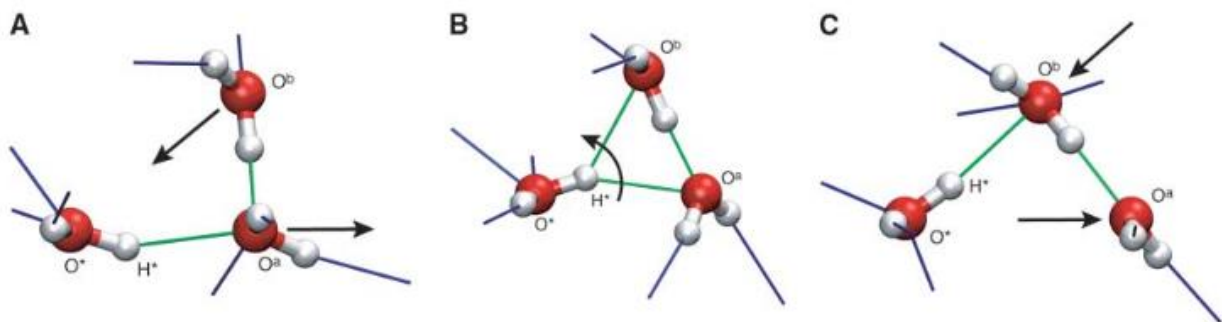
Figure 2.1 The leading Mechanism of water dynamics and Hydrogen Bonding Reforming [35].

A) H* is bonded to O^a in the first hydration shell, with O^b further apart in the second hydration shell. Because of the collective fluctuations O^a is over coordinated while O^b is undercoordinated. This causes O^a to move away from O^* while O^b moves toward O^*. **B)** O^a and O^b have the same coordination number and are equidistant from O^*. H* flips from O^a toward O^b. **C)** O^b forms hydrogen bond with H^* and becomes over coordinated while O^a loses a bond and become undercoordinated.

The fluctuations of the hydrogen bond are connected to both dynamics and structural fluctuations. H-bond cleavage and the molecular orientation is said to be occurring concertedly and not successively as assumed in many recent studies. The life time of hydrogen bond is evaluated from simulation models to be on the scale of 1.4 ps   [30]. When discussing the hydrogen bond, it is important to define the criteria for a hydrogen bond to be in existence between two water molecules [36]: i) the distance between them should be less than 3.6 A. ii) Their Oxygen-Hydrogen-Oxygen angle is more than 150°. The Laage and Hynes model of molecular jump mechanism for water reorientation that claims the reorientation of water molecule involves large amplitude rotation or jumps where the initial H-bonding hydrogen and oxygen oscillate around the possible new oxygen atom axis until collective fluctuations of the hydrogen bonding network reorganize the environment in such a way the hydrogen atoms can form a new hydrogen bond with a new neighboring oxygen atom or water molecule thus obeying

the fundamentals of chemical engineering thermodynamics in lowering the cost of energy used in forming the new hydrogen bond.

2.5 Properties of Water

The first part of this dissertation began with a consideration of the motions associated with bulk viscosity in neat water. The bulk viscosity is also known as the second viscosity coefficient, the dilational viscosity or the volume viscosity corresponds to the viscous (not elastic) response to volume change – compression or expansion. This project has already resulted in a peer-reviewed publication [1]. The main goal of the study was to connect equilibrium molecular motions to rheological timescales for bulk viscosity.

Viscosity emerges directly from the propensity of the molecules to move and reorganize the local structure on the molecular scale. On the human scale a relationship can be expressed quantitatively as a pair of coefficients relating stress to the rate of strain in the generalized form of Newton's law of viscosity [37]:

$$\sigma_{ij} = \eta \left(\frac{\partial v_j}{\partial x_i} + \frac{\partial v_i}{\partial x_j} \right) + \left(\frac{2}{3}\eta - \zeta \right) \left(\frac{\partial v_x}{\partial x_x} + \frac{\partial v_y}{\partial x_y} + \frac{\partial v_z}{\partial x_z} \right) \delta_{ij} \tag{2.1}$$

Here, σ_{ij} is the stress tensor, and v is the velocity tensor, both which are a function of the Cartesian coordinates x, y, and z. δ_{ij} is the unit tensor. The two coefficients, η and ζ, are the shear viscosity and bulk viscosity, respectively. The bulk viscosity is alternately referred to as the volume viscosity or dilatational viscosity, reflecting the viscous resistance to volume change.

The notion that a characteristic internal (molecular) relaxation time determines the viscosity of a liquid is quite old. Maxwell[38] proposed the concept, recognizing a fundamental molecular relaxation time, τ_M, emerges as the ratio of shear viscosity, η, to infinite shear modulus, G_∞. This relationship distinguishes the timescales at which the mechanical response of a liquid will be solid-like ($\tau < \tau_M$) or liquid-like ($\tau > \tau_M$).

The Kubo-Green formula [39] is another such approach which shows that the steady-state shear viscosity η, is described by the time fluctuation of the stress tensor $p^{(s)}$ as:

$$\eta = \frac{V}{k_B T} \int_0^\infty dt \{p_{xz}^{(s)}(0) p_{xz}^{(s)}(t) 2 \tag{2.2}$$

where k_B and T stand for the Boltzmann constant and the absolute temperature, respectively. The model states that the shear viscosity is determined by the fluctuations of the stress tensor – or how rapidly the internal stress is reset due to molecular rearrangement, in other words the way the molecules rearrange themselves in respond to the stress is what determines the shear viscosity. This is a way to understand the connection to the timescale of structural changes in the liquid. The bulk viscosity can be understood in the same way, with the difference being that the internal stress reset is in the diagonal terms of the stress tensor. This corresponds to the viscous part of volumetric changes[40].

I accomplished the goal of studying the molecular origins of bulk viscosity in liquid water using two experimental approaches – inelastic light scattering and inelastic neutron scattering. Inelastic light scattering – specifically Brillouin scattering – was used to experimentally illustrate the bulk viscosity timescale. While inelastic neutron scattering was used to directly measure

molecular relaxation and associated structures. These experimental techniques are explained in chapter 3 and the work on bulk viscosity of liquid water is explained in details in chapter 4.

To be able to compare hydration and bulk population of water in the work on Polyethylene glycol hydrogels in chapter 5 of this dissertation. An approach of coupled translational-rotational dynamics was used. A model that consists of a Cole-Davidson function (coupled translational-rotational dynamics) and Brownian oscillator function (liberational motions) was fitted to the data. The experimental values obtained by Cole-Davidson function should be interpreted with caution and translated to William-Watts [41] relaxation time τ_{ww} and stretching exponent β_{ww} that account for the stretching away from the actual or average relaxation time. These were used to find the self-diffusion coefficient of bulk water and the molecular relaxation times that were used in studying the perturbation to water dynamics in PEG hydrogels. Fitting the resulting relaxation times of pure water values with a power law should result in a -2 exponential dependence with a constant that is the self-diffusion coefficient of water.

2.6 Aqueous Solutions

In aqueous solutions, any cite on the surface of the solute is surrounded and in contact with a water, because a vacuum space is not possible in aqueous solutions. During a hydration process the sum of all free energies due to interaction of water molecules with the solute is the free energy of hydration. An interacting cite of a solute can be defined as any volume around the solute molecule that is thermodynamically altered or perturbed by the solute[42]. This can be direct immobilization of the solvent molecules or a momentary slowdown of the translational and rotational motions of water which affects the rate of structural re-organization of the population near the surface of the solute.

Such perturbation to the water molecular dynamic will result in changes to the macroscopic physical properties of the system[43] [44]. Since the origin of such properties are the dynamics of water at the nanoscale. In this dissertation I focused on such perturbation.

Two main properties should be considered regarding the chemistry of the aqueous solutions, the chemical activity of water and the osmotic pressure. Water activity is a physicochemical property. It is defined as the ratio of the partial pressure of water in a sample to the vapor pressure of pure water at the same temperature[45]. It is important in biology, especially for enzymatic reactions and food industry since its stability depends on the availability of water[46]. Thermodynamic models have been used to correlate and predict the water activity in solutions[47, 48]. The models use a coefficient known as the activity coefficient or introduce a correction to the Raoult's law of ideal solutions [49]. Due to hydration and other interactions in the presence of water, not all water molecules will be behaving ideally and therefore the corresponding mechanical properties will be altered. The activity phenomenon can be understood as a correction factor to the concentration expressed in molality and mole fractions[50], where it is ideally supposed to be a linear relationship between water activity and molality.

So, if we think of solutes in aqueous solutions and how they screen charges over a certain volume of water and give a rise to changes in water potential energy or activity, this is a starting point in explaining the two different water populations, bulk, and hydration. This is also seen in industrial applications such as food industry where water activity plays a big role in food preservation, but it was found that the molecular specificity of the solute material affects the state of water in different manners [51]. In context of mass transfer; the most important parameter for osmotic

solutions is its water activity [52]. This is because the solutions used in osmosis in food industry are real solutions that deviate from the ideal solution behavior even at low concentrations.

Another way of explaining water activity of an aqueous solution is through the non simplified Van Hoff model[52]. The model is as follows:

$$\Delta \Pi = \frac{-RT}{V_m} \, ln a_w \qquad (2.3)$$

where V_m and a_w are the partial molar volume and activity of water, respectively. The difference in water activity or the deviation from ideality is how we explain the presence of bulk water population which refers to ideal conditions and hydration or disturbed water which deviates from such ideality. Therefor understanding the extent of this deviation is important in many industrial fields just like the case of food industry. Water forms a layer around the solute in a process called solvation and the number of water molecules around the solute will decrease with increasing solute concentration and therefore water activity [37]. Stokes and Robinson have developed a model where it treats the solvent-solute interaction as an equilibrium. This is important in systems where the solute can form hydrogen bonding with water.

In explaining the chemistry happening during hydration we can define water activity as the equilibrium amount of water available for hydration. Water activity is therefore equal to unity when available for hydration. At hydrophobic surfaces, the water molecules have weaker hydrogen bonds and consequently higher water activity. Such water has the gradient to move toward lower activity bulk. If the surface is hydrophilic and forms hydrogen-bonds, then the

hydration water will have lower activity. This causes the movement inward and so causes increased osmotic pressure. Which therefore effects diffusion and viscosity of the system.

In my dissertation I focus on studying the relationship between the extent of perturbation and the viscoelastic and transport properties. Which indeed will be related to water activity.

Another concept to cover is the excluded volume concept which is the result of the above phenomenon. Molecular theories of fluids explain intermediate and macro scale properties based on local molecular structure and motions[53]. Broadly, these consider non interactive molecules which primarily via excluded volume (Leonard-Jones concept), and liquids/mixtures in which the molecules have directional attractive/repulsive interactions, such as the hydrogen bond. The excluded volume concept showed that the structure of non-polar fluids is predominantly controlled by strong short-range repulsive interactions. Systems such as hydrocarbons, metallic liquids and low temperature gasses can be described with these models[54]. Yet when it comes to water, the excluded volume concept describes only a part of the molecular picture. When hydrogen bonds are factored in, the orientation of the water molecule now impacts the local forces between molecules in an angular dependence, as does the special case where a proton is shared in the hydrogen bond – introducing transient changes in network connectivity. Because of the added complexity, and the substantial importance of water quasi-molecular, phenomenological, and descriptive models have been developed.

For instance, shear viscosity is an important transport coefficient of liquids which describes the resistance to flow and plays an important role in explaining flow systems in chemical engineering, readily apparent in the basic equations of fluid dynamics[55]. In another prospective, the shear

viscosity of a solvent is regarded as a measure of the rates of structural reorganization of the water molecules in respond to external and flow occurs. Therefore, it makes sense to understand shear viscosity in terms of microscopic structure and intermolecular interaction.

The origin of diffusion coefficients can be treated in a similar manner using the Green-Kubo formalism, where it is used in molecular dynamics simulation to estimate the diffusion coefficient. In this formalism transport or diffusional coefficients are related to integrals of the time-correlation functions. The self-diffusion coefficient is given by[56]:

$$D_i = \frac{1}{3N_i} \int_0^\infty dt < \sum_{k=1}^{N_i} v_i^k(0).v_i^k(t) > \tag{2.4}$$

where $v_i^k(t)$ resembles the velocity vector of a molecule k of species i. the equation yields the self-diffusion coefficient of component i with an averaging over N_i molecules, again connecting a molecular origin to the property. Indeed, in the case of shear viscosity and the diffusion coefficient of a solute, the molecular origin is shared as is famously embodied in Einstein's fluctuation-dissipation theorem [57]: $D = \frac{k_B T}{f}$, Where f is a friction force coefficient.

2.7 Polyethylene Glycol Hydrogels

The chemistry and biological applications of polyethylene glycol "PEG" have been the subject of intense study in both academia and in industry. One of the most common applications is the use of PEG hydrogels for drug delivery and in wound covering [58] [59] due to its availability in different multifunctional derivatives. These lead to forming many varieties of cross-linked PEG hydrogels [60]. The suitability and performance of hydrogels in biomedical materials and

applications depend mainly on their fully swollen structure [61] and this final bulk structure is defined and explained in terms of three structural parameters which are the polymer volume fraction in the fully swollen gel (ϕ), the molecular weight of the polymer between cross-links (M_C), and the polymer free space a solute can diffuse in which is called the mesh size (ξ) [61]. The above parameters provide a complete information of the way the solvent is stored and retained by the hydrogel.

The mechanical properties of hydrogels depend largely on their water content and understanding the role of water is the main key to understand the system because it is composed of 90% water or more. It is known that hydrogels contain two types of water 'bound' or hydration water and free water. As mentioned before the bound population will have slower dynamics than the bulk population. In this dissertation I studied in detail the extent and degree of this slower dynamics. This reduction in the mobility of water molecules near polymer surfaces demonstrate the effect of the hydration water on the viscous and transport properties without any other factors in the system that contribute to changes in these properties.

Hydrogels are dilute polymer solutions in which the polymer chains are chemically crosslinked to create a swollen network structure[62]. This family of materials can be generated from a wide variety of polymer chemistries and adapted for a huge variety of applications. Variation in polymer volume fraction, cross-link density, molecular weight, polymer type, co-polymers and compositing of nano/micro particles; can all be used to engineer the properties of hydrogels to suit numerous applications. Polyethylene glycol (PEG) hydrogels are perhaps the most ubiquitous polymer gels used in drug delivery[63], tissue engineering and wound treatment, along with many other applications. The PEG polymer itself is favorable in these roles because of its low

interaction with other dissolved solutes – theorized to originate with the minimal disruption the PEG molecule has upon the surrounding water structure.

This polymer/water interaction is at the heart of theory describing the swelling and physical properties of hydrogels. Competing driving forces determine total swelling of the hydrogels. The swelling degree depends on the solvent quality referred to interaction parameter between the solvent and the polymer chains or solute [64]. In the case of hydrogels, the polymer chains with a specific molecular weight will be crosslinked in situ and form a new system with a specific molecular weight between crosslinks in the swollen state[65, 66]. This is all from the competing interactions that specify the nature and the structure of the new system and therefore they will predict the macroscopic properties of the hydrogels.

The mentioned competing driving forces are either swelling driving or swelling resistant. The swelling driving forces are the gain in entropy by mixing of the solvent and the polymer. While the swelling resistance is the loss of entropy in network chains as they are stretched. This entropy competing process defines and determines the final state of the gel and the degree of swelling[67]. In more details the free energy of mixing is as known the product of the temperature and change in entropy upon mixing subtracted from the change in enthalpy upon mixing. The best model to describe the change in the system energy upon mixing is Flory-Huggins solution theory [68].

Flory-Huggins solution theory considers a lattice model to explain the thermodynamics of polymer solution which considers the dissimilarity in the molecular sizes for the purpose of

estimating the entropy of mixing of the system. The Gibbs free energy change ΔG_m of mixing of the polymer and the solvent is achieved.

The thermodynamic equation for the Gibbs energy change during mixing at constant temperature and pressure is given by[69]:

$$\Delta G_m = \Delta H_m - T\Delta S_m \tag{2.5}$$

The change from pure substances properties to a solution is addressed by Δ. The Florry-Huggins approach lattice model leads to an explicit formula for the enthalpic and entropic changes associated with the mixing process. The resulting formula is[70]:

$$\Delta G_m = RT[n_1 ln\phi_1 + n_2 ln\phi_2 + n_1\phi_2\chi_{12}] \tag{2.6}$$

where n_1 and n_2 are the number of moles of the solvent and the polymer respectively, ϕ_1 and ϕ_2 are the volume fractions. χ is the solvent-solute interaction parameter that takes into account the energy of mixing polymer and solvent molecules. Here the entropy is thought of an increase in the randomness of the distribution of the molecules when they are interspersed. The obvious differences in the molecular size was considered by assuming that individual polymer segments and individual solvent molecules occupy sites on a lattice. Where each site is occupied by either one water molecule or one monomer of the polymer chain.

On the other hand, the elastic contribution to the hydrogel free energy is well explained by the rubber elasticity theory which accounts for the entropic retraction force that restrains swelling[71]. This process has no enthalpic term. It defines the entropic change in network change due to stretching. It treats the polymer coils as freely joined chains and the entropic

change is determined by finding the product of all possible probabilities for each end-to-end distance of the polymer chains in both the stretched and the relaxed states. The entropic change which is gives the free energy change is given by[68, 72]:

$$\Delta G_{el} = -T\Delta S_{el} = \frac{3}{2} k_b T v_e [\alpha^2 - 1 - ln\alpha] \tag{2.7}$$

Where α is the factor of stretching or the ratio of the stretched to unstretched length and v_e is the number density of elastically active chains.

Flory-Rehner equation describes the mixing of a polymer and liquid molecules as predicted by swelling equilibrium theory. It takes into account the same three forces considered in Flory-Huggins theory to find the change in Gibbs free energy and gives arise to a model that predicts the molecular mass between cross-links M_c as follows[72]:

$$-[\ln (1 - \phi + \phi + \chi_1\phi^2] = \frac{V_1}{\bar{v}M_c} \left(1 - \frac{2M_c}{M_n}\right)(\phi^{\frac{1}{3}} - \frac{\phi}{2}) \tag{2.8}$$

where $\bar{v}$ is the specific volume of the polymer and V_1 is the solvent's molar volume and M is the molecular weight of the polymer.

Also the Peppas-Merrill equation is used to evaluate the molecular weight between cross-links which is prepared in the absence of a solvent[73]. The Peppas-Merrill equation hence takes into account the polymer volume fraction in the relaxed state ϕ_r . The relaxed state is the state of the gel is the state after polymerization but before the solvent is introduced or swelling is allowed in the presence of water. The Flory-Rehner equation can be achieved by sitting the ϕ_r term equal to unity. Below is the Peppas-Merrill equation[73]:

$$\frac{1}{M_c} = \frac{2}{M_n} - \frac{(\bar{v}/V_1)\left[\ln(1-\phi)+\phi+\chi_1\phi^2\right]}{\phi_r\left[\left(\frac{\phi}{\phi_r}\right)^{\frac{1}{3}}-\left(\frac{\phi}{2\phi_r}\right)\right]} \qquad (2.9)$$

Crosslinked polymeric networks are conveniently characterized by the cross-linking density which is inversely proportional to the average molecular weight per cross-linking unit M_c. Through the theory of rubber elasticity it is known that when an initially unswollen cross-linked gel is first swollen so that the volume fraction of polymer decreases to ϕ, where the remainder is solvent, the tensile stress T is related to the extension ratio α by the equation:

$$\frac{T}{\left[\alpha-(1/\alpha^2)\right]} = RT\frac{\phi_r}{M_c}\left(1 - \frac{2M_c}{M_n}\right)\phi^{\frac{1}{3}} \qquad (2.10)$$

The above formalism which is derived from Flory-Huggins and Peppas-Merrill relations will ease the comparison of different gels and find their modulus through swelling and mechanical experiments. So, it is clear from performing swelling experiment we can predict mechanical properties of the hydrogels. The difference in moduli between hydrogels is due to the amount of water in the hydrogel and the modulus can be expressed as [74]:

$$G = \frac{\rho RT}{M_c\phi^{\frac{1}{3}}}\left(1 - \frac{2\,M_c}{Mn}\right) \qquad (2.11)$$

where ρ is the network density.

In the case of drug delivery, Lusting and Peppas [75] described the solute transport within non-porous polymer hydrogels. The model depends on the mesh size and the solute size to be diffusing within the hydrogel network as:

44

$$\frac{D}{D_0} = \left(1 - \frac{a}{\xi}\right) e^{\left(\frac{-1}{Q_v - 1}\right)} \tag{2.12}$$

where D is the diffusion coefficient, D_0 is the diffusion of the solute in water, a is the molecular radius and Q_v is the equilibrium swelling ratio.

For water transport within the polymer chains can be described by the following equation which contains contribution from Fickian diffusion and polymer relaxation[76]:

$$\frac{M_t}{M_\infty} = k_1 t^{1/2} + k_2 t \tag{2.13}$$

where M_t is the total amount of water that is absorbed at time t and M_∞ is the amount at equilibrium. $k_1 \ and \ k_2$ are constants.

The goal in this dissertation is to find the molecular origin for the macroscopic differences in mechanical properties and structure of PEG hydrogels due to the water content as explained before.

The polymer elasticity also plays an important role in explaining the macroscopic properties. In swollen states the swelling ratio and the young modulus are related as explained above and different swelling ratios will have different modulus and gel viscoelastic properties

In this dissertation, I aimed to develop a dataset of to directly look at the dynamical changes in water within PEG hydrogels. This developed a framework to connect observed changes in water dynamics to the equilibrium properties of PEG gels. I studied the difference in dynamics of bound and bulk water, and the effect of initial polymer concentration on the swelling degrees and therefore mechanical properties of the hydrogels. I also studied in detail the structural characteristics discussed earlier along with the polymer dynamics in the hydrogels. This is the

heart of chapter 5. Inelastic neutron scattering measurements were used to look directly at the changes in water dynamics within PEG gels of differing volume fraction using BASIS/CNCS; and then attempt to understand the connection of the equilibrium water dynamics within PEG hydrogels to the polymer dynamics. For this I used NSE to observe the polymer chain motions and SANS to understand the polymer network structure.

To access the water dynamics directly, the quasielastic neutron scattering (QENS) techniques which will be discussed in details in the next chapter were measured using the Backscattering Spectrometer (BASIS), and inelastic neutron scattering using the Cold Neutron Chopper Spectrometer (CNCS), Both the instruments are at the Oak Ridge National Laboratory Spallation Neutron Source. The hydration water is important to explain both the structure and the function of the hydrogel [77]. Where it is the key factor to both structural flexibility and responses to external stimuli [78] [79] [80]. So, a complete picture of water dynamics surrounding the macromolecule is needed to understand the system. The way bulk water is believed to diffuse is through jumps occurring between cages of neighboring molecules and performing a local motion in between [81] [12, 82]. On the other hand, the motion of water molecules in the hydration shell around a macromolecule wither polymer chains or a protein is different and is perturbed by the macromolecule with respect to bulk water [12] [7].

The analysis of this data followed the approach in Perticaroli et al.[6] where the water dynamics addressed as two populations; one bulk water population representing water that is structurally and dynamically unaffected by the solute, and a 'bound' or hydration water population representing water which is dynamically altered by its proximity to the polymer chains. The result of this analysis are two parameters used to explain the extent of perturbation through the

46

hydration number N_H and the magnitude of this perturbation through retardation factor, R_H . The hydration number describes the extent of perturbation in terms of the number of water molecules per monomer unit which are dynamically altered, while the retardation factor describes the degree of the observed perturbation as defined by the ratio of characteristic relaxation times of hydration water to bulk water. The dynamics of hydration water has only sparsely been investigated due to the experimental difficulty in accessing this time and length scale regime.

The PEG gels were generated using a photo-initiated thiol-ene click reaction [83], in collaboration with Prof. Seidlits at the University of California at Los Angeles. The monomer 4 Arm-PEG-SH (MW:20 KDa) is cross-linked by an 8 Arm PEG Norbornene (MW 20 KDa) in a water bath under photo-initiation to form a cross-linked hydrogel. This polymerization chemistry is like most others and is expected to generated an inhomogeneous cross-linking reaction resulting in inhomogeneities in the polymer gels [84] [85]. According to the de Genne's C* theorem, the scattering function from polymer gels can be treated as the case of polymer solutions[86, 87]. Hence the scattering intensity of a gel is given by Ornstein-Zernike function with a second term describing the static concentration fluctuations due to any inhomogeneities. This model provided the correlation length at each polymer volume fraction of in the hydrogel [88]. While the main Ornstein-Zernike formalism describes the describes the thermal fluctuations in a semi dilute polymer solutions[86]. For swollen gels, the polymer concentration lies typically in the semi dilute regime. Hence the scattering function for a polymer solution can be used and excess scattering from cross-links can be neglected [89]. In my work I believe that the PEG hydrogels are in equilibrium swelling and that the O-Z model fits well to our scattering intensity from SANS. The

EQ-SANS instrument at the neutron spallation source in Oak Ridge National Lab is the instrument chosen for the SANS measurement for the gels, which is one of the broadest applications of neutron scattering, is a structural probe applicable to length scales ranging from 14 to around 6400 Angstroms [90]. Due to the power of SANS to access inhomogeneities and the important properties of hydrogels such as the polymer volume fraction in the swollen [61].

As mentioned, the chain diffusion coefficient is calculated from the relaxation times from Neutron Spin Echo (NSE). Theories on polymer dynamics are explained in more detail in the next section.

2.8 Polymer Dynamics

Polymers are made up of large number of monomers linked together through covalent bonds. According to the bead and spring model the flexible polymer is composed of several equal statistical segments[91]. The distribution of the end-to-end distance is gaussian due to the assumption that each segment is actually made up of enough real segments. There are continuous collisions occurring between the beads and with the solvent molecules in a solution. where a bead here is referred to either a monomer or larger part of the chain. Also, the movement of the polymer through the solvent will induce a velocity field in the solvent which will be experienced by other parts of the chain or let's say the beads. If we neglect the hydrodynamic interactions for simplicity as starting point to understand the polymer dynamics, which is not a good assumption for dilute polymer solutions. The bead will experience a viscous and a random force acting on it. The Rouse model neglects any hydrodynamic interactions and excluded volume effects and considers the polymer chain as a gaussian chain which consists of freely joined Gaussian segments or beads of a certain length. The forces experienced by the bead are

summarized in the Langevin equation for the Rouse model [92], where it gives the sum of the velocity due to a stochastic forces from random motion and due to potential field:

$$\frac{dR_n}{dt} = \frac{-1}{\varsigma}\frac{\partial U}{\partial R_n} + g_n \tag{2.14}$$

where ς is the friction coefficient experienced by the bead, R_n is the position of bead N, g_n is the change in velocity due to stochastic force caused by the random Brownian motion and U is the potential energy of the bead which can be explained by the bead and spring model [93]:

$$U = \frac{1}{2}k_{spr}\sum_{n=1}^{n=N}(R_n - R_{n-1})^2 \tag{2.15}$$

where k_{spr} is the spring constant and the sum is for the whole chain of length ℓ. combining the expression for U and the Langevin equation:

$$\frac{dR_n}{d_t} = \frac{k_{spr}}{\varsigma}(R_{n+1} + R_{n-1} - 2R_n) + g_n \tag{2.16}$$

For n=0 and n=N the same expression can be used if we apply $R_{-1} = R_0$ and $R_{N+1} = R_N$.

Solving equation (2.16) by cos-Fourier transformation results in a spectrum of normal modes p which involves the vibrational modes along with the relaxation motions. The rouse relaxation time is then (τ_r) the longest relaxation time in the mode spectrum called the Rouse relaxation time [94]:

$$\tau_r(q) = \frac{1}{12}\frac{k_bT}{\varsigma}l^2q^4 \tag{2.17}$$

From here it is important for us to conclude that the dynamic structure factor for the Rouse dynamics is proportional q^4. Moving to explain the Zimm dynamics there is an addition consideration of hydrodynamic interactions between different segments which needs to be considered in the Langevin equation. This leads to a different longest relaxation time due to different forces acting on the beads and different distribution of the modes. This is seen in different dependence on p ($\frac{1}{\tau_p} \propto \frac{1}{\tau_z} p^{\frac{3}{2}}$ compared to $\frac{1}{\tau_p} \propto \frac{1}{\tau_r} p^2$) and hence a different q dependence (q^3 instead of q^4). Where the characteristic polymer relaxation time of the Zimm dynamics is given by:

$$\tau_z(q) = \frac{1}{6\pi} \frac{k_b T}{\eta} q^3 \tag{2.18}$$

As mentioned, I used neutron spin echo (NSE) to observe the polymer dynamics in PEG hydrogels. The observed experimental quantity is the intermediate scattering function which states the fraction of pair correlations that are still in existence after a given time interval. The relaxation times are extracted then as a function of the momentum transfer vector. It usually takes the shape of an exponential decay just because lower number of correlations remain at longer probe durations. In this case, the diffusion coefficient is not simply proportional to the exponential decay constant and the square of the length scale probed; but rather a sub-diffusive length scale dependence is seen. Upon comparison, the dynamics of the polymeric chains are not altered significantly in the concentration range studied for the PEG gels experimentally. This comes despite the clear structural changes in the gel at the level of polymer network mesh size. We can

conclude that the polymer chains are not directly interacting with nearby chains in this concentration regime, nor is there significant internal chain deformation being induced. This correlates directly into the network elasticity concepts discussed above and show that water interaction – and entropy gain - is the primary driver of swelling and the mechanical properties of the gel.

2.9 Protein Solutions

Soluble proteins can be considered as nano colloids and studied using theories of colloidal suspension. Colloids can be defined as species that are dissolved in solution and exhibit irregular motion caused by random collisions between the solvent and the colloidal particles. Those collisions are of thermal origin and requires the colloidal particles to be larger than the water particles but small enough to experience Brownian motion[95]. As we know Brownian motions are characterized by properties of the solvent such as its viscosity. Such characterization requires the ability to distinguish between the interactions of the colloidal species within themselves and the interactions with the solvent which therefore requires the colloidal particles to be sufficiently larger than the solvent particles. This means the interactions can be averaged and many solvent molecules will be interacting with the colloidal particle at the same time. The size of a colloidal species is ten times larger than that of the solvent molecule. In the case of aqueous solutions this means the colloidal particles have a radius in the order of nanometers[96]. This means colloidal species are in size range where thermal motions determine its displacement. Not small that it cannot be distinguished experimentally from the solvent and not large that it experiences other effects such as gravity and buoyant forces. Colloidal particles can be classified as rigid, macromolecules or small molecules just like micro-emulsions. Proteins can be under the second

class of colloidal particles (macromolecules). Proteins lie down in the lower limit of a colloidal particle size. The main goal of this part of my dissertation is to model the green fluorescent protein (GFP) as colloidal particle and explain its self-diffusion using colloidal theories.

2.10 Diffusion in Colloidal Solutions

Self-diffusion and collective diffusion are the two types of diffusion process that are considered in colloidal solutions theories. Self-diffusion is observing the diffusion of a certain or tagged particle in a suspension crowded with other particles, the tagged particle is usually referred as a tracer [97]. Collective diffusion involves many particles due to their cooperative movements that restores a local homogenous density in the system [98]. At infinite dilution both the processes are identical to a free particle diffusion at infinite dilution D_0 [99]. In the very dilute limit, the diffusion explained by solely a particle undergoing random motion due to the collision between the particles and the solvent molecules where the diffusion coefficient depends on the pure solvent viscosity. Above this concentration direct and indirect interactions start resulting in an increase in the friction coefficient experienced by the colloidal particle.

In order to track the self-diffusion coefficient of a labelled tracer colloidal particle, one must analyze its mean square displacement (MSD). As a function of time different characteristic times of the colloidal particles can be distinguished. For times much below a momentum relaxation time τ_m the particle is not affected by the solvent and hence its displacement is the product of the particle's velocity and the time of travel. On the other hand, for times much larger than the momentum relaxation time but before collisions between particles occur, the colloidal particle's movement is explained by a Brownian motion where it have experienced enough collisions with the solvent particles. For times above that where interactions are significant then direct

interactions between the particle's molecules play a role in determining the nature of the diffusion. In other words, as concentration increases D_0 is reduced due to the indirect hydrodynamic interactions between the particles at short times and at longer times when the particle's start interacting directly. It is important to mention that the long self-diffusion coefficient of colloidal particles are still dominated by hydrodynamic interactions even at a longer observing time[100]. For collective diffusion coefficient where it is a collective motion of many particles dependent on density fluctuations it similarly can be explained by the observed time scales. Also, the collective diffusion coefficient is scale dependent where at short length scales (smaller than the nearest neighboring distance) the collective diffusion coefficient goes to the self-diffusion coefficient[101].

The motivation to study and analyze protein solutions and the change in dynamics with concentration arise from the fact that the living cells are crowded with protein's and other macromolecules at volume fractions ranging from 20 to 40%[102]. Several studies focusing on the dynamics of protein's in concentrated solutions have been done [102, 103]. Bovine serum albumin (BSA) have been studied [102] and showed a reduction in the self-diffusion coefficient with concentration and their finding is described very well in terms of colloidal short-time self-diffusion outlying the importance of hydrodynamic interactions on crowding behavior. Another study on Hemoglobin was investigated using neutron spin echo (NSE) and revealed the fact that the collective diffusion goes to the self-diffusion at q values above the structure maximum. They showed similar conclusion of the reduction in the self-diffusion coefficient of proteins[101]. The collective diffusion coefficient in another study on Myoglobin was found to increase at low q values at increased concentrations due to increased direct interactions[104]. It is concluded from

several studies on protein solutions that the size of the protein has to be renormalized to an effective larger volume fraction. This is due to the fact that proteins are structurally different from nano colloids where proteins are defined as macromolecules with non spherical shape and nonhomogeneous topology. Therefor it is a challenge to colloid theory [105]. But it has been proven that considering a protein as a sphere with equivalent radius in simulations results in reasonable approximation to its diffusion coefficient[106]. In this dissertation I use the hydrodynamic radius estimated from the perturbed water molecules in the first two hydration shells from a previous GFP study [6]on the water dynamics in GFP solutions to be the key to normalize the protein volume fraction.

For biological solutions such as GFP, the question is whether diffusion can be understood based on concepts explaining the case for uncharged colloidal particles. For a colloids hydrodynamic interaction which is mediated by the solvent acts as an important role. Where basically particles suspended in a fluid mediate long-ranged flows while moving and move in response to the solvent motion. By reaction to the solvent's dynamics, the colloidal particles experience what is called hydrodynamic interaction with each other. So, particles will experience indirect solvent-mediated forces, apart from the other direct interactions. The flow velocity due to these hydrodynamic interactions decays in a fast rate proportional to the distance scale squared [107]. Hydrodynamic interactions explain the equilibrium dynamics of colloidal systems. At equilibrium the average distance between particles is determined by the potential energy, therefore the overall structure of the system is not affected. However hydrodynamic interactions divert and determine the movement of the particles, and this effect influences the crystallization processes of such system which will is usually proportional to the solvent viscosity.

The Brownian motion strength of particles can be estimated by the diffusion time τ_D which the particle takes to travel a distance comparable to its radius or size. For a sphere which has a radius a this time is given by:

$$\tau_D = \frac{a^2}{D_0} \propto \eta \frac{a^3}{T}$$ (2.19)

where D_0 is translational diffusion coefficient $D_0 = \frac{K_b T}{f_0}$.

Any flow that is described as a stokes flow can be associated with a fluid stress described in terms of a stress tensor σ. This means that a surface dS immersed in the fluid experiences a hydrodynamic drag dF exerted by the fluid is given by:

$$dF = \sigma\, n\, dS$$ (2.20)

In this dissertation I observed the reduced mobility in GFP with increasing volume fractions and shows that the reduction in the self-diffusion coefficient is well-explained by the colloidal theories.

2.11 Crowded Solutions

Crowded solutions especially protein solutions are of vital importance in the design of pharmaceuticals and understanding the natural biological environment within a cell. The translational diffusion constant of proteins has been seen to be reduced by five times according to NMR experiments [101]. The reduced mobility is believed to be due to excluded volume effects in crowded media as mentioned in the previous sections. However, the weak dependence of the collective diffusion constant suggests that other factors such as hydrodynamic interaction terms are likely to be involved. The dynamic structure factor obtained by NSE can give information

about inter-particle correlations and their time evolution. This way we can obtain the collective diffusion coefficient by fitting an exponential function.

2.12 Hydration Water in Green Fluorescent Protein

Previous work [6] focused on the hydration water in GFP solutions. Where the structurally and dynamically perturbed water surrounding the protein was the main aspect of the study. This is due to the earlier discussed influence of the water dynamics on the properties and function of such biological systems. Therefor the degree of perturbation was studied. It was shown that less than two shells were perturbed. The dynamics were found to be 2-10 times slower than bulk water as a function of q which reflects the distance from the protein and the probing length measurement. This shows that the hydration water undergoes a sub diffusive motion, where in case of bulk or neat water it is diffusive behavior. As previously mentioned, two parameters; the retardation factor and the hydration number are used to quantify the extent and degree of perturbation. For hydration shell information MD simulations were performed to evaluate the number of water molecules in the perturbed water shells. For the first shell one of the hydrogen atoms of the water molecules must be within 3.3 Angstroms radius from the protein surface, and for the second shell it should be located within 3.3 to 5.5 Angstroms. This tells us that around 863 water molecules are in the first shell and the total of perturbed water molecules was 1706 within the two shells. The neutron scattering experimental description showed that around 1470 were perturbed which are slightly less than two complete shells. These water molecules are believed to be impacting the protein's diffusion coefficient and impacting the determined hydrodynamic radius. The results showed that water was perturbed by a factor of 4-10 in the first shell and 2-5 in the second shell.

As a continuation for this project I studied the protein dynamics itself. previous experimental observations showed that diffusion coefficients of hemoglobin decreases exponentially with concentration [108]. Such reduction in mobility is believed to be due to excluded volume effects in crowded media. The independence of the collective diffusion coefficient on concentration reflects the fact that there is another interaction playing the role of reduced self-diffusion coefficient. The collective diffusion coefficient is considered unaffected, and this is due to the equality of osmotic and friction forces. Molecular interactions are established on a length scale of few nanometers and this range can be accessed by neutron scattering and particularly neutron spin echo technique. In sections 1.9 and 1.10 I discussed the concepts of hydrodynamic interaction in colloidal particles. The question I am addressing here is whether such concepts can be applied to the GFP solution at high concentration and to understand the molecular dynamics that dominate in long range molecular transport. Hydrodynamic interactions dominate at the short times and direct forces are significant and formed during the structural relaxation time. It is of a great interest to measure prove that hydrodynamic interactions relate to the immobility experienced by the protein. the no dependence of the collective diffusion coefficient is a hint that there is a hydrodynamic interaction dominating in determining the diffusion coefficient of such protein crowded in solution.

2.13 Green Fluorescent Protein

Green Fluorescent Protein was by coincidence discovered by Shimomura [109] as an associate to aequorin from Aequorea jelly fish. It was found during purification of aequorin where a protein that gave rise to a greenish solution in sunlight was observed. Also, it shows no toxicity, this
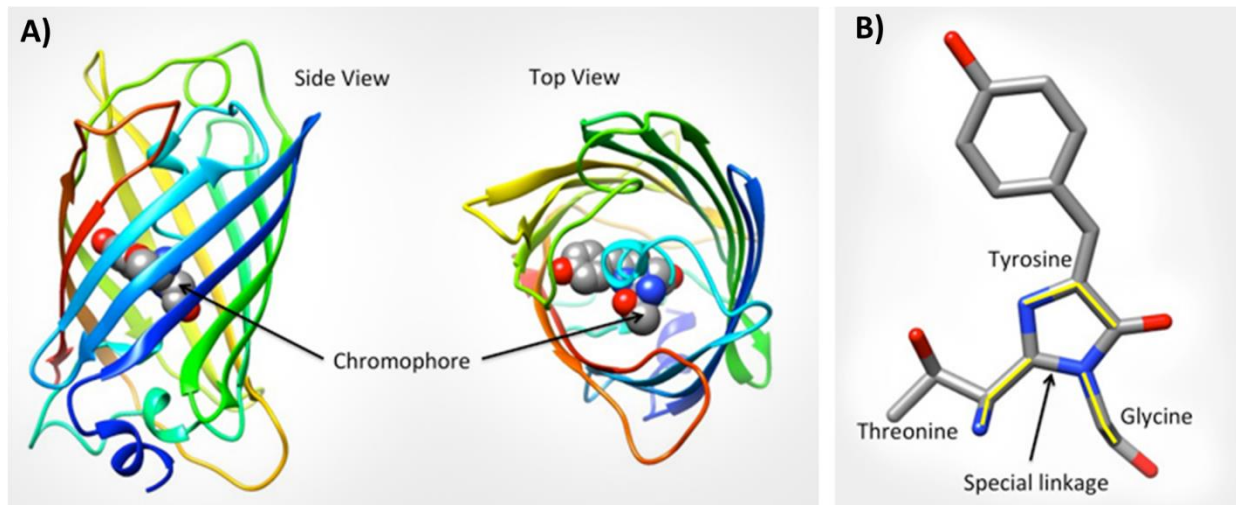
Figure 2.2 Structure of Green Fluorescent Protein. A) Green Fluorescent Protein (GFP). B) The chromophore [110]

makes GFP ideal in many investigations and applications. GFP is also known to be resistant to heat and high pH[111]. Some of the many applications of the protein are studying protein dynamics in living cells using fluorescent microscopy[112]. It is also used in cell biology and biotechnology[113], fungal biology[114], in mouse embryos[115], in bacterial protein stabilization[116], and many other applications. GFP exhibits a bright green florescent when exposed to light in the blue to ultraviolet range [117]. GFP has a beta barrel structure which is nearly a prefect cylinder around 42 Angstroms long with a radius of about 24 Angstroms[118]. Eleven beta strands result in the beta-barrel and an alpha helix fills the center. The chromophore which his responsible for the green light is found in the middle of the beta-barrel which is referred to light of the barrel[119]. The structure of GFP is shown in Figure 2.2.

References

1. Yahya, A., et al., *Molecular origins of bulk viscosity in liquid water.* Physical Chemistry Chemical Physics, 2020. **22**(17): p. 9494-9502.
2. Perticaroli, S., et al., *Description of Hydration Water in Protein (GFP) Solution.* Biophysical Journal, 2017. **112**(3): p. 201a.
3. Nickels, J.D., et al., *Lipid rafts: buffers of cell membrane physical properties.* The Journal of Physical Chemistry B, 2019. **123**(9): p. 2050-2056.
4. Berens, S.J., et al., *Transition between Different Diffusion Regimes and Its Relationship with Structural Properties in Nafion by High Field Diffusion NMR in Combination with Small-Angle X-ray and Neutron Scattering.* The Journal of Physical Chemistry B, 2020. **124**(40): p. 8943-8950.
5. Perticaroli, S., et al., *Dynamics of hydration water in sugars and peptides solutions.* The Journal of Physical Chemistry B, 2013. **117**(25): p. 7729-7736.
6. Perticaroli, S., et al., *Description of hydration water in protein (green fluorescent protein) solution.* Journal of the American Chemical Society, 2017. **139**(3): p. 1098-1105.
7. Nickels, J.D., et al., *Dynamics of protein and its hydration water: neutron scattering studies on fully deuterated GFP.* Biophysical journal, 2012. **103**(7): p. 1566-1575.
8. Poole, P.H., et al., *Phase behaviour of metastable water.* Nature, 1992. **360**(6402): p. 324-328.
9. Mahoney, M.W. and W.L. Jorgensen, *A five-site model for liquid water and the reproduction of the density anomaly by rigid, nonpolarizable potential functions.* The Journal of Chemical Physics, 2000. **112**(20): p. 8910-8922.
10. Kell, G.S., *Density, thermal expansivity, and compressibility of liquid water from 0. deg. to 150. deg.. Correlations and tables for atmospheric pressure and saturation reviewed and expressed on 1968 temperature scale.* Journal of Chemical and Engineering Data, 1975. **20**(1): p. 97-105.
11. Errington, J.R. and P.G. Debenedetti, *Relationship between structural order and the anomalies of liquid water.* Nature, 2001. **409**(6818): p. 318-321.
12. Tan, P., et al., *Gradual crossover from subdiffusion to normal diffusion: a many-body effect in protein surface water.* Physical review letters, 2018. **120**(24): p. 248101.
13. Berendsen, H., et al., *Intermolecular forces*. 1981, Reidel, Dordrecht Jerusalem, Israel.
14. Morisaku, T., et al., *Hydration of phosphorylcholine groups attached to highly swollen polymer hydrogels studied by thermal analysis.* Polymer, 2008. **49**(21): p. 4652-4657.
15. Fulton, A.B., *How crowded is the cytoplasm?* Cell, 1982. **30**(2): p. 345-347.
16. Syková, E. and C. Nicholson, *Diffusion in brain extracellular space.* Physiological reviews, 2008. **88**(4): p. 1277-1340.
17. Jhon, M.S. and J.D. Andrade, *Water and hydrogels.* Journal of biomedical materials research, 1973. **7**(6): p. 509-522.
18. Quinn, F.X., et al., *Water in hydrogels. 1. A study of water in poly (N-vinyl-2-pyrrolidone/methyl methacrylate) copolymer.* Macromolecules, 1988. **21**(11): p. 3191-3198.
19. Pascal, T.A., et al., *Thermodynamics of water stabilization of carboxybetaine hydrogels from molecular dynamics simulations.* The Journal of Physical Chemistry Letters, 2011. **2**(14): p. 1757-1760.
20. Choudhury, N. and B.M. Pettitt, *Dynamics of water trapped between hydrophobic solutes.* The Journal of Physical Chemistry B, 2005. **109**(13): p. 6422-6429.
21. Muhr, A.H. and J.M. Blanshard, *Diffusion in gels.* Polymer, 1982. **23**(7): p. 1012-1026.
22. Wilson, D.K., F.B. Rudolph, and F.A. Quiocho, *Atomic structure of adenosine deaminase complexed with a transition-state analog: understanding catalysis and immunodeficiency mutations.* Science, 1991. **252**(5010): p. 1278-1284.

23. Sovago, M., et al., *Hydrogen bonding strength of interfacial water determined with surface sum-frequency generation.* Chemical Physics Letters, 2009. **470**(1-3): p. 7-12.

24. Merzel, F. and F. Avbelj, *Why do water molecules around small hydrophobic solutes form stronger hydrogen bonds than in the bulk?* Biochimica et Biophysica Acta (BBA)-General Subjects, 2020. **1864**(4): p. 129537.

25. Iglič, A., E. Gongadze, and K. Bohinc, *Excluded volume effect and orientational ordering near charged surface in solution of ions and Langevin dipoles.* Bioelectrochemistry, 2010. **79**(2): p. 223-227.

26. Kaplan, W.D. and Y. Kauffmann, *Structural order in liquids induced by interfaces with crystals.* Annu. Rev. Mater. Res., 2006. **36**: p. 1-48.

27. Drost-Hansen, W., *Structure of water near solid interfaces.* Industrial & Engineering Chemistry, 1969. **61**(11): p. 10-47.

28. Teixeira, J., et al., *Experimental determination of the nature of diffusive motions of water molecules at low temperatures.* Physical Review A, 1985. **31**(3): p. 1913.

29. Eisenberg, D., W. Kauzmann, and W. Kauzmann, *The structure and properties of water*. 2005: Oxford University Press on Demand.

30. Luzar, A. and D. Chandler, *Hydrogen-bond kinetics in liquid water.* Nature, 1996. **379**(6560): p. 55-57.

31. Shinohara, Y., et al., *Viscosity and real-space molecular motion of water: Observation with inelastic x-ray scattering.* Physical Review E, 2018. **98**(2): p. 022604.

32. Frank, H.S. and W.-Y. Wen, *Ion-solvent interaction. Structural aspects of ion-solvent interaction in aqueous solutions: a suggested picture of water structure.* Discussions of the Faraday Society, 1957. **24**: p. 133-140.

33. Dhopatkar, N., A.P. Defante, and A. Dhinojwala, *Ice-like water supports hydration forces and eases sliding friction.* Science advances, 2016. **2**(8): p. e1600763.

34. Singwi, K. and A. Sjölander, *Diffusive motions in water and cold neutron scattering.* Physical Review, 1960. **119**(3): p. 863.

35. Laage, D. and J.T. Hynes, *A molecular jump mechanism of water reorientation.* Science, 2006. **311**(5762): p. 832-835.

36. Rani, P. and P. Biswas, *Diffusion of hydration water around intrinsically disordered proteins.* The Journal of Physical Chemistry B, 2015. **119**(42): p. 13262-13270.

37. Stokes, R. and R. Robinson, *Interactions in aqueous nonelectrolyte solutions. I. Solute-solvent equilibria.* The Journal of Physical Chemistry, 1966. **70**(7): p. 2126-2131.

38. Maxwell, J.C., *IV. On the dynamical theory of gases.* Philosophical transactions of the Royal Society of London, 1867. **157**: p. 49-88.

39. Plumari, S., et al., *Shear viscosity of a strongly interacting system: Green-Kubo correlator versus Chapman-Enskog and relaxation-time approximations.* Physical Review C, 2012. **86**(5): p. 054902.

40. Hirai, N. and H. Eyring, *Bulk viscosity of liquids.* Journal of Applied Physics, 1958. **29**(5): p. 810-816.

41. Lindsey, C. and G. Patterson, *Detailed comparison of the Williams–Watts and Cole–Davidson functions.* The Journal of chemical physics, 1980. **73**(7): p. 3348-3357.

42. Timasheff, S.N., *Protein-solvent preferential interactions, protein hydration, and the modulation of biochemical reactions by solvent components.* Proceedings of the National Academy of Sciences, 2002. **99**(15): p. 9721-9726.

43. Constantinides, G., et al., *Probing mechanical properties of fully hydrated gels and biological tissues.* Journal of biomechanics, 2008. **41**(15): p. 3285-3289.

44.   Yakimets, I., et al., *Mechanical properties with respect to water content of gelatin films in glassy state.* Polymer, 2005. **46**(26): p. 12577-12585.

45.   Ninni, L., M. Camargo, and A. Meirelles, *Water activity in poly (ethylene glycol) aqueous solutions.* Thermochimica acta, 1999. **328**(1-2): p. 169-176.

46.   Troller, J., *Water activity and food*. 2012: Elsevier.

47.   Sereno, A.M., et al., *Prediction of water activity of osmotic solutions.* Journal of Food Engineering, 2001. **49**(2-3): p. 103-114.

48.   Rupley, J.A., E. Gratton, and G. Careri, *Water and globular proteins.* Trends in Biochemical Sciences, 1983. **8**(1): p. 18-22.

49.   Guggenheim, E., *The theoretical basis of Raoult's law.* Transactions of the Faraday Society, 1937. **33**: p. 151-156.

50.   Mazurkiewicz, J., P. Tomasik, and J. Zapłotny, *Relationships between water activity and viscosity of solutions.* Food hydrocolloids, 2001. **15**(1): p. 43-46.

51.   Miyawaki, O., et al., *Activity and activity coefficient of water in aqueous solutions and their relationships with solution structure parameters.* Bioscience, biotechnology, and biochemistry, 1997. **61**(3): p. 466-469.

52.   Gekas, V., et al., *Mass transfer properties of osmotic solutions. I. Water activity and osmotic pressure.* International Journal of Food Properties, 1998. **1**(2): p. 95-112.

53.   Gray, C.G., K.E. Gubbins, and C.G. Joslin, *Theory of Molecular Fluids: Volume 2: Applications*. Vol. 10. 2011: Oxford University Press.

54.   Mason, T.G., et al., *Nanoemulsions: formation, structure, and physical properties.* Journal of Physics: condensed matter, 2006. **18**(41): p. R635.

55.   Kikuchi, N., et al., *Transport coefficients of a mesoscopic fluid dynamics model.* The Journal of chemical physics, 2003. **119**(12): p. 6388-6395.

56.   Fernández, G., J. Vrabec, and H. Hasse, *Self diffusion and binary Maxwell–Stefan diffusion in simple fluids with the Green–Kubo method.* International journal of thermophysics, 2004. **25**(1): p. 175-186.

57.   Kubo, R., *The fluctuation-dissipation theorem.* Reports on progress in physics, 1966. **29**(1): p. 255.

58.   Harris, J.M., *Poly (ethylene glycol) chemistry: biotechnical and biomedical applications*. 2013: Springer Science & Business Media.

59.   Zarzycki, R., Z. Modrzejewska, and K. Nawrotek, *Drug release from hydrogel matrices.* Ecol Chem Eng S, 2010. **17**(2): p. 117-36.

60.   Harris, J.M. and K. Yoshinaga, *Assessment of the Effects of Attaching an Enzyme to Glass by a Poly (ethylene glycol) Tether.* Journal of bioactive and compatible polymers, 1989. **4**(3): p. 281-295.

61.   Peppas, N.A., et al., *Hydrogels in biology and medicine: from molecular principles to bionanotechnology.* Advanced materials, 2006. **18**(11): p. 1345-1360.

62.   Hoffman, A.S., *Hydrogels for biomedical applications.* Advanced drug delivery reviews, 2012. **64**: p. 18-23.

63.   Cheng, J., et al., *Formulation of functionalized PLGA–PEG nanoparticles for in vivo targeted drug delivery.* Biomaterials, 2007. **28**(5): p. 869-876.

64.   Donnelly, R.F., et al., *Hydrogel-forming microneedles prepared from "super swelling" polymers combined with lyophilised wafers for transdermal drug delivery.* PLoS One, 2014. **9**(10): p. e111547.

65.   Temenoff, J.S., et al., *Effect of poly (ethylene glycol) molecular weight on tensile and swelling properties of oligo (poly (ethylene glycol) fumarate) hydrogels for cartilage tissue engineering.* Journal of Biomedical Materials Research: An Official Journal of The Society for Biomaterials, The

Japanese Society for Biomaterials, and The Australian Society for Biomaterials and the Korean Society for Biomaterials, 2002. **59**(3): p. 429-437.

66. Peppas, N., et al., *Hydrogels in pharmaceutical formulations.* European journal of pharmaceutics and biopharmaceutics, 2000. **50**(1): p. 27-46.

67. Ostroha, J., et al., *Controlling the collapse/swelling transition in charged hydrogels.* Biomaterials, 2004. **25**(18): p. 4345-4353.

68. Young, R.J. and P.A. Lovell, *Introduction to polymers*. 2011: CRC press.

69. Cengel, Y.A., *Introduction to thermodynamics and heat transfer*. Vol. 846. 1997: McGraw-Hill New York.

70. Bower, D.I., *An introduction to polymer physics*. 2003, American Association of Physics Teachers.

71. Deiber, J.A., et al., *Characterization of cross-linked polyampholytic gelatin hydrogels through the rubber elasticity and thermodynamic swelling theories.* Polymer, 2009. **50**(25): p. 6065-6075.

72. Flory, P.J. and J. Rehner Jr, *Statistical mechanics of cross-linked polymer networks I. Rubberlike elasticity.* The journal of chemical physics, 1943. **11**(11): p. 512-520.

73. Peppas, N.A. and E.W. Merrill, *Poly (vinyl alcohol) hydrogels: Reinforcement of radiation-crosslinked networks by crystallization.* Journal of Polymer Science: Polymer Chemistry Edition, 1976. **14**(2): p. 441-457.

74. Bell, C.L. and N.A. Peppas, *Water, solute and protein diffusion in physiologically responsive hydrogels of poly (methacrylic acid-g-ethylene glycol).* Biomaterials, 1996. **17**(12): p. 1203-1218.

75. Lustig, S.R. and N.A. Peppas, *Solute diffusion in swollen membranes. IX. Scaling laws for solute diffusion in gels.* Journal of Applied Polymer Science, 1988. **36**(4): p. 735-747.

76. George, K.A., et al., *Investigation into the diffusion of water into HEMA-co-MOEP hydrogels.* Biomacromolecules, 2004. **5**(4): p. 1194-1199.

77. Niebuur, B.-J., et al., *Water Dynamics in a Concentrated Poly (N-isopropylacrylamide) Solution at Variable Pressure.* Macromolecules, 2019. **52**(5): p. 1942-1954.

78. Aseyev, V., H. Tenhu, and F.M. Winnik, *Non-ionic thermoresponsive polymers in water*, in *Self Organized Nanostructures of Amphiphilic Block Copolymers II*. 2010, Springer. p. 29-89.

79. Bellissent-Funel, M.-C., et al., *Water determines the structure and dynamics of proteins.* Chemical reviews, 2016. **116**(13): p. 7673-7697.

80. Laage, D., T. Elsaesser, and J.T. Hynes, *Water dynamics in the hydration shells of biomolecules.* Chemical reviews, 2017. **117**(16): p. 10694-10725.

81. Laage, D., et al., *Reorientation and allied dynamics in water and aqueous solutions.* Annual review of physical chemistry, 2011. **62**: p. 395-416.

82. Philipp, M., et al., *From molecular dehydration to excess volumes of phase-separating PNIPAM solutions.* The Journal of Physical Chemistry B, 2014. **118**(15): p. 4253-4260.

83. Hoyle, C.E. and C.N. Bowman, *Thiol–ene click chemistry.* Angewandte Chemie International Edition, 2010. **49**(9): p. 1540-1573.

84. Saffer, E.M., et al., *SANS study of highly resilient poly (ethylene glycol) hydrogels.* Soft Matter, 2014. **10**(12): p. 1905-1916.

85. Mendes, E., et al., *Soft order in high-functionality star polymer solutions and gels: A small-angle neutron scattering study.* Macromolecules, 1995. **28**(1): p. 174-179.

86. De Gennes, P.-G. and P.-G. Gennes, *Scaling concepts in polymer physics*. 1979: Cornell university press.

87. Matsunaga, T., et al., *SANS studies on Tetra-PEG Gel under uniaxial deformation.* Macromolecules, 2011. **44**(5): p. 1203-1210.

88. Matsunaga, T., et al., *SANS and SLS studies on tetra-arm PEG gels in as-prepared and swollen states.* Macromolecules, 2009. **42**(16): p. 6245-6252.

89. Higgins, J. and H. Benoit, *Polymers and neutron scattering. Clarendon*. 1994, Oxford.

90. Heller, W.T. and K.C. Littrell, *Small-angle neutron scattering for molecular biology: basics and instrumentation*, in *Micro and Nano Technologies in Bioanalysis*. 2009, Springer. p. 293-305.

91. Rouse Jr, P.E., *A theory of the linear viscoelastic properties of dilute solutions of coiling polymers.* The Journal of Chemical Physics, 1953. **21**(7): p. 1272-1280.

92. Doi, M. and S. Edwards, *Dynamics of concentrated polymer systems. Part 1.—Brownian motion in the equilibrium state.* Journal of the Chemical Society, Faraday Transactions 2: Molecular and Chemical Physics, 1978. **74**: p. 1789-1801.

93. Lodge, A.S. and Y.-J. Wu, *Constitutive equations for polymer solutions derived from the bead/spring model of Rouse and Zimm.* Rheologica Acta, 1971. **10**(4): p. 539-553.

94. Ewen, B. and D. Richter, *Neutron spin echo investigations on the segmental dynamics of polymers in melts, networks and solutions.* Neutron Spin Echo Spectroscopy Viscoelasticity Rheology, 1997: p. 1-129.

95. Dhont, J.K., *An introduction to dynamics of colloids*. 1996: Elsevier.

96. Ross, S. and E. Morrison, *Colloidal systems and interfaces.* 1988.

97. Jönsson, B., et al., *Self-diffusion of small molecules in colloidal systems.* Colloid and Polymer Science, 1986. **264**(1): p. 77-88.

98. Ladd, A.J., et al., *Time-dependent collective diffusion of colloidal particles.* Physical review letters, 1995. **74**(2): p. 318.

99. Nägele, G., *The physics of colloidal soft matter*. 2004: Centre of Excellence for Advanced Materials and Structures Warsaw.

100. Tokuyama, M. and I. Oppenheim, *Dynamics of hard-sphere suspensions.* Physical Review E, 1994. **50**(1): p. R16.

101. Doster, W. and S. Longeville, *Microscopic diffusion and hydrodynamic interactions of hemoglobin in red blood cells.* Biophysical journal, 2007. **93**(4): p. 1360-1368.

102. Roosen-Runge, F., et al., *Protein self-diffusion in crowded solutions.* Proceedings of the National Academy of Sciences, 2011. **108**(29): p. 11815-11820.

103. Harada, R., Y. Sugita, and M. Feig, *Protein crowding affects hydration structure and dynamics.* Journal of the American Chemical Society, 2012. **134**(10): p. 4842-4849.

104. Le Coeur, C. and S. Longeville, *Microscopic protein diffusion at high concentration by neutron spin-echo spectroscopy.* Chemical Physics, 2008. **345**(2-3): p. 298-304.

105. Piazza, R., *Protein interactions and association: an open challenge for colloid science.* Current opinion in colloid & interface science, 2004. **8**(6): p. 515-522.

106. Ando, T. and J. Skolnick, *Crowding and hydrodynamic interactions likely dominate in vivo macromolecular motion.* Proceedings of the National Academy of Sciences, 2010. **107**(43): p. 18457-18462.

107. Diamant, H., et al., *Hydrodynamic interaction in quasi-two-dimensional suspensions.* Journal of Physics: Condensed Matter, 2005. **17**(31): p. S2787.

108. Everhart, C.H. and C.S. Johnson Jr, *The determination of tracer diffusion coefficients for proteins by means of pulsed field gradient NMR with applications to hemoglobin.* Journal of Magnetic Resonance (1969), 1982. **48**(3): p. 466-474.

109. Shimomura, O., F.H. Johnson, and Y. Saiga, *Extraction, purification and properties of aequorin, a bioluminescent protein from the luminous hydromedusan, Aequorea.* Journal of cellular and comparative physiology, 1962. **59**(3): p. 223-239.

110. https://pdb101.rcsb.org/learn/paper-models/gfp-activity-page.

111. Bucka-Kolendo, J. and B. Sokołowska, *Lactic acid bacteria stress response to preservation processes in the beverage and juice industry.* Acta Biochimica Polonica, 2017. **64**(3): p. 459–464-459–464.

112.   Bastiaens, P.I. and R. Pepperkok, *Observing proteins in their natural habitat: the living cell.* Trends in biochemical sciences, 2000. **25**(12): p. 631-637.

113.   Misteli, T. and D.L. Spector, *Applications of the green fluorescent protein in cell biology and biotechnology.* Nature biotechnology, 1997. **15**(10): p. 961-964.

114.   Lorang, J., et al., *Green fluorescent protein is lighting up fungal biology.* Applied and Environmental Microbiology, 2001. **67**(5): p. 1987-1994.

115.   Zernicka-Goetz, M. and J. Pines, *Use of green fluorescent protein in mouse embryos.* Methods, 2001. **24**(1): p. 55-60.

116.   Phillips, G.J., *Green fluorescent protein–a bright idea for the study of bacterial protein localization.* FEMS microbiology letters, 2001. **204**(1): p. 9-18.

117.   Prendergast, F.G. and K.G. Mann, *Chemical and physical properties of aequorin and the green fluorescent protein isolated from Aequorea forskalea.* Biochemistry, 1978. **17**(17): p. 3448-3453.

118.   Brejc, K., et al., *Structural basis for dual excitation and photoisomerization of the Aequorea victoria green fluorescent protein.* Proceedings of the National Academy of Sciences, 1997. **94**(6): p. 2306-2311.

119.   Zimmer, M., *Green fluorescent protein (GFP): applications, structure, and related photophysical behavior.* Chemical reviews, 2002. **102**(3): p. 759-782.

Chapter 3 :   Methods

3.1 Introduction to Neutron Scattering

The main tool used throughout my PhD work is neutron scattering, with contributions from MD simulation, optical spectroscopy. The molecular scale relaxations of water have been studied extensively by simulation. and experimental techniques such as: infrared spectroscopy [1], terahertz spectroscopy [2], optical Kerr-effect spectroscopy [3], X-ray scattering [4], and neutron scattering [5]. Each technique has specific advantages and distinct time and length scales associated with the measurement; with inelastic neutron scattering perhaps the most powerful of these methods where it can access up to sub nanometer length-scale and up to nanosecond to sub-picosecond time scale.

Beyond the length-scale resolved spectroscopic description of the molecular motions; the inelastic neutron scattering technique can probe both the self-motion of hydrogen atoms within water[6], as well as resolving the atomic pair lifetimes associated with the water network; depending upon the isotopic variants of water used. The isotopic sensitivity of neutrons to hydrogen is a powerful tool [7]– with hydrogen (^{1}H) possessing a high incoherent scattering cross section and small negative coherent scattering length; compared to deuterium (^{2}H) which has a small incoherent cross section and a large positive coherent scattering length. The way that these scattering properties manifest into scattering experiments differs by the type of neutron scattering measurements being performed. There are several varieties of neutron scattering will be utilized: small angle neutron scattering (SANS), neutron diffraction (ND), quasielastic neutron scattering (QENS), and neutron spin echo spectroscopy (NSE).

Neutrons produced by either a reactor or an accelerator-based sources typically have wavelengths on the order of Ångstroms [8]; and hence are very suitable for probing the structures and motions of molecules in soft condensed matter. From the de Broglie relation[9]: the neutron has a wavelength:

$$\lambda = \frac{h}{mv} \tag{3.1}$$

where h is Plank's constant, m is the mass of the neutron, and v is the neutron velocity. During the scattering experiment, the neutrons experience a change in momentum after interacting the sample[10]. This means the scattered neutron had a change in direction and/or the velocity. This momentum change is described by a momentum transfer vector called the scattering vector represented by q. and is defined as the vector difference between the incoming k_i and the scattered vector k_s. besides the change in direction, the magnitude of the incident neutron wave vector can change too where it means the neutron gained or lost energy due to interacting with the sample. Scattering is totally elastic if there is no energy exchange. The absolute magnitude of the scattering wave vector is given by the Brag relationship $q = 2\pi/d$. Where d represents the probe length in the sample.This is visually explained in Figure 3.1

Neutrons penetrate deeply into matter since they are uncharged and scatter primarily from nuclear interactions (although they also possess a magnetic moment which does interact in very useful ways with magnetic structures)[11]. These nuclear interactions vary with element and isotope. This is in contrast with X-ray photons which interact with the electron clouds, meaning that the scattering density scale with atomic number[12]. The isotopic sensitivity of neutron scattering is especially useful in biological materials due to the high amount of hydrogen.
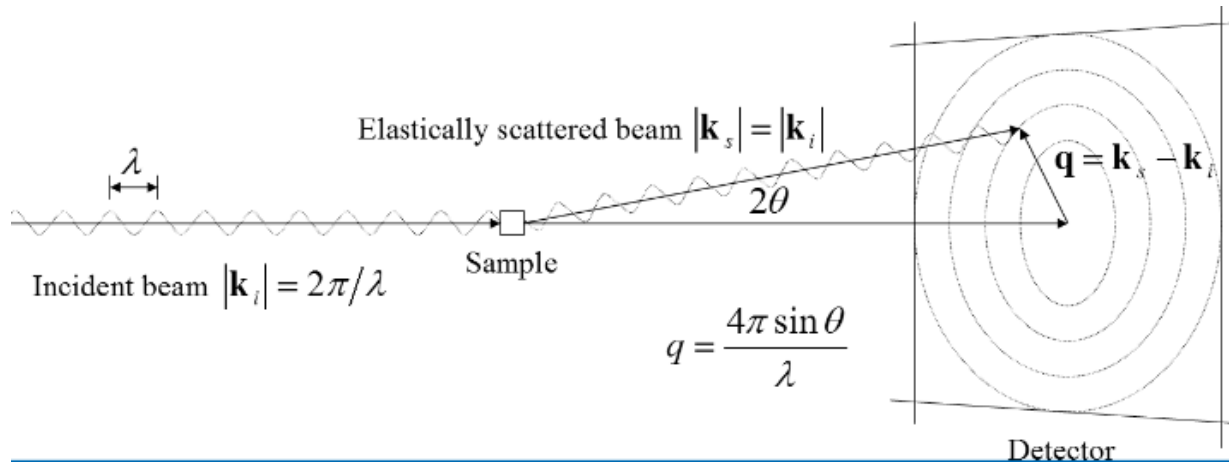
Figure 3.1 Momentum change in neutron scattering [13].

The high differences in the scattering cross sections and scattering lengths between isotopes provides the possibility of using isotopic substitution to emphasize or eliminate the scattering from a certain part of a molecule or molecular arrangement.

3.2 Elastic Scattering

Here there is no change in the energy of the incident neutron during the scattering. It is the direction of the neutron vector than changes not the magnitude. [14]. In other words, scattering events in which no energy is exchanged are called elastic scattering events, and for most experiments comprises more than 99% of scattering observed. These methods are used for structural studies and predominantly observe coherent scattering from atom pairs or macromolecules/structures.

In this work we use cold and thermal neutrons which corresponds to wavelengths on the order of 1 -10 Angstroms [10]. It is convenient to explain the difference between elastic and inelastic scattering using a comparison of the incident and scattered neutron's respective wave vectors.

These scattering wave vectors are defined by a velocity and direction. The wave vector and the velocity vector are correlated by the equation:

$$\frac{hk}{2\pi} = mv \qquad\qquad (3.2)$$

where h is the planks constant, m is the mass of the neutron and mv is the momentum of the neutron.

The momentum transferred during the scattering event can now be defined as the difference between the incident neutron wave vector and the scattered neutron's wave vector which we define it as q. The momentum transfer is then simply $\frac{h}{2\pi}q = \frac{h}{2\pi}(k_i - k_s)$. Where k_i is the wave vector of the incident neutrons and k_s is the wave vector of the scattered neutrons. In elastic scattering there is no energy exchange between the incident neutrons and the sample, or $|k_i| = |k_s|$. We can now discuss q as it relates to the scattering experiment where it describes both the physical angle on the scattered neutron through $q = \frac{4\pi}{\lambda}\sin(\theta/2)$, where θ is the scattering angle; and as the physical distance between two scatterers where $q = \frac{2\pi}{d}$ where d is the distance separating two scattering centers. In the case where there is a change in energy, the scattering is said to be inelastic which is discussed in the next section.

3.3 Small Angle Neutron Scattering (SANS)

Small-angle neutron scattering (SANS) is a diffraction study in the range where the magnitude of the momentum transfer, q, is much smaller than the position of the first peak in the structure factor[10]. Thus, SANS is used to study structures with dimensions in the range of almost 14 to

6400 Angstroms [15]. SANS is the technique usually used in investigating the structure of biological materials as it can probe the shape, size and conformation of macromolecules in aqueous solutions and systems on a length scale from ten to several thousand Angstroms[16].

Compared to Synchrotron X-rays, the single significant disadvantage of neutrons is that neutron fluxes are several orders of magnitude less. This translates into much longer experimental times and lower throughput. However, neutrons scatter not from the electron density as X-rays but from the scattering length density associated with the atomic nuclei. Neutron scattering length varies by element and isotope in a non-systematic way [17].

The SANS experiment is performed by observing the number and angle of scattered neutrons from a given sample. Neutrons are generated by a spallation source or reactor first pass through a monochromator or chopper that defines the wavelengths [18] and collimating optics define the angular divergence of the beam. The observed scattering is expressed as the quantity I(q), where q is the scattering wave vector. Scattering measurements are performed in the reciprocal space. As noted above, q can be defined as $q = \frac{4\pi}{\lambda} \sin (\theta/2)$, where θ is the physical scattering angle on the detector. The scattering wave vector, q, is also related to the physical spacing of scattering centers, d, in the sample via $q = \frac{2\pi}{d}$ [19]. The SANS q range is typically from 0.001 Å^{-1} to 0.45 Å^{-1}. [19]. The configuration of SANS is shown in Figure 3.2.
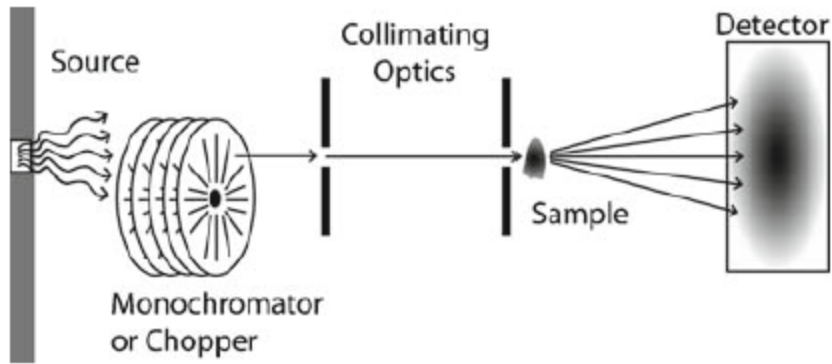
Figure 3.2 Schematic of SANS instrument [13].

The scattering intensity reflects the local differences in scattering length density, p, within the sample due to the molecular structure. The scattering length density is defined as the sum of all coherent lengths of all atoms divided by the volume they occupy. The scattering resulting from a given spatial distribution therefore reflects the distribution of the atoms in the sample [20]. The most general form to describe the scattering is the Fourier transform of the pair distribution function, scaled by the scattering length density:

$$I(q) = \left| \langle \int_V (\rho(r) - \rho_s) e^{-ir} d^3r \right|^2 \tag{3.3}$$

In many cases this can be simplified to describe the distribution of atoms or solutes in terms of two main factors; a form factor, P(q), that represents the interference of neutron scattered from different parts of the same object, and a structure factor S(q), that represents the interference of neutrons scattered from different objects. This is seen in the equation below:

$$I(q) = \frac{N}{V} (\rho_{s1} - \rho_{s2})^2 V_p^2 P(q)S(q) \tag{3.4}$$

where ρ_{s1} and ρ_{s2} are the scattering length density of the scattering and the surrounding medium or the solvent buffer respectively, N is the number of scattering centers, V is the volume of a scattering center, P(q) is the form factor and depends on the shape of the object, finally S(q) is the structure factor and it depends on the interaction between the objects in the system and it is related to the probability distribution function of inter-particles distances, If the system has no interparticle interactions, i.e. a dilute solutions, then S(q)=1. In practice, the observed scattering is fit against models of the sample molecular structure which are represented in the form factor and/or structure factor.

3.4 Neutron Diffraction

Broadly, SANS can be classified as neutron diffraction, but here we refer to high q diffraction, measuring shorter length scale structure. Here, the scattered intensity is modeled only by the structure factor, reflecting atom pairs, rather than molecular structures. Again, there are no energy change considered since this is elastic scattering. The measured intensity is therefore proportional to the structure factor only which is given by[10]:

$$S(q) = \sum_i b_i \, e^{iq.r_i} \qquad (3.5)$$

where b_i is the scattering length.

3.5 Inelastic Neutron Scattering

In contrast to the case of elastic scattering described above, some collisions between neutrons and atoms in a sample result in an exchange of energy. Since we know the energy of the incident neutron and we assume mass is conserved, the gained or lost energy must come from the motion of the atom in the sample from which the neutron has scattered. In this way, inelastic neutron

scattering allows us to directly observe molecular motions of water, macromolecules, and other solutes.

In our case we are mostly concerned with observations of water diffusion, molecular rotation, and local vibrations (nanosecond and picosecond time scales) and protein and polymer diffusion over tens of nanometers (tens to hundreds of nanoseconds timescale). There are a number of techniques under the umbrella of inelastic scattering by which this can be accomplished, each probing a specific time and length scale.

Here, incoherent scattering plays a more significant role than the background seen in elastic scattering methods. Here, the inelastic incoherent scattering is associated with the self-motions of individual atoms, while inelastic coherent scattering reflects the changing of distance between pairs of atoms or structures[21]. Quasielastic neutron scattering is a form of inelastic neutron scattering where the energy transfer peak is located around E=0[22]. Which indicates that each form of the scattering access different time scales kinetics. Where in quasielastic it is the slowest which is set by the width of the instrument resolution. Slower motions must be measured using other technologies such as neutron spin echo which encodes velocity in the spin of the neutron. The various elastic/quasielastic neutron scattering instruments have specific energy/length scale windows shown in the (q, E) space. To have a full information and to access all the dynamics we are concerned of we will be using different instrumentation with different resolutions. Figure 3.3 [23] shows the different energy window governed by each technique and how the dynamics of different biological systems impose more than one window covered by a single instrumentation.
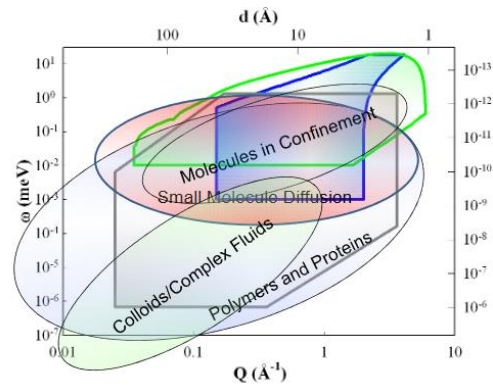
Figure 3.3 Energy window for different scattering methods. Back scattering shown in blue, Cold neutron chopper in green, and neutron spin echo in grey.

Combing two instruments of different design allows an expanded dynamical range for our observations of water dynamics. I have used two main instruments together in this dissertation, the direct geometry instrument CNCS, and the indirect geometry instrument Back Scattering Spectrometer (BASIS)) to obtain a dynamic range covering ~100 fs to 3 ns. For both geometries, I observe both coherent and incoherent scattering. In conjunction with NSE for longer timescales. As mentioned before such a combination was used to construct an experimental description of bulk water and compare its motions to those in hydration water around GFP [24]. Dynamics were collected with a combination with BASIS and CNCS instrumentation. The two instruments measure the dynamic structure factor in an overlapping range. Figure 3.4 from a recent study [25]shows how the dynamics range overlap and can be combined to give a susceptibility formalism spectrum.
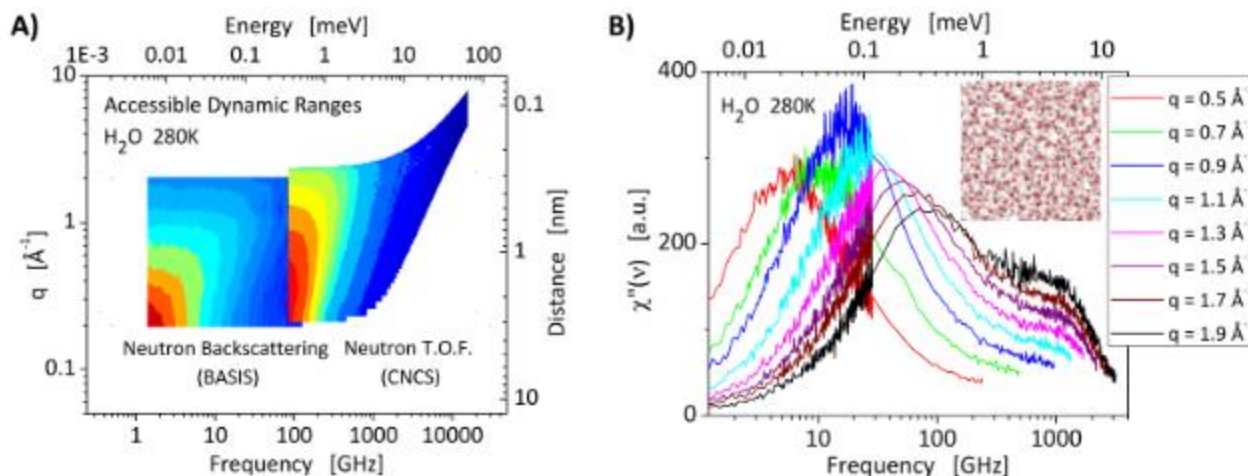
Figure 3.4 Water Dynamics. A) Experimental NS spectra of pure H_2O registered on the BASIS and CNCS instrument. B) Stitched spectra of H_2O from the two instruments.

3.6 Direct Geometry (Time-of-Flight) Inelastic Neutron Scattering

Direct geometry methods observe the time difference between the incident beam and the neutrons traveling faster or slower due to interaction with the sample by the timing of scattered neutrons proceeding directly from the sample to a detector array. The resulting energy resolution is limited by electronics within the detector and the physical space between the sample and the detector bank, while the q range is again defined by angle and wavelength. In general, these instruments measure fast dynamics, phonons, and other collective modes, molecular rotation, and vibration which result in large changes of momentum in the scattered neutron – i.e. large changes in velocity.

I used one such instrument in this work, the Cold Neutron Chopper Spectrometer (CNCS) at ORNL. CNCS is a time of flight spectrometer. It can access sub fs to 50 ps and in a q range from 0.3 to 2 $Å^{-1}$. The operation is simple to explain where it receives beam from a cold coupled moderator.
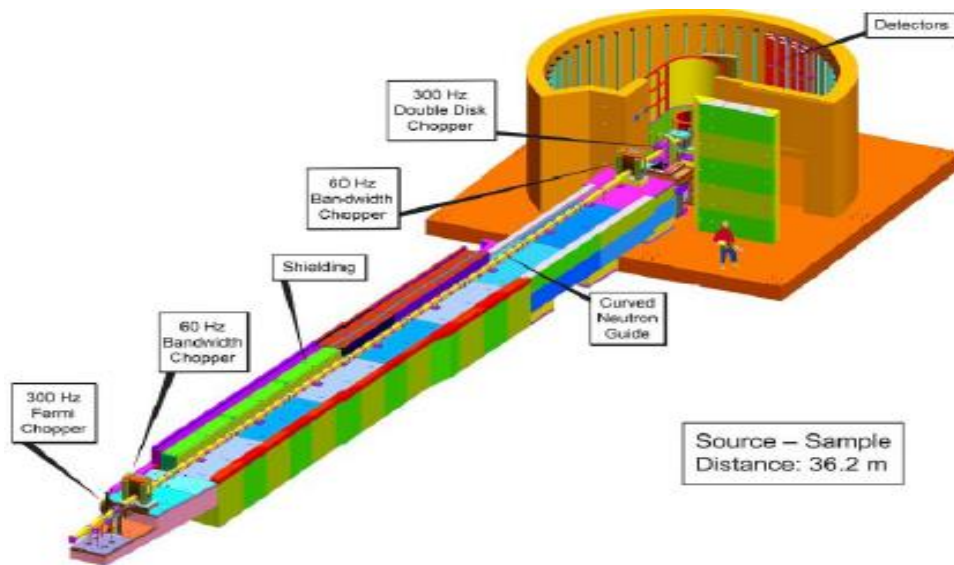
Figure 3.5 Cold Neutron Chopper Spectrometer layout.

Short pulses of a neutron beam are directed onto the sample after defining a certain wavelength band and finally the location and the time of flight of the detected neutrons are used to determine the energy gained or lost by the neutron or in another word the momentum exchange that occurred between the incident neutron beam and the sample. The layout of the CNCS instrument is shown in Figure 3.5.

3.7 Indirect Geometry

The direct geometry has fundamental limitations in the electronic timing of scattered neutrons, so a few more complex geometries have been developed to access smaller energy transfers. These instruments measure what is called quasielastic scattering (QENS), or the limiting case of energy resolution in which the inelastic scattering is often not fully distinguished from the inelastic scattering centered at $\omega = 0$. Here we primarily use the Back Scattering Spectrometer (BASIS)
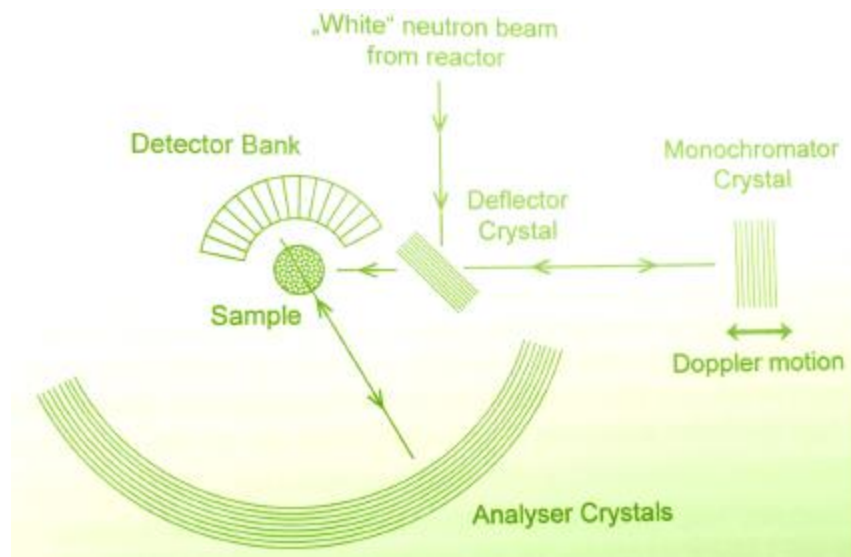
Figure 3.6 BASIS configuration.

at the Spallation Neutron Source at Oak Ridge National Laboratory. This pulsed source instrument utilizes an extremely long beam guide and physical choppers to regulate the incident energy into a narrow wavelength band. A pulse of neutron with a defined wavelength band then interacts with the sample, and scattered neutrons gain or lose energy and proceed at various angles. These scattered neutrons next interact with an analyzer crystal (silicon i111 or i311) which reflects only one specific wavelength (speed) of neutron into the detector bank. Combining the time at which the neutrons hit the sample detector with the fact that all neutrons hitting the detector have the exact same wavelength (velocity), we can back calculate the energy change, benefitting from the extremely good resolution of the Bragg reflection from the analyzer crystal. Depending on the analyzer crystal type we can have a q range from 0.2 to 2.0 Å^{-1}. And the dynamics range here are slower than in CNCS ranging from 10 ps to 10 ns. Just like how discussed above this was used along with CNCS to observe the dynamics of water in PEG hydrogels and have an experimental description of the perturbation in water dynamics around the polymer chains.

3.8 Neutron Spin Echo (NSE)

NSE is another inelastic scattering technique, unique because it is capable of measuring slower dynamic from picoseconds to hundreds of nanoseconds. This time range is useful to observe the motion of macromolecules such as proteins (diffusion, rotation, internal motions) and polymers (diffusion, chain, and segmental dynamics). NSE achieves this high resolution by measuring such small velocity changes via the spin of the neutron. By polarizing incident neutrons and regulating their precession through identical, opposing magnetic fields, the neutron spin precession acts as a clock by which velocity changes can be measured. The neutrons are allowed to spin in a magnetic field before interacting with the sample and encoding of the individual velocities of the incoming neutrons into precession angles occurs. In elastic scattering where there is no change of energy, a symmetric magnetic field compensates for the precession angle accumulated. This leads to the restoration of polarization by spin re-phasing which is why it is called spin-echo. But since this is an inelastic scattering measurement and the neutron velocity is changed, the re-phasing will become incomplete by the asymmetric magnetic field and there will be a loss of polarization, This reflects actually the distribution of differences in the time the neutrons need to fly through the magnetic fields. By variation of the detector position and magnetic field strength, the intermediate scattering function I(Q, t) can be observed. This is different from the dynamic structure factor observed in the other inelastic scattering methods discussed above, relaying information about molecular motions in the time domain. A wide q-range is accessible by the NSE technique, complementing structural observations in the SANS and diffraction ranges
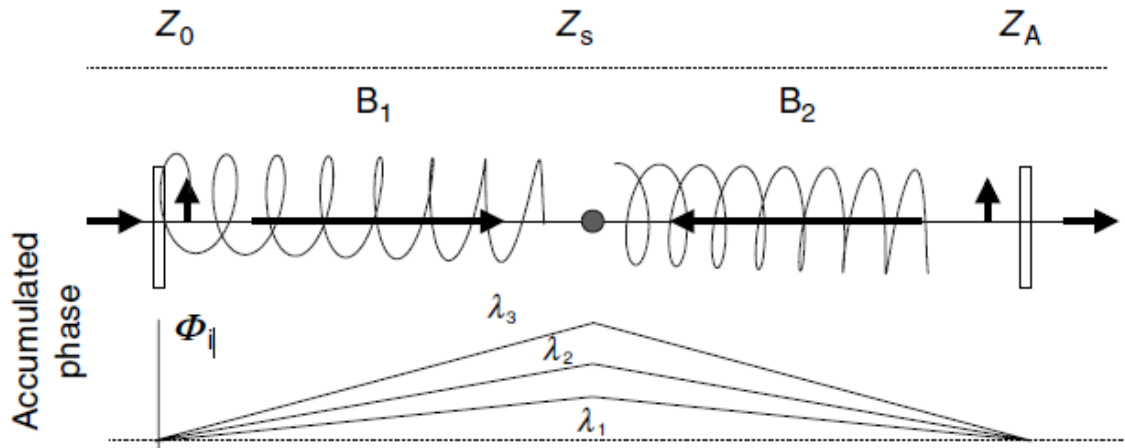
Figure 3.7 Neutron Spin Echo Spectrometer Principle [10].

(approx. 0.05 to 2 Å^{-1}). Another important distinction is that NSE typically probes changes in coherent scattering – not incoherent scattering as the other methods just discussed. One caveat of the NSE instrument at the SNS is a time-of-flight based instrument which results in lower flux than continuous source instruments.

3.9 Dynamic Light Scattering (DLS)

Dynamic light scattering measures the fluctuations in the scattering intensity from particles in solution undergoing Brownian motion. Where the diffusion coefficient and they hydrodynamic radius of the particle can be estimated[26]. I used this method specifically to estimate the free-particle diffusion coefficient of green fluorescent protein at infinite dilution D_0. An estimation of the protein's size is obtained through the Stokes-Einstein formalism. It is an important experimental technique in industry and research, and it has the ability to measure the size of particles in a range of 0.001 to several microns[27]. The operation is basically a beam is illuminated on a sample and what is measured is the intensity of the scattered light $I(q, \theta)$. When light hits the sample and as long the particles are smaller than the wavelength, the light is scattered in all directions (Rayleigh scattering)[27]. the fluctuation in the intensity is originating

from the distance between the particles continuously changing due to random Brownian motions[28]. The light undergoes either constructive or destructive interference by the surrounding particles and from this intensity fluctuation we access the time dependent movement of the particles which leads to a diffusion coefficient which reflects the size of the sample travelling in medium with known viscosity. This dynamic information is presented in what is called autocorrelation of the intensity recorded during the experimental duration as[29]:

$$g^2(q,\tau) = \frac{\langle I(t)I(t+\tau)\rangle}{\langle I(t)\rangle^2}$$
(3.6)

where $g^2(q,\tau)$ is the autocorrelation function as a function of scattering wave vector q and delay time τ and I is the intensity.

This second order autocorrelation function is converted to a first order autocorrelation function through[30, 31]:

$$g^2(q,\tau) = 1 + \beta_{DLS}[g^1(q,\tau)]^2$$
(3.7)

where β_{DLS} is a correction factor depending on the alignment of the laser during the experiment.

Then simply the first auto-correlation function is treated as a single decaying curve with a decaying constant of $\Gamma_{DLS} = q^2D$ [32]. Where the diffusion coefficient is the translational diffusion coefficient.

Figure 3.8 shows the optical configuration for dynamic light scattering. where the detector which is in most cases is a photomultiplier tube that measures the intensity of scattered light. The amplifier removes the background noise before the pulses being analyzed by the correlator that
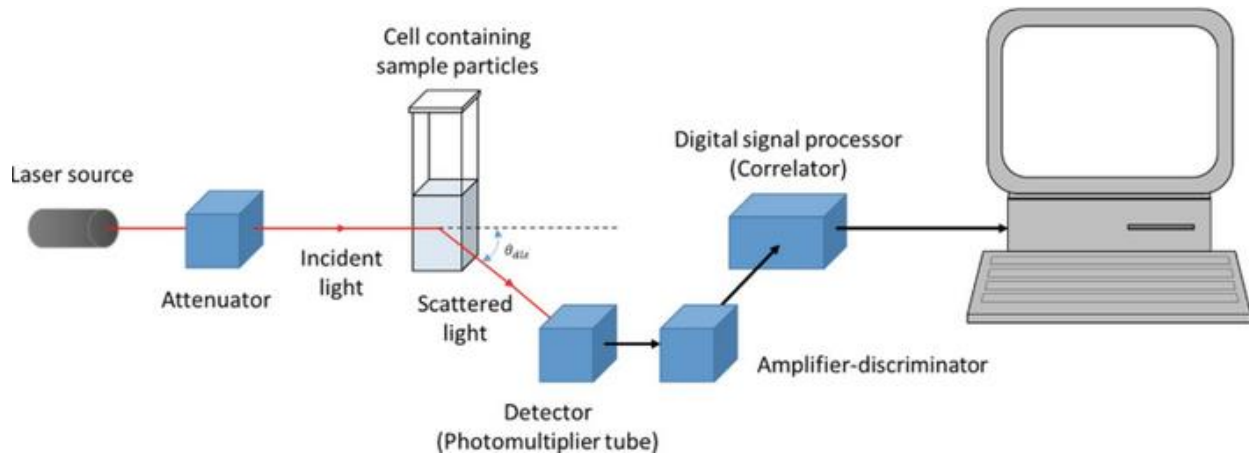
Figure 3.8 Optical configuration for typical experimental setup for DLS measurements [33].

auto correlates the rate of the modulated pulses by comparison of the scattered light intensity for given periods of time.

3.10 Brillouin Light Scattering

The Rayleigh-Brillouin light scattering is an inelastic light scattering technique that allows determination of the directional dependence of the acoustic velocities in materials[34]. It is an inelastic scattering of light where thermal motions in the sample results in fluctuations in the number density as a function of position and time and the light experiences the particle as a dipole that results in a doppler shift of the scattered light[35]. The resultant scattered light has a wavevector and frequency that depends on both the incident light and the wavevector and frequencies that are present in the sample's density fluctuations. Brillouin scattering measures the density fluctuations that probe elastic properties at micro scale. This results in triplet spectrum consisting of a central Rayleigh band at the incident light frequency ω_0 which has a width determined by thermal diffusivity and Brillouin doublets shifted by a frequency of $\pm\,\omega(q)$ corresponding to doppler shifts produced by the sound modes. The doublets have a width of $q^2\Gamma$ that corresponds to the attenuation coefficient[28]. The observed intensity, I(ω) is a function of

frequency ω. The observed spectra in this dissertation was modeled with a damped harmonic oscillator [28]. The two doublets are two Lorentzian lines symmetrically shifted and are used to obtain the sound velocity through[36]:

$$\pm\omega(q) = \pm c_L q \tag{3.8}$$

And the width at half maximum is corresponding to the longitudinal kinematic viscosity and the thermal diffusivity as[28]:

$$\Gamma_B = \Gamma q^2 = \left[\frac{\zeta + \frac{4}{3}\eta}{\rho} + D_{TH}\right] q^2 \tag{3.9}$$

where the first term in the brackets represent the longitudinal diffusivity and ζ and η are the bulk and shear viscosities and ρ is the density. Where q in the case of Brillouin light scattering is given as:

$$q = \frac{4\pi n}{\lambda} \sin\left(\frac{\theta}{2}\right) \tag{3.10}$$

where n is the refractive index.

References

1. Woutersen, A., U. Emmerichs, and H. Bakker, *Femtosecond mid-IR pump-probe spectroscopy of liquid water: Evidence for a two-component structure.* Science, 1997. **278**(5338): p. 658-660.
2. Rønne, C., P.-O. Åstrand, and S.R. Keiding, *THz spectroscopy of liquid H 2 O and D 2 O.* Physical review letters, 1999. **82**(14): p. 2888.
3. Winkler, K., et al., *Ultrafast Raman-induced Kerr-effect of water: Single molecule versus collective motions.* The Journal of Chemical Physics, 2000. **113**(11): p. 4674-4682.
4. Iwashita, T., et al., *Seeing real-space dynamics of liquid water through inelastic x-ray scattering.* Science advances, 2017. **3**(12): p. e1603079.
5. Teixeira, J., et al., *Experimental determination of the nature of diffusive motions of water molecules at low temperatures.* Physical Review A, 1985. **31**(3): p. 1913.
6. Nickels, J.D., et al., *Dynamics of protein and its hydration water: neutron scattering studies on fully deuterated GFP.* Biophysical journal, 2012. **103**(7): p. 1566-1575.
7. Meilleur, F., K.L. Weiss, and D.A. Myles, *Deuterium labeling for neutron structure-function-dynamics analysis*, in *Micro and Nano Technologies in Bioanalysis*. 2009, Springer. p. 281-292.
8. Prask, H., et al., *The NIST cold neutron research facility.* Journal of research of the National Institute of Standards and Technology, 1993. **98**(1): p. 1.
9. Cubitt, R. and G. Fragneto, *Neutron reflection:: Principles and examples of applications*, in *Scattering*. 2002, Elsevier. p. 1198-1208.
10. Fitter, J., T. Gutberlet, and J. Katsaras, *Neutron scattering in biology: techniques and applications*. 2006: Springer Science & Business Media.
11. Voigt, J., *2 Neutron Sources.* Neutron Scattering, 2013.
12. Shapiro, D., et al., *Biological imaging by soft x-ray diffraction microscopy.* Proceedings of the National Academy of Sciences, 2005. **102**(43): p. 15343-15346.
13. Heller, W.T. and K.C. Littrell, *Small-angle neutron scattering for molecular biology: basics and instrumentation*, in *Micro and Nano Technologies in Bioanalysis*. 2009, Springer. p. 293-305.
14. Pynn, R., *Neutron scattering by rough surfaces at grazing incidence.* Physical Review B, 1992. **45**(2): p. 602.
15. Hammouda, B., *A tutorial on small-angle neutron scattering from polymers.* Gaithersburg: National Institute of Standards and Technology, 1995.
16. Shibayama, M., T. Tanaka, and C.C. Han, *Small angle neutron scattering study on poly (N-isopropyl acrylamide) gels near their volume-phase transition temperature.* The Journal of chemical physics, 1992. **97**(9): p. 6829-6841.
17. Sears, V.F., *Neutron scattering lengths and cross sections.* Neutron news, 1992. **3**(3): p. 26-37.
18. Heller, W.T., *Small-angle neutron scattering and contrast variation: a powerful combination for studying biological structures.* Acta Crystallographica Section D: Biological Crystallography, 2010. **66**(11): p. 1213-1217.
19. Hammouda, B., *Probing nanoscale structures-the sans toolbox.* National Institute of Standards and Technology, 2008: p. 1-717.
20. Jackson, A.J., *Introduction to small-angle neutron scattering and neutron reflectometry.* NIST Center for Neutron Research, 2008: p. 1-24.
21. Bellissent-Funel, M.-C. and J. Teixeira, *Dynamics of water studied by coherent and incoherent inelastic neutron scattering.* Journal of molecular structure, 1991. **250**(2-4): p. 213-230.
22. Middendorf, H., *Biophysical applications of quasi-elastic and inelastic neutron scattering.* Annual review of biophysics and bioengineering, 1984. **13**(1): p. 425-451.
23. Bée, M., *Quasielastic neutron scattering.* 1988.

24.   Perticaroli, S., et al., *Description of Hydration Water in Protein (GFP) Solution.* Biophysical Journal, 2017. **112**(3): p. 201a.

25.   Perticaroli, S., et al., *Description of hydration water in protein (green fluorescent protein) solution.* Journal of the American Chemical Society, 2017. **139**(3): p. 1098-1105.

26.   Arzenšek, D., R. Podgornik, and D. Kuzman. *Dynamic light scattering and application to proteins in solutions*. in *Seminar, Department of Physics, University of Ljubljana*. 2010.

27.   Goldburg, W.I., *Dynamic light scattering.* American Journal of Physics, 1999. **67**(12): p. 1152-1160.

28.   Berne, B.J. and R. Pecora, *Dynamic light scattering: with applications to chemistry, biology, and physics*. 2000: Courier Corporation.

29.   Provencher, S.W. and P. Štêpánek, *Global analysis of dynamic light scattering autocorrelation functions.* Particle & particle systems characterization, 1996. **13**(5): p. 291-294.

30.   Frisken, B.J., *Revisiting the method of cumulants for the analysis of dynamic light-scattering data.* Applied optics, 2001. **40**(24): p. 4087-4091.

31.   Topel, Ö., et al., *Determination of critical micelle concentration of polybutadiene-block-poly (ethyleneoxide) diblock copolymer by fluorescence spectroscopy and dynamic light scattering.* Journal of Molecular Liquids, 2013. **177**: p. 40-43.

32.   Chang, C.-C., et al., *Protein folding by a quasi-static-like process: a first-order state transition.* Physical Review E, 2002. **66**(2): p. 021903.

33.   Leong, S.S., et al., *Dynamic Light Scattering: Effective Sizing Technique for Characterization of Magnetic Nanoparticles*, in *Handbook of Materials Characterization*. 2018, Springer. p. 77-111.

34.   Speziale, S., H. Marquardt, and T.S. Duffy, *Brillouin scattering and its application in geosciences.* Reviews in Mineralogy and Geochemistry, 2014. **78**(1): p. 543-603.

35.   Takagi, Y. and K. Kurihara, *Application of a microscope to Brillouin scattering spectroscopy.* Review of Scientific Instruments, 1992. **63**(12): p. 5552-5555.

36.   Palombo, F. and D. Fioretto, *Brillouin light scattering: applications in biomedical sciences.* Chemical reviews, 2019. **119**(13): p. 7833-7847.

Chapter 4 :   Molecular Origins of Bulk Viscosity in Liquid Water

4.1 Abstract

The rapid equilibrium fluctuations of water molecules are intimately connected to the rheological response; molecular motions resetting the local structure and stresses seen as flow and volume changes. In the case of water or hydrogen bonding liquids generally, the relationship is a non-trivial consideration due to strong directional interactions complicating theoretical models and necessitating clear observation of the timescale and nature of the associated equilibrium motions. Recent work has illustrated a coincidence of timescales for short range sub-picosecond motions and the implied timescale for the shear viscosity response in liquid water. Here, neutron and light scattering methods are used to experimentally illustrate the timescale of bulk viscosity and provide a description of the associated molecular relaxation. Brillouin scattering has been used to establish the timescale of bulk viscosity; and borrowing the Maxwell approach, the ratio of the bulk viscosity, ζ, to the bulk modulus, K, yields a relaxation time, τ_B, which emerges on the order of 1–2 ps in the 280 K to 303 K temperature range. Inelastic neutron scattering is subsequently used to describe the motions of water and heavy water at the molecular scale, providing both coherent and incoherent scattering data. A rotational (alternatively described as localized) motion of water protons on the 1–2 ps timescale is apparent in the incoherent scattering spectra of water, while the coherent spectra from D_2O on the length scale of the first sharp diffraction peak, describing the microscopic density fluctuations of water, confirms the relaxation of water structure at a comparable timescale of 1–2 ps. The coincidence of these three

timescales provides a mechanistic description of the bulk viscous response, with the local structure resetting due to rotational/localized motions on the order of 1–2 ps, approximately three times slower than the relaxations associated with shear viscosity. In this way we show that the shear viscous response is most closely associated with changes in water network connectivity, while the bulk viscous response is associated with local density fluctuations.

4.2 Introduction

Water is perhaps the most important and intriguing molecule in the human experience. Important because of its ubiquitous presence in daily life, its role as solvent and reagent in biology and industrial applications, and as a vital environmental resource. Intriguing because of the complex way that structure and hydrogen bonding (HB) combine to produce a rich phase diagram[1, 2] and anomalous physical properties[3-5] (especially near surfaces). We call the properties of water anomalous because models and theoretical frameworks[3, 6-9] which exist to predict local structure, dynamics, macroscopic transport and thermodynamic properties for monoatomic liquids[10-14] and Lennard-Jones fluids[15-18], struggle to predict properties of water accurately. This is due to the local ordering of the molecules and dynamical complexity introduced by electrostatic and HB interactions, including vibrational, rotational, and translational components[19, 20] of molecular motions, along with the kinetics of the HB itself[19].

Viscosity is a property of water describing resistance to flow, and it emerges directly from the propensity of the molecules to move and reorganize the local structure on the molecular scale. On the human scale a relationship can be expressed quantitatively as a pair of coefficients relating stress to the rate of strain in the generalized form of Newton's law of viscosity[21]:

$$\sigma_{ij} = \mu\left(\frac{\partial v_j}{\partial x_i} + \frac{\partial v_i}{\partial x_j}\right) + \left(\frac{2}{3}\mu - \zeta\right)\left(\frac{\partial v_x}{\partial x_x} + \frac{\partial v_y}{\partial x_y} + \frac{\partial v_z}{\partial x_z}\right)\delta_{ij} \tag{4.1}$$

Here, σ_{ij} is the stress tensor, and v_{ij} is the velocity tensor, both which are a function of the Cartesian coordinates x, y, and z. δ_{ij} is the unit tensor. The two coefficients, μ and ζ, are the shear viscosity and bulk viscosity respectively. The bulk viscosity is alternately referred to as the volume viscosity or dilatational viscosity; reflecting the viscous resistance to volume change.

The notion that a characteristic internal (molecular) relaxation time determines the viscosity of a liquid is quite old. Maxwell[22] proposed the concept, recognizing a fundamental molecular relaxation time, τ_M, emerges as the ratio of shear viscosity, μ, to infinite shear modulus, G_∞. This relationship distinguishes the timescales at which the mechanical response of a liquid will be solid-like ($\tau < \tau_M$) or liquid-like ($\tau > \tau_M$). As nicely articulated in a recent review[23] of dynamics in liquids; the molecular scale origin of shear viscosity emerges from the timescale of the shear stress correlations within the liquid. This Maxwell relaxation time, τ_M, can be expressed using the Green-Kubo approach within the fluctuation-dissipation theorem[24, 25], formulated as;

$$\tau_M = \int_0^\infty \frac{\langle \sigma_{xy}(0)\,\sigma_{xy}(t)\rangle}{\langle(\sigma_{xy}(0))^2\rangle}\,dt \tag{4.2}$$

where $\sigma_{xy}(t)$ is the shear stress at time, t. This macroscopic conceptualization over generic volume V, can in turn be connected to the molecular scale via the relation;

$$V\sigma_{xy} = \sum_i \Omega_i \sigma_{xy}(k) \tag{4.3}$$

where V is the macroscopic volume, Ω_i is the molecular volume, and $\sigma_{xy}(k)$ is the shear stress of the kth molecule.

In this way, the molecular shear stress is connected to the local molecular configuration[26], and we can conceive that molecular rearrangements reset local correlations in the shear stress.

Borrowing the approach for the shear viscosity, Hall [27] uses the ratio of ζ to the bulk modulus, K, to yield a relaxation time, τ_B, of the bulk viscous response. This timescale is obtained experimentally here using Brillouin scattering to establish the timescale of fundamental bulk viscosity relaxation time at 1–2 ps. Inelastic neutron scattering measurements show the motions of water and heavy water at the molecular length scale and the nanosecond to picosecond timescale. The individual molecular motions seen via incoherent scattering of H_2O are well-described as a coupled translation/rotation mechanism; the rotational component of which also is observed around 2 ps. Coherent scattering of D_2O reveals an ~2 ps timescale associated with the lifetime of the intermolecular correlations comprising the first sharp diffraction peak. The coincidence of timescales suggests a mechanistic description of coordinated rotational motions allowing structural reorganization as the equilibrium motions responsible for bulk viscosity in liquid water.

4.3 Results and Discussion

Both the local molecular configuration and the lifetime of local molecular correlations[11] are experimentally accessible using scattering methods. Here, neutron scattering measurements are made to obtain the average molecular structure and dynamics of water/heavy water on length scales from approximately 3 Å to 3 nm and timescales from the nanosecond to sub-picosecond time range. A schematic depiction of the local structure of water is shown in Figure 4.1, noting the approximate atomic distances to near neighbor molecules of liquid water[28-32]. This descriptions of the average structure of the fluctuating tetrahedral network in liquid water can
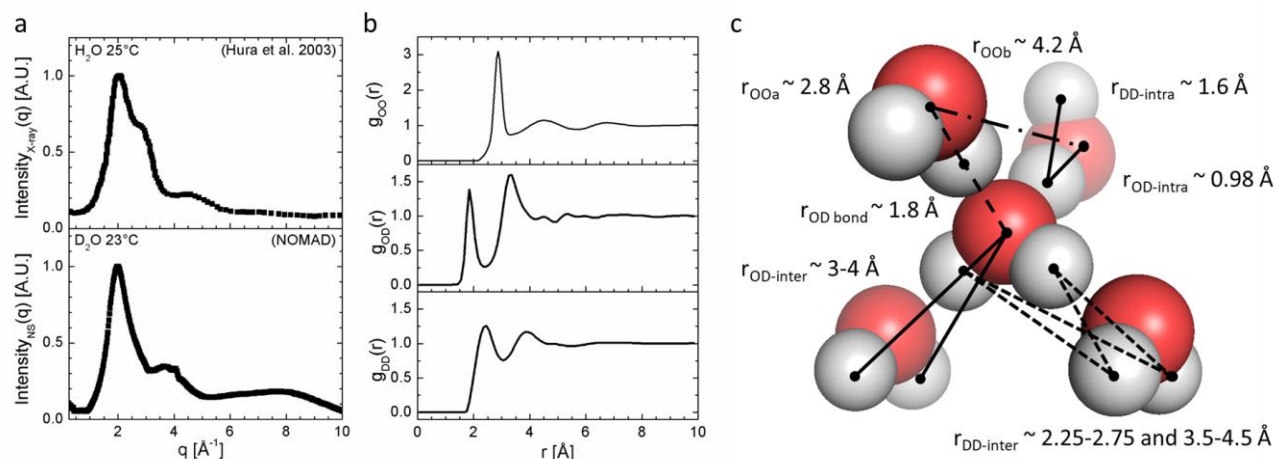
Figure 4.1 Schematic description of the local structure of water.

(a) X-ray (XRD)[29] and neutron (ND) diffraction data from liquid water (X-ray at 25°C, ND at 23°C). (b) Pair distribution functions for atoms pairs in H for liquid water at 25°C from Soper and Williams[31]. (c) Scattering data has contributed to the structural understanding of liquid water, shown here with approximate atomic pair distances annotated[28-32], R_{OOa} denotes O-O spacing within the first neighboring shell, while r_{OOb} denotes the second shell.

be experimentally obtained at the molecular/atomic scale using scattering methods. The early X-ray studies of Bernal[28] provide a surprisingly accurate understanding of the molecular spacing and tetrahedral organization of water molecules within the liquid. This understanding has been significantly refined using neutron diffraction[30-32] which adds detail about hydrogen positions explicitly, as neutrons scatter strongly from both hydrogen (deuterium) and oxygen[33], while X-rays scatter predominately from oxygen. In Figure 4.1, the static structure factor (the experimental quantity we obtain from elastic scattering experiments) of water/D_2O at 300K from both neutron and X-ray scattering is shown (X-ray data from Hura et al.[29]), in addition to pair distribution functions extracted from scattering measurements from the literature[31].

This structural picture is relevant in order to define which atomic/molecular correlations contribute to the coherent inelastic neutron scattering in our experimental window. This is

defined by the scattering wave vector, q, between 0.2 to 2.0 Å^{-1}; and specifically around the q-range of first sharp diffraction peak of D_2O, q<1.3 Å^{-1}. This equates to real space distances less than ~4.5 Å, corresponding to $d < 2\pi/q$, and greater than ~3 Å, as defined by our instrumental constrains of q<2.0 Å^{-1}. Within this range there are relevant pair-distances of all atom pairs; O-O correlations ~2.8 Å, and second shell correlations around 4.2 Å, D-D correlations ~4 Å, and O-D correlations ~3.5 Å. Note, many of the smallest correlations such as the O-D spacing of the hydrogen (deuterium) bond at ~1.8 Å are outside of the range of the q-range of the inelastic measurements presented here. This also illustrates a key difference with respect to X-ray measurements which reflect only the O-O correlations between neighboring molecules; indeed, this is why the shape of the first sharp diffraction peak in Figure 4.1 differs between the two methods.

The molecular scale relaxations of water have been studied extensively by simulation[7, 19, 34] and experimental techniques such as: infrared spectroscopy[35-37], terahertz spectroscopy[38], optical Kerr-effect spectroscopy[39], X-ray scattering[40], and neutron scattering[20]. Each technique has specific advantages and distinct time and length scales associated with the measurement; with inelastic neutron scattering perhaps the most powerful of these methods over the sub nanometer length-scale and nanosecond to sub-picosecond time-scale. Beyond the length-scale resolved spectroscopic description of the molecular motions; the inelastic neutron scattering technique can probe both the self-motion of hydrogen atoms within water, as well as resolving the atomic pair lifetimes associated with the water network; depending upon the isotopic variants of water used[33]. Hydrogen, [1]H (or simply H), has a large incoherent scattering cross-section. This means that we observe predominately incoherent inelastic neutron scattering

from H_2O, reflecting the motions of individual hydrogen atoms and the associated length scale of motion. Whereas [2]H (or D) has a small incoherent cross-section and larger coherent cross-section, meaning that scattering from D_2O primarily reflects the lifetime of spatial correlations between nearby atoms.

The inelastic neutron scattering spectra of H_2O and D_2O were measured at 280 K, 290 K and 300 K. In this case, we obtain a dynamic range of up to three decades in frequency, ~1 GHz to greater than 1,000 GHz, for probe lengths ranging from ~3 Å to 3 nm (q from 0.2 Å^{-1} to 2 Å^{-1}). The stitched inelastic neutron scattering spectra of H_2O and D_2O at 300 K are shown in Figure 4.2 as a function of q and υ. The observed quantity from these experiments is the dynamic structure factor $S(q,E)$, where E is energy transfer, and q is the scattering wave vector. The energy axis is converted to angular frequency, v, and $S(q,E)$ transformed into the susceptibility formalism, $\chi''(q,\upsilon)$, as described in the methods and seen in Figure 4.2. This formalism is advantageous for several reasons, such as the emphasis of the inelastic/quasielastic regions of the spectra and the fact that well-separated dynamical processes appear as distinct maxima.

The scattering spectra of H_2O in this frequency/probe length range is dominated by the incoherent contribution, meaning that these spectra reflect the distribution of times needed for individual ^{1}H atoms to move a defined distance relative to their initial position. A strong q-dependence is observed in the main feature of the scattering; with the peak maxima trending to higher frequency with increasing q (or shorter distances). The inelastic spectra of D_2O differ from that of H_2O based on a simple visual inspection of the scattering data in Figure 4.2, with the strongest spectral feature emerging around 100 GHz only for the larger values of q, closely following that of the static structure factor. This is consistent with the notion that the scattering

observed from D_2O is primarily coherent scattering reflecting the distribution of atom pair lifetimes, with a minor incoherent contribution superimposed that parallels the dynamic of H_2O. This incoherent contribution is also apparent as a weak, q-dependent, feature visible only at low q. A direct comparison of the spectra of H_2O and D_2O at a common q value highlights these differences in Figure 4.2. At low q (q = 0.7 Å^{-1} for instance), there is a clear parallel between the incoherent feature in H_2O and the weak incoherent feature observed in D_2O. Noting the feature for D_2O appears at lower frequency in agreement with the lower self-diffusion coefficients of D_2O[41].

A quantitative description of the molecular motions has been obtained from modeling these spectra. Beginning with H_2O, a description can be obtained using three distinct contributions[20]; a Debye function to represent the translational motions (analogous to a Lorentzian distribution in the intensity formalism), another Debye function to represent the rotational motions, and a damped harmonic oscillator (DHO) to account for the intermolecular collective modes of H-bond bending motions at ~1500 GHz[42-44]. The DHO is given by the relation:

$$\chi_{DHO}{}'' = \mathcal{I}m\{\Delta_{DHO}\omega_0^2[\omega^2 - \omega_0^2 - i\omega\Gamma]^{-1}\} \tag{4.4}$$

where ω_0 is the position, Γ is the width, and Δ_{DHO} is the amplitude.
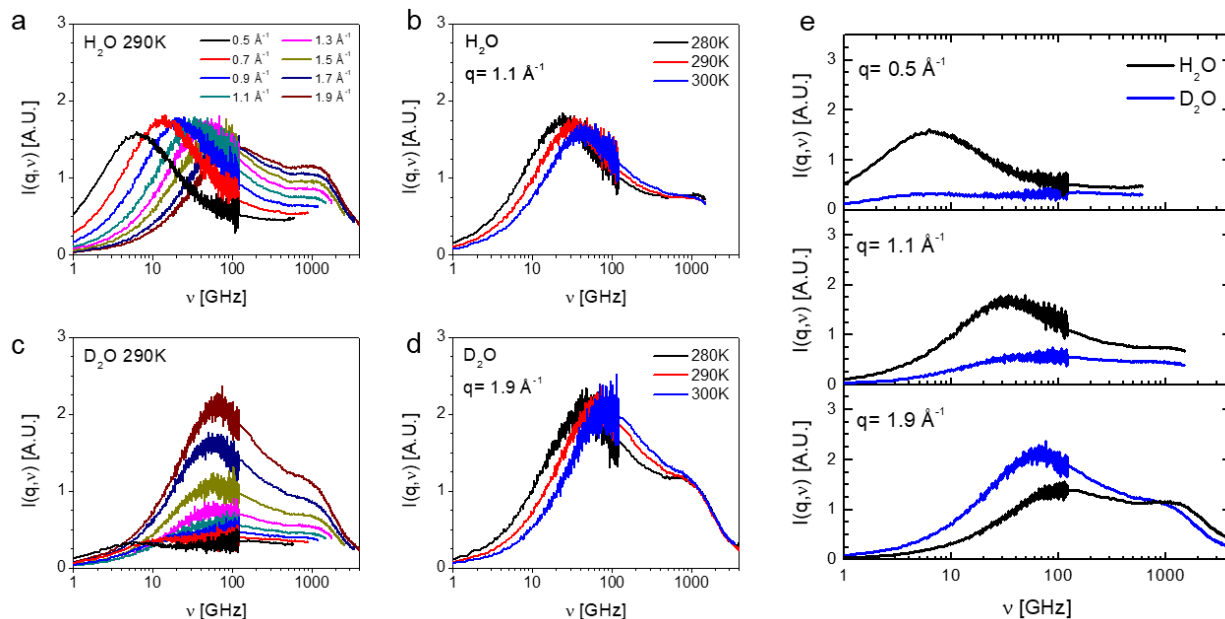
Figure 4.2 Inelastic neutron scattering spectra of H_2O and D_2O at 290 K.

Spectra of **(a)** H_2O and **(c)** D_2O for a range of q-values. **(a)** Illustrates the strong q-dependence of the incoherent scattering feature; while **(d)** demonstrates the q-independence of the coherent scattering feature with a maximum intensity at the length scale of the first sharp diffraction peak. **(b)** and **(d)** show the temperature dependence of the scattering, with the peak positions shifting to higher frequency with increasing temperature. **(e)** directly compares H_2O and D_2O spectra at various q-values.

The results of this data treatment, shown in Figure 4.3 , produce a close agreement with literature[20]; with the translational relaxation times, τ_T,, decreasing with a near q^2 dependence in agreement with a jump diffusion motions and the rotational relaxation times, τ_R, not changing greatly with q. The relative amplitudes of these two contributions are inversely related, with the translational contribution dominant at longer length scales (low-q) and the rotational contribution dominating at shorter length scales (high-q). The observed rotational relaxation time at q=1.9 $Å^{-1}$ was found to vary from 1-2 ps over the range of 280K-303K; while the translational motions occurring on this length scale were somewhat slower and varied from ~2-5 ps in temperature, both in good agreement with prior work[20].
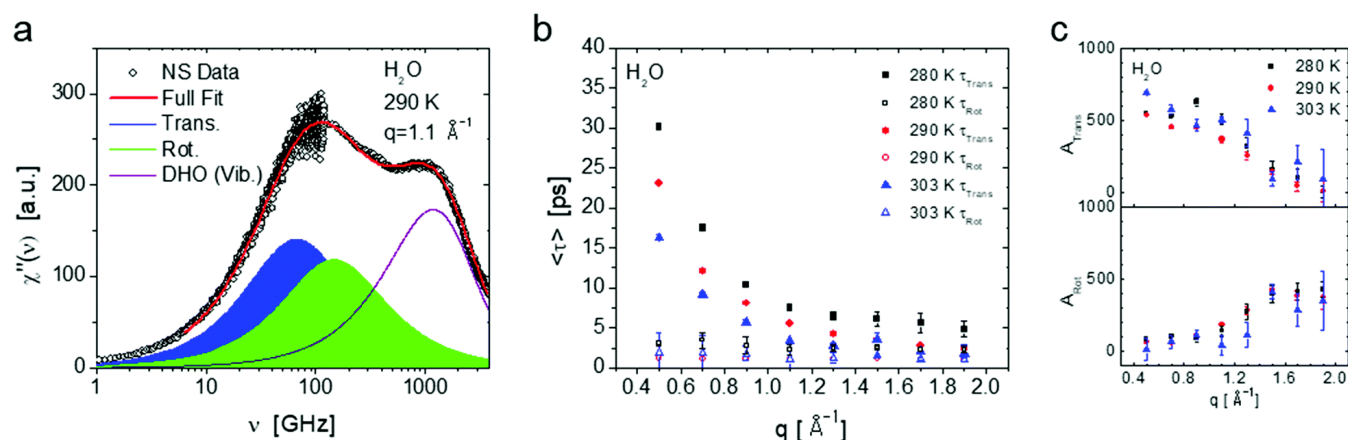
Figure 4.3 Fitting of the predominantly inelastic neutron scattering spectra from H_2O. (a) A two-Debye model was used with the inclusion of a damped harmonic oscillator to account for the vibrational modes at high frequency. This treatment is a frequency domain analog to that performed by Teixeira and co-workers[45] and yielded comparable results. (b) Relaxation times for the two Debye functions corresponding to translational τ_T and rotational τ_R motions. (c) The relative amplitudes of the two Debye functions. Note the translational contribution dominates the amplitude of the scattering at low-q and the rotational component is larger at high q.

The preceding data treatment decomposes water dynamics into pure translational and rotational motions for the purpose of simplifying the nature of the motions. Moreover, this treatment seems to imply a decoupling which is not the complete picture of water motions[34]. Translation and rotation are actually coupled over the length scales probed in this experiment, weakly at low q (≤1 Å^{-1}) and strongly at high q (>1Å^{-1})[46]. The extended jump model for water reorientation proposed by Laage and Hynes[34] suggests a picture of this coupled local reorientation occurring on the order of 4 ps, via a concerted mechanism with a water molecule breaking its hydrogen bond with an over-coordinated first shell neighbor, and forming a new hydrogen bond with an uncoordinated water molecule in the second shell; undergoing a rapid ~60° angular rotation and

changing the distance between the initial oxygen-oxygen pair from ~2.8 Å in the first shell to ~4.2 Å in the second shell.

Indeed, it is sometimes convenient in this experimental window to treat H_2O inelastic spectra using a single Cole-Davidson (CD) function, $\chi_{CD}'' = -\mathcal{I}m\{\Delta_{CD}[1 + i\omega\tau_{CD}]^{-\beta}\}$, to represent the coupled translational and rotational dynamics in this range. The relevant terms in this fitting include a stretching exponent β (0.7 used), Δ_{CD} being the amplitude and τ_{CD} being the relaxation time. The consistency of this approach is illustrated in Perticaroli et al.[47], with τ_{CD} transitioning smoothly between the time reported in the decoupled model, and the amplitude of the coupled feature closely resembling the sum of the decoupled components. The approach is especially useful to simplify the treatment of two separate water populations (bulk and interfacial) when it is practical to replicate the incoherent contribution of water dynamics via a single functional form; such as bulk and hydration in analyses of water in the presence of solutes or surfaces[47-49]. Another useful approach to the fitting of the water spectra is the relaxing cage model [50-52] which has proven valuable to some investigators seeking to understand structural dynamics of water from the perspective of mode coupling theory or within a continuous random walk model[50]. This approach is used in the treatment and separation of the bulk and hydration water in Polyethylene glycol hydrogels in the next chapter.

To quantify the timescale of the observed scattering for D_2O – physically the superposition of atom pair lifetimes at the length scale of the scattering wave vector – a fitting procedure was used where the coherent scattering is represented as an additional Debye function, with the vibrational motions at high frequency again represented with a DHO, and the incoherent contribution represented by two Debye functions as seen in the case of H_2O. The two incoherent

contributions are clearly minor contributions at high q and can be constrained in the fitting process by fixing the respective time constants based on the observations from H_2O and the observed diffusion constants in literature[53]; as well as fixing the amplitude of the incoherent contributions at high q based upon observed amplitude of the incoherent translational feature at low q in D_2O where the incoherent feature is apparent and can be scaled to that observed for H_2O.

The amplitude of the observed coherent feature emerges in line with the first sharp diffraction peak at q > 1.3 $Å^{-1}$, corresponding to real space atomic correlations of 2.5 to 4.2 Å. There is a clear amplitude agreement with the static structure factor, confirming the coherent nature of the observed feature. The observed time scale at which these correlations are broken varied between ~1 and ~2 ps over the 280 K to 303 K temperature range, very much in line with what could be expected by obtaining the peak maximum. The observed timeframe agrees with the slower mode reported by Iwashita et al.[40] using inelastic X-ray scattering on H_2O and was assigned to the local molecular rearrangements between the second shell oxygen atoms. Here, the large coherent scattering length of both deuterium and oxygen mean that the correlations observed in this study include D–D and O–D, in addition to O–O. Despite of well-known differences in the structure and hydrogen/deuterium bond between H_2O and D_2O [54], the observation of a coincidence in approximate timescales for the molecular rotation of water, and the disruption of local structure seen in the first sharp diffraction peak of D_2O clearly identifies the 1–2 ps timeframe as relevant to the structural relaxation controlling bulk viscosity.
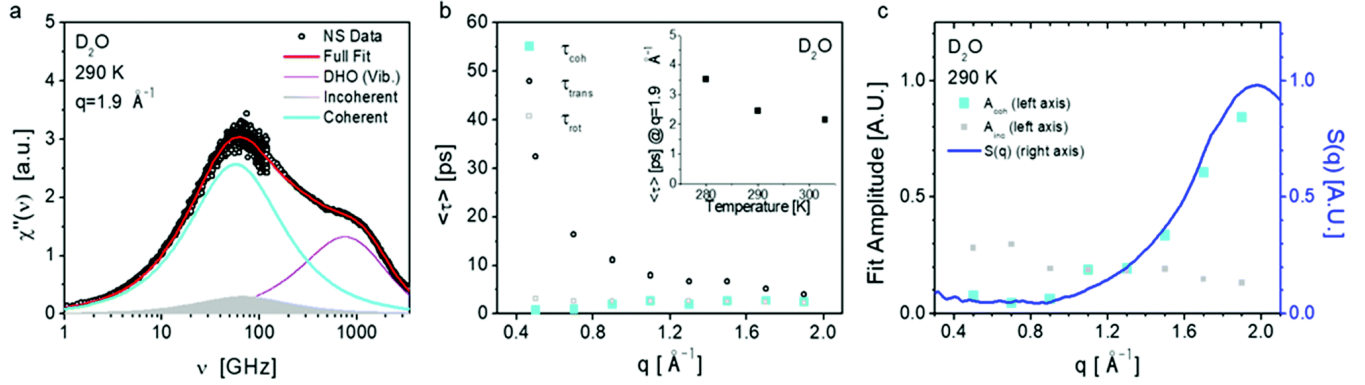
Figure 4.4 Fitting of the inelastic neutron scattering spectra from D_2O.

(a) The fit is comprised of two Debye functions representing the incoherent scattering (shown together in grey), an additional Debye function representing coherent inelastic scattering, and a DHO representing the vibrational component. (b) The average relaxation time from the coherent contribution was observed at ~2 ps. (c) The amplitude of the coherent component (cyan square) clearly follows the static structure factor of D_2O, supporting the notion that this feature is coherent in origin – reflecting the average lifetime of correlations making up this structural feature; namely, O–O, D–O, and D–D correlations noted in Figure 4.1.

Both the bulk viscosity, ζ, and the bulk modulus, K, can be obtained experimentally from Brillouin scattering[55]. Brillouin scattering is an inelastic light scattering technique which can be used to probe sound waves propagating in a medium. The observed spectra, Figure 4.5(a-d), were collected as observed intensity, $I_B(v)$, as a function of frequency, v. The longitudinal mode apparent in the observed spectra can be modelled using a damped harmonic oscillator model, (DHO)[55, 56]:

$$I_B(v) = A\frac{\Gamma_L\Omega_L}{(v^2+\Omega^2)^2+(\Gamma_L v)^2} + y_0 \qquad (4.5)$$

where Ω_L is the oscillator frequency and Γ_L is the full width at half-maximum of the spectral feature. A and y_0 are the amplitude and background. The spectra are collected on both the Stokes and anti-Stokes regions but have been fitted only on the Stokes side. The fit parameters, Ω_L and Γ_L are used to obtain the longitudinal sound velocity, c_L, the bulk viscosity, ζ, and the bulk modulus, K. In the backscattering geometry, the sound velocity can be calculated as:

$$c_L = \frac{\Omega_L \lambda}{2n},$$

(4.6)

where λ is the incident wavelength and n is the refractive index. The bulk modulus, K, can be calculated using the calculated c_L, the constant volume and constant pressure heat capacities, C_V and C_P, and the density, ρ, using:

$$K = c_L{}^2 \rho \frac{C_V}{C_P},$$

(4.7)

The bulk viscosity is obtained from the damping of the longitudinal mode observed here as the linewidth. For the case of H_2O and D_2O in the temperature range considered here, the ratio of constant volume to constant pressure specific heat is close to unity, so contributions from thermal conductivity can be neglected, resulting in the simplified relation:

$$\zeta = \frac{\rho c_L{}^2 \Gamma_L}{4\pi^2 \Omega_b{}^2} - \frac{4}{3}\mu,$$

(4.8)

The relevant time scale for the molecular motions governing the bulk viscosity of water can now be estimated using the relation $\zeta/K = \tau_B$. All calculated parameters have been summarized in
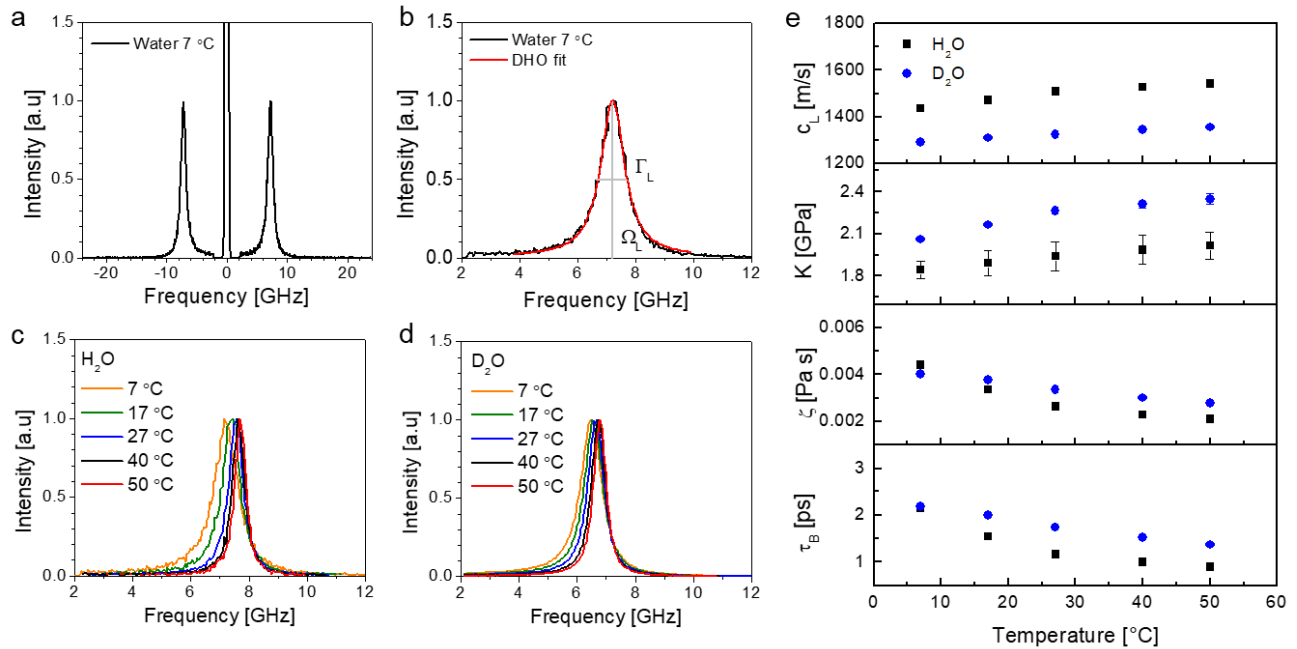
Figure 4.5 Brillouin scattering measurements can be used to measure the longitudinal sound velocity, c_L, bulk modulus, K, bulk viscosity, ζ, and associated relaxation time, τ_B.

(a) Representative spectrum from H_2O showing the symmetric Stokes and anti-Stokes features. (b) The spectra can be described as a damped harmonic oscillator (DHO), extracting the oscillator frequency and the full-width at the half-maximum of the feature. (c) and (d) show the temperature dependences of the spectra for both H_2O and D_2O. (e) Computed properties obtained as a function of temperature, identifying the relevant timescale of molecular relaxation for bulk viscosity.

Figure 4.5 as a function of temperature. The sound velocity is seen to increase with temperature, and as expected for both H_2O and D_2O; the bulk modulus goes through a maximum above the temperature range considered here. The resulting time scales of molecular relaxation are found on the order of ~1 to 2 ps, significantly slower than the motions governing the shear behavior of water as seen recently by Iwashita et al.[40] That study investigated the timeframe of local molecular rearrangements in water using a real-space analysis to extract the van Hove [57] function from inelastic X-ray scattering experiments. This allowed the authors to follow the time and space correlations of the oxygen atoms, showing the loss of correlation between oxygen

atoms of neighboring molecules. The observations seem to identify a distinct decay time for the correlations of the neighboring oxygen atoms; providing a dynamical time scale comparable to the predicted Maxwell relaxation time from shear viscosity for liquid water below the viscosity crossover temperature ~60 °C, [23] in potential agreement with ultrafast spectroscopy [37]

The dynamic hydrogen bond network in water constantly changes connectivity in a complex dance of this attractive interaction and rapid molecular motions. The breaking of a single hydrogen bond is associated with local reorientations of water molecules on the sub-picosecond timescale [19], which appear to provide sufficient molecular flexibility to relieve the molecular scale shear stress within the network. Moreover, the rapid motions associated with shear viscosity are consistent with the translational jump timescale predicted from a jump diffusional model [40, 45, 58]. This makes a logical and expected connection of translational diffusion and shear viscosity.

Alternately referred to as the volume viscosity or dilatational viscosity; the bulk viscosity describes the viscous resistance to volume change. It is reasonable then to consider that the timescale of microscopic density fluctuations within the material will be relevant. Indeed, coherent neutron scattering observations of D_2O at the length scale of the first sharp diffraction peak reflect a weighted average lifetime of the correlations contributing to the structural peak, providing an experimental description of the lifetime of microscopic density fluctuations at 1–2 ps, coinciding closely with the bulk modulus relaxation time.

The further coincidence of rotational dynamics of water identifies a timescale of molecular motions as well. As we have emphasized earlier, the assumption of pure rotational dynamics

made in this analysis is based on a common[59] and classical approach[45] of analytical simplicity

and does not reflect recent development such as the extended jump model for water

reorientation proposed by Laage and Hynes[34]. As noted above, a more generic localized motion

within a cage, or local energy basin, is a common alternate interpretation of the observed proton

motions in incoherent inelastic neutron scattering. This concept is extensively developed by

Qvist, Schober and Halle[50] and leads into a number of recent analyses of water properties[52].

The reader should be clear that many more models of water dynamics are proposed than are

discussed here, however. Regardless of any existing debate about the exact nature of these

motions, it is clear that protons in water are moving in a highly localized (<1 Å) fashion on the

timescale of 1–2 ps, and that these motions coincide with the bulk viscous response.

4.4 Conclusion

As can be seen in Figure 4.6 , the timescale observed for bulk viscosity, on the order of 1–2 ps,

compares favorably to the structural reorganization occurring on the order of 1–2 ps in D_2O at

temperatures ranging from 280 K to 303 K. The approach of Hall [27] to the calculation of a

Maxwell time for bulk viscosity predicts a timescale for molecular rotations or localized motions

to act as density fluctuations which permit a reset of the local volume to conform to the local

pressure. This is in parallel to shear viscosity, where the molecular configurations reset the local

stress tensor. The first sharp diffraction peak reflects a collection of atomic correlations resulting

from the local molecular spacing, and it is logical that the lifetime of the correlations is intimately

connected to the bulk viscous response. The rotation of the water molecule can be understood

to disrupt many of the atomic correlations within liquid water. Specifically, considering those just
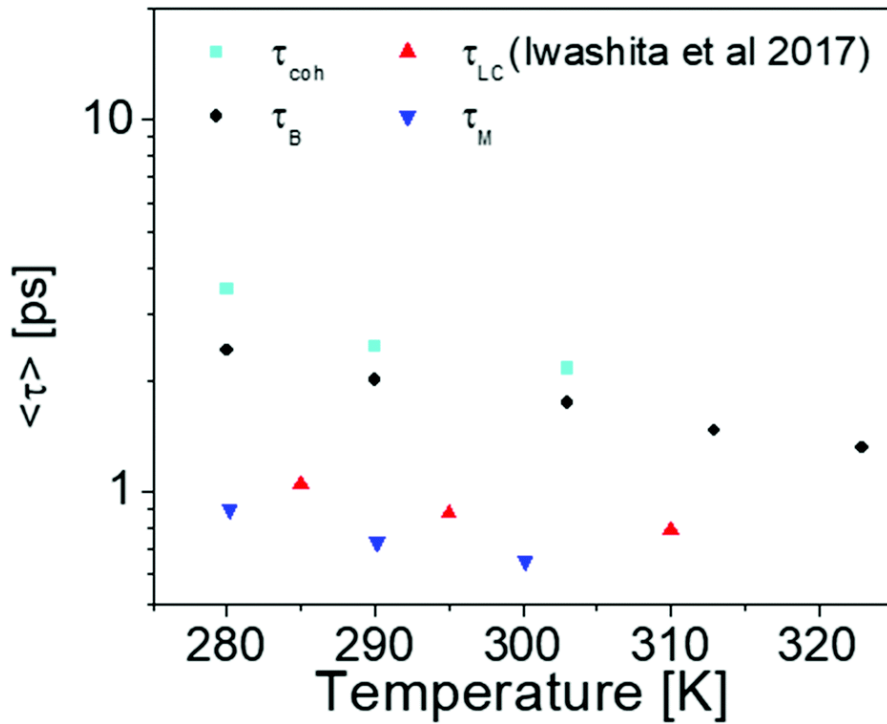
Figure 4.6 Comparison of rheological timescales for bulk and shear viscosity.

Here, τ_{coh} and τ_B are reported for D_2O while τ_M and τ_{LC} are reported from Iwashita et al.[40] for H_2O. This figure illustrates that rapid fluctuations on the sub-picosecond timescale are sufficient to relieve local shear stress, whilst slower motions related to water rotation control reset structure on the order of the first sharp diffraction peak and limit the viscous response to local volume changes.

noted as comprising the first sharp diffraction peak for neutrons. O–H, O–O, and H–H atom pairs in Figure 4.1. All would all disrupted by a 60 degree rotation of the water molecule, consistent with the mechanism of rotation and coincident with the timescale identified as resetting of the local volume. The implications of this work are twofold. Firstly, I have illustrated the fundamental molecular timescale of bulk viscosity in liquid water and correlating it to a specific molecular spacing and relaxation using light and neutron scattering methods. The results illustrate a connection between rotational motions on the length scale of the first sharp diffraction peak for neutrons; and the viscous response to rapid volume changes. Secondly, I show that the motions

associated with the bulk viscous response occur two to three times slower than those associated with the shear viscous response; with the connectivity of the fluctuating hydrogen bond network varying faster than the local density fluctuations.

4.5 Methods

Neutron diffraction measurements were conducted at the Nanoscale Ordered Materials Diffractometer (NOMAD)[60] at the Spallation Neutron Source, Oak Ridge National Laboratory. D2O was measured in a 2.5 mm quartz capillary tube 30°C. Diffraction spectra were obtained in the q range from 0.2 to 50 $Å^{-1}$. Data were normalized against a solid V rod, and the capillary background was subtracted. Data from all detector banks were combined to improve the counting statistics in the low q region.

The inelastic neutron scattering spectra of H_2O and D_2O were measured at 280 K, 290 K and 300 K, using two spectrometers, BASIS[61] and CNCS[62] at the Spallation Neutron Source, Oak Ridge National Laboratory, Tennessee, USA. The energy axis is converted to angular frequency, *v*. These spectrometers were utilized in a configuration which results in an overlapping *q-v* range, allowing the datasets to be combined. The observed spectra were first processed into slices along the energy axis, binning the data at defined q-values common to both instruments, and then transformed into the susceptibility formalism, *χ''(q,v)*, as seen in Figure 4.2, according to the relation:

$$\chi''(q,v) \propto S(q,v)/n_B(v) \tag{4.9}$$

where *S(q,v)* is the measured dynamic structure factor and:

$$n_B(\nu) = [\exp(h\nu/kT) - 1]^{-1} \qquad (4.10)$$

is the Bose occupation number[63]. This formalism is advantageous for several reasons, such as the emphasis of the inelastic/quasielastic regions of the spectra and the fact that well-separated dynamical processes appear as distinct maxima. The later point facilitates the stitching of neutron data from different spectrometers at common q-values to achieve a larger dynamic range than possible from a single spectrometer. In this case, we obtain a dynamic range of up to three decades in frequency, ~1 GHz to greater than 1,000 GHz, for probe lengths ranging from ~3 Å to 3 nm (q from 0.2 Å^{-1} to 2 Å^{-1}).

Brillouin scattering measurements were performed in a polarized, backscattering configuration using a Sandercock tandem Fabry-Perot interferometer with a 532 nm single-mode solid state laser. A 6mm mirror separation was used, giving a free spectral range of 24 GHz. 300 μL samples of H_2O and D_2O were sealed and placed in a Linkam temperature control cell. The samples were allowed to equilibrate for a minimum of 30 minutes at each temperature prior to measurement. Spectra were collected over approximately 60 minutes.

4.6 Acknowledgments

References

1. Poole, P.H., et al., *Phase behaviour of metastable water.* Nature, 1992. **360**(6402): p. 324-328.
2. Bridgman, P., *The Pressure-Volume-Temperature Relations of the Liquid, and the Phase Diagram of Heavy Water.* The Journal of Chemical Physics, 1935. **3**(10): p. 597-605.
3. Mahoney, M.W. and W.L. Jorgensen, *A five-site model for liquid water and the reproduction of the density anomaly by rigid, nonpolarizable potential functions.* The Journal of Chemical Physics, 2000. **112**(20): p. 8910-8922.
4. Kell, G.S., *Density, thermal expansivity, and compressibility of liquid water from 0. deg. to 150. deg.. Correlations and tables for atmospheric pressure and saturation reviewed and expressed on 1968 temperature scale.* Journal of Chemical and Engineering Data, 1975. **20**(1): p. 97-105.
5. Errington, J.R. and P.G. Debenedetti, *Relationship between structural order and the anomalies of liquid water.* Nature, 2001. **409**(6818): p. 318-321.
6. Sanz, E., et al., *Phase diagram of water from computer simulation.* Physical review letters, 2004. **92**(25): p. 255701.
7. Stillinger, F.H. and A. Rahman, *Improved simulation of liquid water by molecular dynamics.* The Journal of Chemical Physics, 1974. **60**(4): p. 1545-1557.
8. Hirai, N. and H. Eyring, *Bulk Viscosity of Liquids.* Journal of Applied Physics, 1958. **29**(5): p. 810-816.
9. Jaeger, F., O.K. Matar, and E.A. Müller, *Bulk viscosity of molecular fluids.* The Journal of Chemical Physics, 2018. **148**(17): p. 174504.
10. Copley, J., SW Lovesey, *The Dynamic Properties of Monoatomic Liquids.* Rep. Prog. Phys., 1975. **38**: p. 461.
11. De Gennes, P.G., *Liquid dynamics and inelastic scattering of neutrons.* Physica, 1959. **25**(7-12): p. 825-839.
12. Thiele, E., *Equation of state for hard spheres.* The Journal of Chemical Physics, 1963. **39**(2): p. 474-479.
13. Wertheim, M., *Exact solution of the Percus-Yevick integral equation for hard spheres.* Physical Review Letters, 1963. **10**(8): p. 321.
14. Irving, J. and J.G. Kirkwood, *The statistical mechanical theory of transport processes. IV. The equations of hydrodynamics.* The Journal of chemical physics, 1950. **18**(6): p. 817-829.
15. Verlet, L., *Computer" experiments" on classical fluids. I. Thermodynamical properties of Lennard-Jones molecules.* Physical review, 1967. **159**(1): p. 98.
16. Nicolas, J., et al., *Equation of state for the Lennard-Jones fluid.* Molecular Physics, 1979. **37**(5): p. 1429-1454.
17. Ashurst, W.-T. and W. Hoover, *Dense-fluid shear viscosity via nonequilibrium molecular dynamics.* Physical Review A, 1975. **11**(2): p. 658.
18. Gray, P. and S.A. Rice, *On the Kinetic Theory of Dense Fluids. XVIII. The Bulk Viscosity.* The Journal of Chemical Physics, 1964. **41**(12): p. 3689-3694.
19. Luzar, A. and D. Chandler, *Hydrogen-bond kinetics in liquid water.* Nature, 1996. **379**(6560): p. 55-57.
20. Teixeira, J., et al., *Experimental determination of the nature of diffusive motions of water molecules at low temperatures.* Physical Review A, 1985. **31**(3): p. 1913-1917.
21. Stokes, G.G., *On the theories of the internal friction of fluids in motion, and of the equilibrium and motion of elastic solids.* Transactions of the Cambridge Philosophical Society, 1880. **8**.
22. Maxwell, J.C., *IV. On the dynamical theory of gases.* Philosophical transactions of the Royal Society of London, 1867. **157**: p. 49-88.

23. Egami, T., *Real-Space Description of Dynamics of Liquids.* Quantum Beam Science, 2018. **2**(4): p. 22.
24. Gary, P.M. and J.E. Denis, *Statistical Mechanics of Nonequilbrium Liquids*. 2007, Canberra: ANU Press.
25. Hansen, J.-P. and I.R. McDonald, *Theory of simple liquids*. 1990: Elsevier.
26. Egami, T. and D. Srolovitz, *Local structural fluctuations in amorphous and liquid metals: a simple theory of the glass transition.* Journal of Physics F: Metal Physics, 1982. **12**(10): p. 2141.
27. Hall, L., *The origin of ultrasonic absorption in water.* Physical Review, 1948. **73**(7): p. 775.
28. Bernal, J.D. and R.H. Fowler, *A theory of water and ionic solution, with particular reference to hydrogen and hydroxyl ions.* The Journal of Chemical Physics, 1933. **1**(8): p. 515-548.
29. Hura, G., et al., *Water structure as a function of temperature from X-ray scattering experiments and ab initio molecular dynamics.* Physical Chemistry Chemical Physics, 2003. **5**(10): p. 1981-1991.
30. Soper, A., *The radial distribution functions of water and ice from 220 to 673 K and at pressures up to 400 MPa.* Chemical Physics, 2000. **258**(2-3): p. 121-137.
31. Soper, A. and M. Phillips, *A new determination of the structure of water at 25 C.* Chemical Physics, 1986. **107**(1): p. 47-60.
32. Zeidler, A., et al., *Isotope effects in water as investigated by neutron diffraction and path integral molecular dynamics.* Journal of Physics: Condensed Matter, 2012. **24**(28): p. 284126.
33. Sears, V.F., *Neutron scattering lengths and cross sections.* Neutron news, 1992. **3**(3): p. 26-37.
34. Laage, D. and J.T. Hynes, *A molecular jump mechanism of water reorientation.* Science, 2006. **311**(5762): p. 832-835.
35. Woutersen, A., U. Emmerichs, and H. Bakker, *Femtosecond mid-IR pump-probe spectroscopy of liquid water: Evidence for a two-component structure.* Science, 1997. **278**(5338): p. 658-660.
36. Asbury, J.B., et al., *Water dynamics: Vibrational echo correlation spectroscopy and comparison to molecular dynamics simulations.* The Journal of Physical Chemistry A, 2004. **108**(7): p. 1107-1119.
37. Fecko, C., et al., *Ultrafast hydrogen-bond dynamics in the infrared spectroscopy of water.* Science, 2003. **301**(5640): p. 1698-1702.
38. Rønne, C., P.-O. Åstrand, and S.R. Keiding, *THz spectroscopy of liquid H 2 O and D 2 O.* Physical review letters, 1999. **82**(14): p. 2888.
39. Winkler, K., et al., *Ultrafast Raman-induced Kerr-effect of water: Single molecule versus collective motions.* The Journal of Chemical Physics, 2000. **113**(11): p. 4674-4682.
40. Iwashita, T., et al., *Seeing real-space dynamics of liquid water through inelastic x-ray scattering.* Science advances, 2017. **3**(12): p. e1603079.
41. Mills, R., *Molecular diffusion.* J Phys Chem, 1973. **77**: p. 685-688.
42. Perticaroli, S., et al., *Broadband depolarized light scattering study of diluted protein aqueous solutions.* The Journal of Physical Chemistry B, 2010. **114**(24): p. 8262-8269.
43. Perticaroli, S., et al., *Extended frequency range depolarized light scattering study of N-acetyl-leucine-methylamide–water solutions.* Journal of the American Chemical Society, 2011. **133**(31): p. 12063-12068.
44. Settles, M. and W. Doster, *Anomalous diffusion of adsorbed water: a neutron scattering study of hydrated myoglobin.* Faraday Discussions, 1996. **103**: p. 269-279.
45. Teixeira, J., et al., *Experimental determination of the nature of diffusive motions of water molecules at low temperatures.* Physical Review A, 1985. **31**(3): p. 1913.
46. Di Cola, D., et al., *Proton dynamics in supercooled water by molecular dynamics simulations and quasielastic neutron scattering.* The Journal of chemical physics, 1996. **104**(11): p. 4223-4232.

47. Perticaroli, S., et al., *Description of hydration water in protein (green fluorescent protein) solution.* Journal of the American Chemical Society, 2017. **139**(3): p. 1098-1105.

48. Tian, J., et al., *The Behavior of Bilayer Leaflets in Asymmetric Model Membranes: Atomistic Simulation Studies.* The Journal of Physical Chemistry B, 2016.

49. Nickels, J.D., et al., *Dynamics of protein and its hydration water: neutron scattering studies on fully deuterated GFP.* Biophysical journal, 2012. **103**(7): p. 1566-1575.

50. Qvist, J., H. Schober, and B. Halle, *Structural dynamics of supercooled water from quasielastic neutron scattering and molecular simulations.* The Journal of chemical physics, 2011. **134**(14): p. 144508.

51. Chen, S.-H., et al., *Observation of fragile-to-strong dynamic crossover in protein hydration water.* Proceedings of the National Academy of Sciences, 2006. **103**(24): p. 9012-9016.

52. Arbe, A., et al., *Dielectric susceptibility of liquid water: Microscopic insights from coherent and incoherent neutron scattering.* Physical review letters, 2016. **117**(18): p. 185501.

53. Mills, R., *Self-diffusion in normal and heavy water in the range 1-45. deg.* The Journal of Physical Chemistry, 1973. **77**(5): p. 685-688.

54. Soper, A. and C. Benmore, *Quantum differences between heavy and light water.* Physical review letters, 2008. **101**(6): p. 065502.

55. Berne, B.J. and R. Pecora, *Dynamic light scattering: with applications to chemistry, biology, and physics*. 2000: Courier Corporation.

56. Bottani, C.E. and D. Fioretto, *Brillouin scattering of phonons in complex materials.* Advances in Physics: X, 2018. **3**(1): p. 1467281.

57. Van Hove, L., *Correlations in space and time and Born approximation scattering in systems of interacting particles.* Physical Review, 1954. **95**(1): p. 249.

58. Teixeira, J., A. Luzar, and S. Longeville, *Dynamics of hydrogen bonds: how to probe their role in the unusual properties of liquid water.* Journal of Physics: Condensed Matter, 2006. **18**(36): p. S2353.

59. Amann-Winkel, K., et al., *X-ray and neutron scattering of water.* Chemical reviews, 2016. **116**(13): p. 7570-7589.

60. Neuefeind, J., et al., *The nanoscale ordered materials diffractometer NOMAD at the spallation neutron source SNS.* Nuclear Instruments and Methods in Physics Research Section B: Beam Interactions with Materials and Atoms, 2012. **287**: p. 68-75.

61. Mamontov, E. and K.W. Herwig, *A time-of-flight backscattering spectrometer at the Spallation Neutron Source, BASIS.* Review of Scientific Instruments, 2011. **82**(8): p. 085109.

62. Ehlers, G., et al., *The new cold neutron chopper spectrometer at the Spallation Neutron Source: design and performance.* Review of Scientific Instruments, 2011. **82**(8): p. 085108.

63. Bee, M., *Quasielastic neutron scattering: principles and applications in solid state chemistry.* Biology and Materials Science, Adam Hilger, Bristol, 1988: p. 193.

Chapter 5 : Origin of Apparent Viscosity Effects and Nonergodicity in PEG Hydrogels

5.1 Abstract

Polyethylene glycol (PEG) hydrogels are a flexible class of materials with diverse applications across the chemical, biomedical and consumer products communities. PEG hydrogels are able meet the demands of these many applications by tuning material properties through basic parameters such as volume fraction, cross-linking density, polymerization conditions or choice of molecular weight; along with more complex strategies such as co-polymerization and compositing. Of the many varieties of PEG hydrogel, those formed from multi-arm PEG prepolymers are especially useful for detailed study, due to their homogeneous structures and defined molecular weight between cross-links. In this work, we have investigated the structure and molecular motions of a series of 4-arm/8-arm PEG hydrogels as a function of volume fraction. Using neutron scattering methods, supported with molecular dynamics simulation and swelling studies, we describe the non-ergodicity of the hydrogel network and its hydrodynamic environment. Small angle neutron scattering shows changes in the average network structure and local polymer conformation as a function of polymer volume fraction, while neutron spin echo measurements show uniform polymer motions as a function of volume fraction matching the predictions of the Zimm model. Incoherent inelastic neutron scattering was then used to measure the dynamical changes in water within the hydrogel. A population of dynamically perturbed water was identified, amounting to 8 to 9 water molecules per PEG monomer. This water population was found to have sub-diffusive dynamics with a decreased self-diffusion coefficient of around two times relative to neat water. This follows closely the increase in specific

viscosity extracted from observations of the polymer chain motions, which was also approximately two times that of neat water. This indicates a close coupling of the sub-diffusive water dynamics and picosecond to hundreds of nanoseconds Zimm dynamics of the polymer chain at all measured volume fractions, while the observed polymer chain conformations show differences in persistence length as a function of volume fraction. The implication of this non-ergodicity is that approximations of chain flexibility from polymer confirmation may not be appropriate in hydrogel materials where the polymer chain itself is not under tension.

5.2 Introduction

The mechanical properties of hydrogels depend largely on their water content which is the main component of the system. Water molecules which are interacting with the solute will experience a thermodynamic effect by the solute [1], which can range from complete immobilization of water molecules on the solute to perturbation of the translational and/or the rotational motions of water by the solute. Therefore, hydrogels will contain two types of water bound or hydration water and a free or bulk neat water. The water activity which can be thought as the amount of water available for hydration which will decrease with increasing concentration and therefore water activity too[2]. This is another way of looking at the two populations but this time in terms of different water activity with a reduced one in the hydration population or in terms of osmotic pressure with a lower one in the bulk population[3].

In this project I am using neutron scattering techniques to study the dynamics of water molecules in Polyethylene Glycol (PEG) hydrogels and observe the effect of polymer concentration on the dynamics of water and the corresponding local viscosity changes due to such perturbation. The chemistry and biological applications of PEG hydrogels have been the subject of increase interest

in both academics and industry. One of the most focused applications is the use of PEG hydrogels

in cell encapsulation, drug delivery and wound covering [4] [5] [6] [7]. Due to the availability of

PEG in different multifunctional derivatives it is used to form cross-linked PEG hydrogels [8]. The

suitability and performance of such hydrogels depend on their bulk structure [9]. This chemically

cross linked polymer chains swell in a certain specific way and conclude its final bulk structure

[10]. This swelling process is defined by the polymer-water interaction which is the heart theory

in explaining the physical properties of hydrogels [11]. Competing interactions which resist, or

favor swelling will be the decider of the final swelling amount of the hydrogel. The swelling driving

force is the gain in entropy by mixing the polymer and the solvent while the swelling resistant is

the loss of entropy in network chains as they are stretched. This is very well presented by Flory-

Huggins model for mixing and the rubber elasticity theory for the entropic stretching component

[12, 13]. The total free energy of the gel is determined by the amount of water entering the gel

and is minimized by the competing entropic changed mentioned above and equilibrium is

achieved when the chemical potential is same as outside the gel.

For the purpose of describing the perturbation of water in the system, two parameters are

typically used; the extent of the perturbation is defined by the hydration number N_H in terms of

the water molecules in the hydration population or surrounding the polymer chains and have

perturbed dynamics. While the retardation factor R_H quantifies the magnitude of perturbation

as the ration of the characteristic relaxation times of the hydration water (τ_H) relative to the bulk

(τ) [14].

Neutron Scattering (NS) spectroscopy is an powerful two-dimensional technique used here to

resolve the atomic correlations and motions in both time and space domains. with suitable

accessible length scales from Angstroms to nanometers; with broad dynamics ranges from hundreds of nanoseconds to femtoseconds that can be accessed by accessing different energy windows from different instruments and combing them. Moreover, The isotopic sensitivity of neutrons to hydrogen is a powerful tool [15]– with hydrogen (^{1}H) possessing a high incoherent scattering cross section and small negative coherent scattering length; compared to deuterium (^{2}H) which has a small incoherent cross section and a large positive coherent scattering length. The way that these scattering properties manifest into scattering experiments differs by the type of neutron scattering measurements being performed, in this project it is used to distinguish the dynamics of the solvent (diffusion, rotation, collective motions and other interatomic interactions) from those of the polymer chains in the hydrogel. There are several varieties of neutron scattering thar are utilized: small angle neutron scattering (SANS), neutron diffraction (ND), quasielastic neutron scattering (QENS), and neutron spin echo spectroscopy (NSE).

In this work I study the effect of water dynamics on the properties of PEG hydrogels. A range of concentration in the semi dilute region of the system is used.

Neutron scattering allowed us to access the perturbation in the hydration or bound population in each gel with an estimate of the water molecules perturbed. Around 8 to 9 water molecules were perturbed per monomer of PEG and the retardation factor was around two for all the gels. This shows that the factor by which the water molecules are perturbed is independent on the concentration, but the amount of water molecules perturbed increases with increasing concentration. Also, it was found that the perturbed water follows exactly the polymer dynamics at high q values which represents the closest water molecules to the polymer surface. Also, the bulk structure of the hydrogels was dependent on concentration this is due to the increased

resistance to swelling via the entropic equilibrium which will reduce the amount of swelling when concentration is increased. Structural measurement via SANS showed that the mesh size which is the length between cross-links decreases with increasing concentration which explains the swelling and structure of each gel. The gels also showed different persistence lengths which reflects into different flexibility and end-to-end distance between cross-links. The dynamics of the protein were shown to be not altered in this concentration range which confirms that water is the main key in explaining the difference in macroscopic properties of hydrogels, those dynamics were perfectly explained by the Zimm polymer dynamics. The amount of perturbed water molecules per monomer of PEG was independent on the concentration but obviously there will be more water molecules perturbed in the system overall. Moreover, the retardation factor was found to be independent on length scale of the observation which was not the case in a previous study on green fluorescent protein (GFP) where it was strongly dependent with an increasing R_H as a function of probe length. This is due to the obvious differences in the topology between the protein and the cross-linked polymers of PEG. In proteins topological disorders of the biomolecule surface plays an important role in the different dynamics of water [16] [17]. Also, the water molecules in the hydration population near the polymer chains were found to behave sub diffusive ($\tau_H \propto q^{-2.25} \sim \tau_H \propto q^{-2.45}$) compared to diffusive motions of bulk water $\tau \propto q^{-2.0}$. where q is the scattering wave vector.

5.3 Gels Preparation and Swelling Experiment

The PEG gels are synthesized and generated using a photo-initiated Thiol-ene click reaction. The monomer 4 Arm-PEG-SH (MW:20 KDa) was purchased from Laysan Bio and cross-linked with an 8 Arm PEG Norbornene (MW 20 KDa) purchased from JenKem Technology USA and all other

materials used in the synthesis were purchased from Sigma-Aldrich. Five different hydrogels were made by weighing out dry monomer precursors in a 1.67:1 functional group ratio standing for thiol: alkene and then adding appropriate deionized water and a solution of the photo-initiator Lithium phenyl-2,3,4, -trimethylbenzoylphosphinate (LAP). The final concentration of LAP in the precursor solution needs to be around 0.05% w/v. For each individual solution the solution was thoroughly mixed using a vortex mixer until a clear solution is achieved. For the purpose of swelling studies 200 micro liters were placed on a customized molds with a Teflon sheet base. Three gels were prepared for each polymer volume fraction at preparation ϕ_0. The solution was then cross-linked in a UV Crosslinker from fisher scientific (Model 13-245-221) with an energy of 12000 joules for 20 minutes. After cross-linking the gels were transferred into tubes containing 5ml of PBS solution and allowed to swell for 24 hours. The gels were weighed after tapping it with weighing paper to remove any remaining buffer. The gels were then transferred to deionized water to swell for 72 hours with the solution being changed every 12 hours in order to remove excess salt from the hydrogels and ensure complete exchange of solvent. The hydrogels were then weighed after gentle dry with a weighing paper. The hydrogels were then frozen and lyophilized in order to determine the dry weight of the gels. The gel preparation experiment was all done at night in complete dark. It is important to note that the cross-linking density is not changed in the gels used here. Figure 5.1 Shows the chemistry of the polymers used in preparation of the crossed-polymer network.

The mass swelling ratio Q_M is defined as [18, 19]:

$$Q_M = \frac{M_S}{M_D} \tag{5.1}$$

where M_D is the dry unswollen polymer mass and M_S is the hydrogel mass at equilibrium swelling (determined by continuing the swelling period until ensuring no increase in mass was observed). The mass swelling ratio was converted to volume swelling ratio Q_V via [19] :

$$Q_V = 1 + \frac{\rho_p}{\rho_s}(Q_M - 1) \qquad (5.2)$$

where ρ_p= 1.12 g cm^{-3} for PEG and the solvent density ρ_s is 1 g cm^{-3} for water and 1.02 g cm^{-3} for PBS. Finally the polymer volume fraction after swelling was calculated as [20]:

$$\phi = \frac{1}{Q_V} \qquad (5.3)$$

With those parameters estimated the longitudinal modulus was calculated according to the following model [21] [22] [23]:

$$M_{os} = \frac{RT\phi^2}{V1}\left(\frac{1}{1-\phi} - 2\chi\right) + v_e RT\left[\frac{1}{2}\left(\frac{\phi}{\phi_0}\right) + \left(\frac{\phi}{\phi_0}\right)^{\frac{1}{3}}\right] \qquad (5.4)$$

Figure 5.1 Chemistry of the multi-arm PEG network. A). 8 arm Polyethylene glycol Norbornene. B) 4 arm Polyethylene glycol thiol. C) The cross-linked network.

where ϕ and ϕ_0 are the polymer volume fraction after and before swelling respectively, $V1$ is the solvent's molar volume, v_e is the concentration of elastically active chains, and χ is the solvent-polymer interaction parameter which has a value of 0.475 for the multi arm 20KDa molecular weight PEG used in the synthesis of the studied gels[23] compared to a value of 0.43 for linear PEG chains in water[24]. Figure 5.2 shows swelling experiment results along with the estimated longitudinal modulus. The elastically active chain concentration was estimated from stoichiometry. It is known from our chemistry ratio that the 4 ARM PEG Norbornene is the limiting reactant for the cross linking, so the number of elastically active chains was estimated as:

$$v_e = \frac{4\,C_{PEG-SH}N_A}{\frac{\phi_0}{\phi}} \tag{5.5}$$

where, C_{PEG-SH} is the concentration of 4-Arm PEG thiol at preparation, N_A is the Avogadro constant, and $\frac{\phi_0}{\phi}$ represents the change in volume upon swelling. This gives reasonable concentration comparable with other multi arm PEG hydrogels studies where v_e was estimated using the modified Flory-Rehner equation assuming complete cross-linking for all arms present [25] [26]. The elastically active chains concentrations used for the estimation of the longitudinal modulus are shown in Table 5.1.

The longitudinal modulus model in equation 5.4 is obtained by $M_{os} = K_{os} + \frac{4}{3} G$. Where, K_{os} is the osmotic modulus and G is the shear modulus. It is known that in polymer gels, there are two contributions to the osmotic pressure. The first is from the free energy of mixing which is clearly representing the first term in the longitudinal modulus estimation in equation 5.4, and the second is from the elasticity of network chains which is the second of the longitudinal modulus equation [27]. It is clear in the results that the hydrogels swollen in PBS have lower osmotic modulus and hence longitudinal modulus this is due to the higher contribution from the free energy of mixing in water compared to in PBS. The number of elastically active chains per volume is slightly more in PBS which is due to less swelling degree compared to water where more solvent was absorbed into the network and lead to less number of v_e. At equilibrium the two contributions in gels are equal [27, 28]which leads to the estimation of v_e for networks which is the previously mentioned Flory-Rehner model.

Table 5.1 Elastically active chains in the PEG hydrogel network in water and in PBS.

ϕ_0	$v_e[mol\ m^{-3}]$	$v_e[mol\ m^{-3}]$
	in water	in PBS
0.036	1.23	1.86
0.050	1.60	2.14
0.071	2.03	2.45
0.143	2.46	3.27
0.286	3.68	4.72

Figure 5.2 shows the volumetric swelling ratio which is the increase of volume compared to volume of the polymer which indicates the total amount of water intake into the hydrogels while Figure 5.2 shows the swelling degree $\frac{\phi_0}{\phi}$ where, ϕ_0 is the
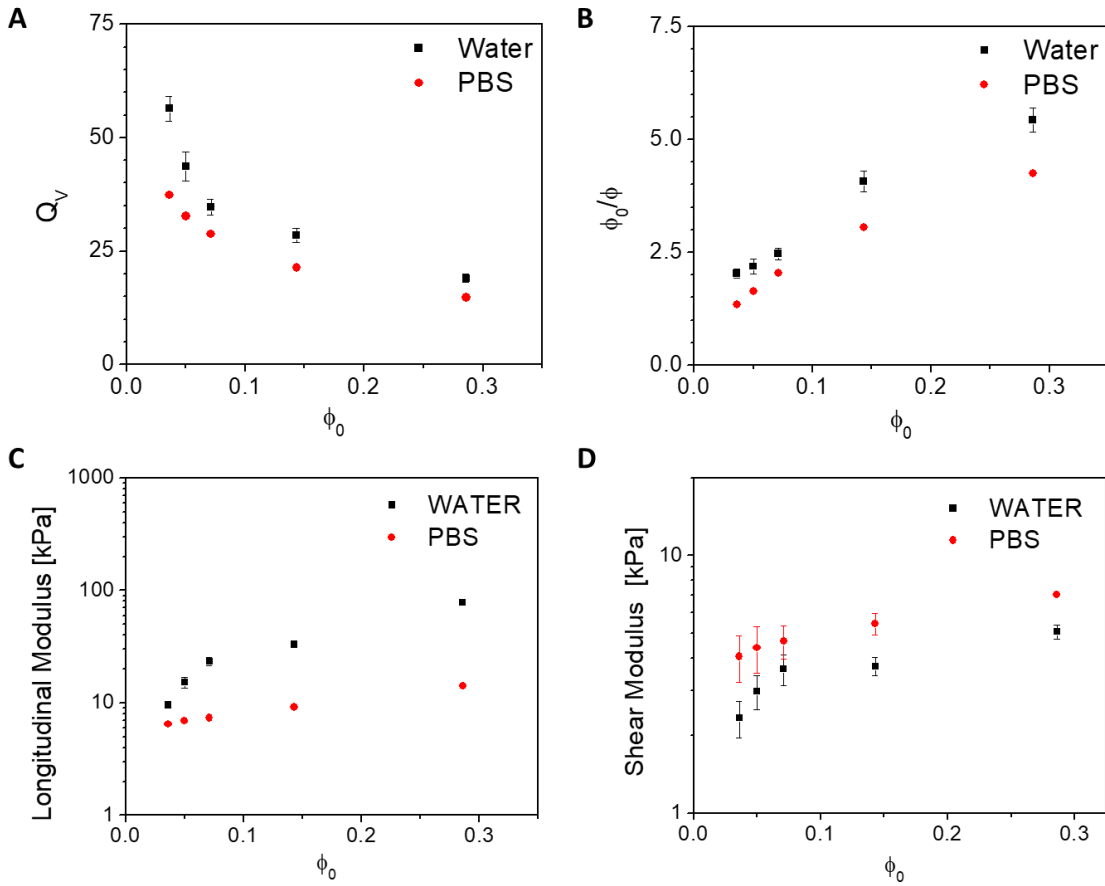
Figure 5.2. Swelling experiment results. A) the volumetric swelling ratio. B) dependence of the swelling degree for the cross-linked multi arm PEG gels. C) Longitudinal Modulus of the Hydrogels. D) Shear Modulus of the Hydrogels.

polymer volume fraction at preparation estimated from the molar volume of PEG. The overlap concentration c* is estimated through[29]:

$$C *= \frac{M}{N_A}(2R_g^3)$$

(5.6)

where M is taken to be M_c the molecular weight between cross-links 7500KDa and R_g is taken from literature to be 4.3nm [30]. The estimated overlap concentration is 0.05 corresponding to $\phi_0 = 0.08$. it means a uniform gel was prepared even with as half of the overlap concentration

which network formation occurs by spontaneously due to chain stretching and reacion of the end groups. The swelling results and structural analysis agree systematically with other swelling studies done on similar multi-arm PEG hydrogel [26] [25] [23] [31] [32].

Table 5.2 Prepared PEG Hydrogels Parameters

Gel	4 Arm-PEG SH [mgml^{-1}]	8 Arm-PEG Norbornene [mgml^{-1}]	ϕ_0	ϕ	f polymer mole fraction swollen state	Hub-Hub Distance estimated [Å]	M_c [gmol^1]
1	12.5	7.5	0.036	0.018	9.26E-06	93.05 $\pm$ 4.45	7500
2	17.5	10.5	0.05	0.023	1.18E-05	85.19 $\pm$6.32	7500
3	25	15	0.071	0.029	1.51E-05	78.77 $\pm$4.02	7500
4	50	30	0.143	0.035	1.83E-05	73.89$\pm$4.23	7500
5	100	60	0.286	0.053	2.83E-05	64.57 $\pm$3.17	7500

Table 5.2 shows all the gels that were prepared and that will be discussed in preceding sections using neutron scattering techniques.

5.4 Structural Analysis on Polyethylene Glycol Hydrogels

PEG hydrogels were first characterized with small angle neutron scattering (SANS). Measurements were carried out at EQ-SANS [33] at the Spallation Neutron Source, Oak Ridge National Laboratory (Tennessee, USA). Over a q-range 0.03-0.45 Å^{-1} shown in Figure 5.3; The spectra was fitted with SASview suite [34] using the Gel Fit Model providing a good fit with the mesh sizes ξ estimated. [35]. The Gel Fit in origin corresponds to Ornstein-Zernike function:

$$I(q) = \frac{(\Delta\rho)^2 RT\,\phi^2}{N_A M_{os}} \left(\frac{1}{1+\xi^2 q^2} + \frac{A_{inhom}}{1+(\epsilon^2 q^2)^2}\right) \tag{5.7}$$

The model is suitable for PEG hydrogels [21] [22] [23] because according to the de Genne's C* theorem, the scattering function for polymer is similar as in polymer solutions [21, 36]. So, The scattering intensity of a gel is given by Ornstein-Zernike function with a second term describing the static concentration fluctuations due to these inhomogeneities. This model will provide the correlation length (mesh size) at known polymer volume fractions studied [23]. While the main Ornstein-Zernike formalism describes the describes the thermal fluctuations in a semi dilute polymer solutions[36]. For swollen gels, the polymer concentration lies typically in the semi dilute regime. Hence the scattering function for a polymer solution can be used and excess scattering from cross-links can be neglected [37] This means the Ornstein-Zernike formalism can be used on the PEG hydrogels to estimate the mesh sizes, the model successfully describing the scattering is shown in Figure 5.3. The values are shown in Table 5.3.
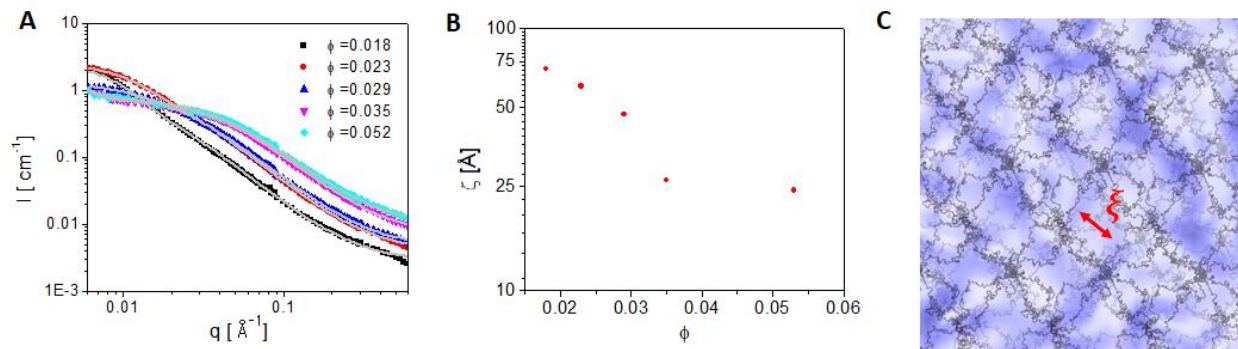
Figure 5.3 Small angle neutron scattering on PEG hydrogels. Measurements were taken at 290 K.

A) raw data of SANS for PEG hydrogels with different polymer volume fraction at swollen state. The spectra show no upturn at low q value which indicates no presence of inhomogeneity; Ornstein-Zernike Fit on the hydrogels to estimate mesh sizes. B) Mesh sizes as function of polymer volume fraction at preparation. C) cross-linked network with an indication of the mesh size.

Table 5.3 Polymer Volume Fractions in Swollen Gels and Mesh sizes

φ	Mesh size (Å)
0.018	70.2 ± 0.3
0.023	60.5 ± 0.2
0.029	47.2 ± 0.1
0.035	26.4 ± 0.1
0.053	24.1 ± 0.1

The most important parameters used in describing the bulk structure of hydrogels are the polymer volume fraction after swelling (ϕ), the molecular weight of the polymer between cross-links (M_C), and the polymer free space or the mesh size (ξ) [9]. The above parameters provide a complete description of the way the solvent is stored in the hydrogel. Also, it provides a measure

of the space or volume between crosslinks and the degree of cross-linking. There were no inhomogeneities observed since the frozen correlation lengths were out of the range of a high value which shows it is not existing, also for confirmation the model was fitted without the second term and the exact mesh sizes were obtained with the model fitting very well. The molecular weight between cross links is fixed in our case because we are not altering any cross-linking density. It is only the entropic effect in stretching that affects the length between cross-links which also reflects amount of swelling. Our molecular weight between cross links is 7.5 KDa which corresponds to an extended chain length of 596.6 Å through simply multiplying the length of a PEG monomer (L_{PEG}= 3.5 Å) [38] by the number of monomers between crosslinks (170.45 monomers).The SANS results showed that the mesh size decrease with increasing polymer concentration which corresponds to lower swelling or water intake. Figure 5.3 shows the mesh sizes for all the Gels. the corresponding osmotic modulus previously mentioned showed that the amount of pressure required to squeeze out water out of the polymer network increased with increasing polymer volume fraction. It makes sense because it is basically the reverse of swelling and should have similar dependence. The mesh sizes on the other hand shows a decrease in value with increasing polymer volume fraction which shows the degree of swelling is less which caused less stretching of the polymer chains.

Another macroscopic parameters that can be estimated from structural analysis is the shear moduli where the difference in moduli between the hydrogels is due to the amount of water in the hydrogel and the modulus can be expressed as [39, 40]:

$$G = v_e RT \frac{\phi^{\frac{1}{3}}}{\phi_0} \tag{5.8}$$

where, v_e is the previously calculated elastically active chains concentration.

In the above model the volume fraction after swelling ϕ decides the factor by which the moduli are increased which reflects the amount of water or degree of swelling which also reduces the amount of elastically active chains per volume of gel. Equation 5.8 also states that each elastically effective chain contributes to the energy required to stretch the chain by a factor of kT[40]. Table 5.4 shows the estimated shear modulus for the gels prepared.

Table 5.4 Shear Modulus of the Gels at 290 K Estimated from Swelling Experiment.

ϕ_0	Shear Modulus [KPa] In Water	Shear Modulus [KPa] In PBS
0.036	2.34 ± 0.38	4.05 ± 0.84
0.050	2.98 ± 0.45	4.39 ± 0.89
0.071	3.62 ± 0.49	4.65 ± 0.70
0.143	3.72 ± 0.30	5.43 ± 0.51
0.286	5.05 ± 0.31	7.03 ± 0.50

In the case of Poisson ratio of 0.5 which is normally assumed in hydrogels the Young Modulus is basically three times the shear modulus [25, 41-43]. The estimated shear modulus for the PEG hydrogels are in agreement with similar multi arm PEG hydrogels studies [44, 45]. The hydrogels studies here consist of different multi-arms configuration and hence different elastically active chains and overall structure. The above swelling study shows a direct relationship between the

structure of the hydrogel and the mechanical properties. Thus, the network architecture which is defined by the molecular design of the hydrogels whether it is the type of polymer, or the degree of swelling and elastic active chains present in the hydrogel is a direct way of producing hydrogels with controlled mechanical properties.

It is also important to introduce the persistence length of this cross-linked polymer network because rheology is effected by the local persistence of the chains [46]. The persistence length is a basic mechanical property quantifying the flexibility or in other words the bending stiffness of a polymer. For polymer chains the polymer will act as a rigid rod for distances shorter than the persistence length. This behavior breaks beyond the persistence length and behave as a flexible chain. The Kratky/ Porod model is usually used for chains with large persistent length [47] [48]. where, the chain is composed of an average linear segments of some length l_k called the Kuhn-step length which is twice as the persistence length l_p [49]. The persistence length can be observed in neutron scattering experiment where the persistence length here is a reflection of the local conformation of the polymer chains. As described by Kratky, the persistence length property is observed in a small angle scattering as a regime of dimension 1. In scattering the mass fractal dimension of an object (d_f) is defined as $I(q) = Bq^{-d_f}$ [50]. A power law of -2 is expected for the Gaussian regime (or a random coil conformation) and a power law of -1 is expected for the persistence length regime (or a rigid rod conformation). The intersection of the two power-law regimes on a log-log scale of I(q) vs q is correlated to the persistence length by

$l_p = \dfrac{6}{\pi q_{intersection}}$ [51]. We observed a -1.5 scaling which is actually more suitable for a good solvent like water.
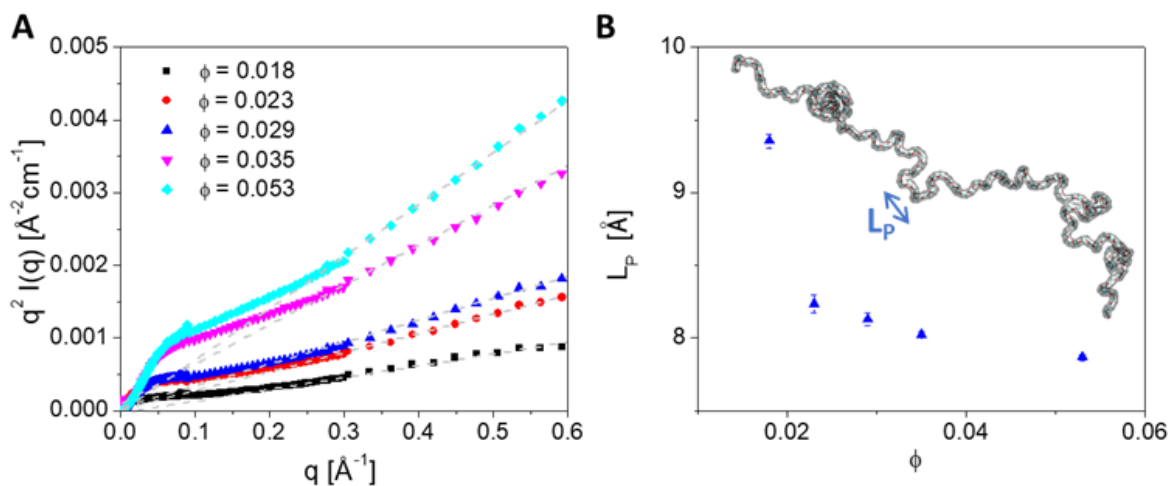
Figure 5.4 A) Kratky Plot for the hydrogels to obtain persistence length. B) Persistence length estimated from SANS.

For the persistence length region, we observed a deviation from -1 to -0.8 which is attributed to noise in the measurement at this high q values. To give a better visualization to the reader we use the Kratky plot where it has the tendency to show the behavior in the Gaussian regime tend toward a horizontal asymptote. From observing the deviation of this asymptotic behavior we can access the persistence length by taking the reciprocal. Both the Kratky plot method and the two-power law model was fit to the SANS data at q range up to 0.6 $Å^{-1}$. The results were consistent with a better visualization using the Kratky plot. This is shown in Figure 5.4.

The results show that the cross over systematically shifts to a lower q for the gels with higher polymer volume fraction. The shift observed was from around 0.24 to 0.20 $Å^{-1}$ which reflects to an increase of 1.5 in persistence length Å which is equal to 43% of the length of a PEG monomer.

Figure 5.4B shows the Persistence length estimated from SANS

5.5 Polymer Chain Dynamics

With this structural information in hand, we can move to the dynamical part of the study, where

the description of the hydration water and the perturbation extent and degree are to be accessed.

Also, it is important to observe the polymer chain dynamics over the used concentration range

and observe any changes in the dynamics if any. So, we have utilized Neutron Spin Echo (NSE) to

measure polymer chain dynamics as a function of concentration in context to the degree of

slowed water dynamics. Measurements were carried out at the Spallation Neutron Source, Oak

Ridge National Laboratory (Tennessee, USA). Over a q-range 0.05-0.30 Å^{-1} covering length scales

where the mesh size, and polymer chain motions between cross-links dominate the scattering.

NSE is an ideal method to describe these motions, which occur at 10's to 100's of nanosecond

timeframe. NSE was performed on each of the hydrogel materials using a 100% D_2O background.

The measurement was carried out at 303K. The results are shown for Gels 1-4 in Figure 5.5.

In Figure 5.5 The observed experimental quantity is the intermediate scattering function which

reflects the fraction of pair correlations still in existence after a given time interval. The relaxation

times τ_0 are extracted then as a function of scattering wave vector. Over here it takes the shape

of a stretched exponential decay. The extracted relaxation times showed a cubic dependence with

q. In this case, the diffusion coefficient is not simply proportional to the exponential decay

constant and the square of the length scale probed; but rather a sub-diffusive length scale

dependence is seen $\tau_0 = 0.015 \pm 0.0027 \, q^{-(-2.8 \pm 0.1)}$. This is shown in Figure 5.6.

Upon comparison, Figure 5.6 shows that the dynamics of the polymeric chains are not altered

significantly in the concentration range studied for the PEG gels experimentally. This comes

despite the clear structural changes in the gel at the level of polymer network mesh size and the
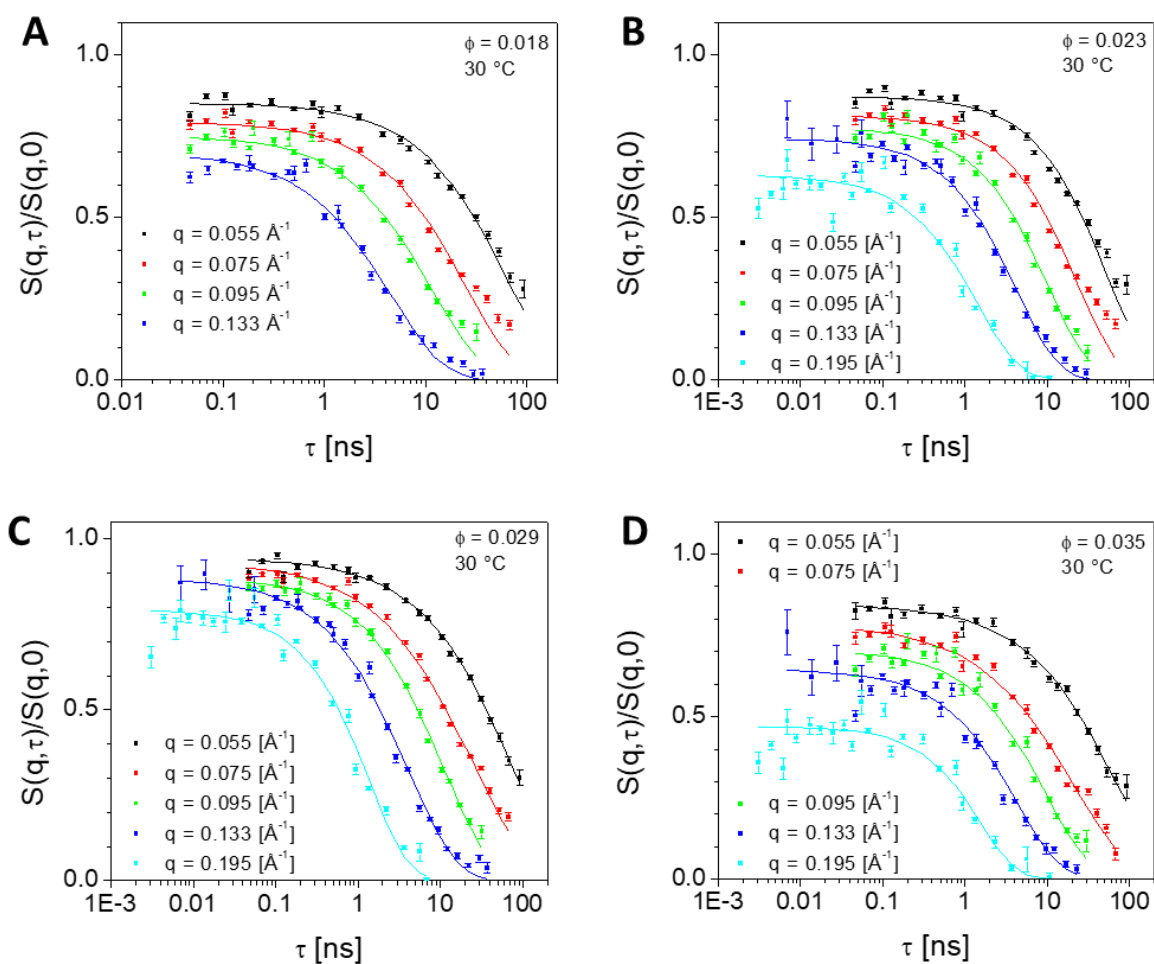
125

Figure 5.5 Intermediate scattering functions obtained from Neutron Spin Echo measurements. A) $\phi = 0.018$. B) $\phi = 0.023$. C) $\phi = 0.029$. D) $\phi = 0.035$. For all samples there is an exponential decay with the time constant decreasing as q increases.

persistence length changes which defines that the chains have different flexibility at different volume fractions.
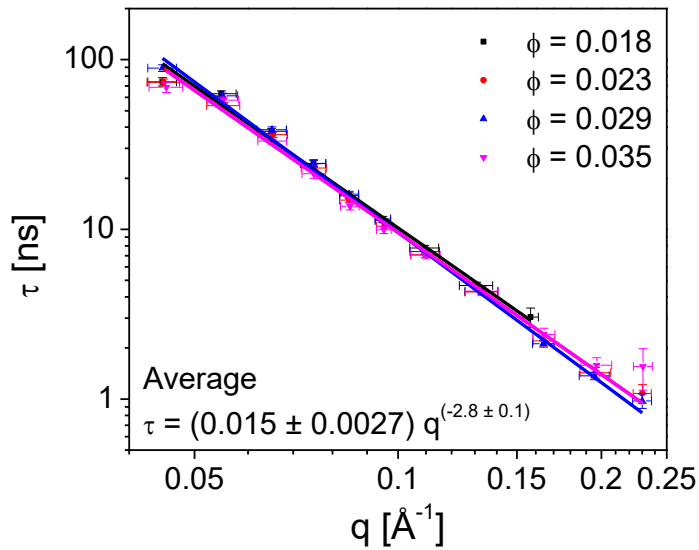
Figure 5.6 Extracted polymer relaxation times from Neutron Spin Echo measurements for the PEG hydrogels.

We conclude that the polymer chains are not interacting with nearby chains in this concentration regime, nor is there significant internal chain deformation being induced. This correlates directly into the network elasticity concepts [52] [53] and show that water interaction – and entropy gain - is the primary driver of swelling and the mechanical properties of the gel. It is interesting finding that the polymer relaxation time follows a cubic dependence with the scattering wave vector. This shows that the dynamics of the cross-linked polymer chains in this concentration regime follows similar dynamics to the Zimm dynamics of polymer solutions where a cubic dependence of q is observed [54]. Where in the Zimm model where the case is dominant by hydrodynamic interaction and the dynamic structure factor depends on the viscosity of the pure solvent and varies with the third power of q [54]. The dynamics of flexible polymers can be explained by the Zimm-Rouse models as mention in the introduction chapter [55] [56] [36] [57]. The Zimm model
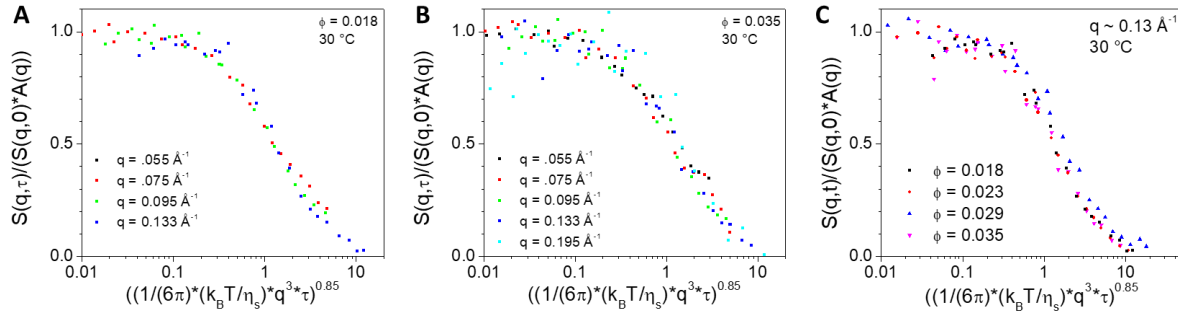
Figure 5.7 The Zimm master curve for A) $\phi = 0.018$ and B) $\phi = 0.035$.

This shows that the zimm model perfectly explains the polymer dynamics independent on volume fraction neither. C) shows the master curve for all the hydrogels at q= 0.13 Å⁻¹. This shows all gels exhibit similar Zimm behavior and the dynamics are not altered with increasing the polymer volume fraction.

describes the chain dynamics in dilute solutions where direct interaction are non-significant and length scales where hydrodynamic interactions are not screened. On the other hand the Rouse model explain the polymer dynamics in concentrated solutions where hydrodynamic interaction are screened [58].

Figure 5.7 shows all the decay curves fall into a one master plot following the Zimm model of the polymer dynamics. This is true for both different q-values and over the concentration range studied here. The apparent viscosity was extracted from the relaxation times of the polymer from NSE fits with $\frac{S(q,\tau)}{S(q,0)} = exp^{(-\tau_{Zimm})^{-0.85}}$. a value of $\beta = 0.85$ is typical for Zimm dynamics [59]. The Zimm diffusion coefficient can be calculated from $D_{Zimm} = \frac{q^{-3}}{\tau_{Zimm}}$ which has the units of $\frac{Å^3}{ns}$ and is related to the apparent viscosity via the famous Stokes-Einstein relation $\eta_{app} = \frac{k_b T}{6\pi D_{Zimm}}$ [60]

Where it is appropriate to represent it in specific viscosity which is a dimension less number to the change in the solvent's viscosity due to the polymer contribution. it is defined as:

$$\eta_{sp} = \frac{\eta_{app} - \eta_s}{\eta_s} \tag{5.9}$$

where η_s is the solvent's viscosity which in this case is water [61, 62].

From Figure 5.6 the average fit value over the concentration range studied is 0.015 $\frac{ns}{Å^3}$ which is the reverse of the Zimm diffusion coefficient. The corresponding η_{app} is calculated as 2.27 mPa.s. which gives a value of η_{sp}=1.85 where the viscosity of water at 300K is 0.797. This shows the origin of the viscosity in PEG hydrogels which is mediated by the perturbation to the neat water dynamics. The amount of perturbation and the dynamics of bulk and hydration water is studied in more details in the next section

The Zimm model gives a description of the dynamics of polymer solutions, where it focuses on the hydrodynamic interactions between the beads of a Gaussian chain which is called the Zimm chain as explained above. The model has mainly two essential basis, the first is modeling actual polymer into statistical segments where the equilibrium distribution of end-to-end distance of each segment is taken as Gaussian which motivates the introduction a harmonic oscillator model. The second fact is the use of averaged hydrodynamic interaction. We observed in the structural analysis that the flexibility of the Gaussian chain is changing with the polymer volume fraction even at very low concentrations where the time average structure parameters specifically the persistence length changes upon increasing polymer volume fraction. On the other hand, the polymer dynamics from NSE. This is an interesting observation which indicated the non ergodicity of the system studied. This is because it breaks the main definition of an ergodic system where

the existence of a connection between the time average of a phase function and a time average of its correlation function [63] which is obviously not observed between the structural time averaged results and the polymer dynamics that depends on this time averaged polymer structure. It indicates that PEG hydrogels are non ergodic aqueous systems. Polymer gels are stated to be non ergodic in previous polymer studies [64] but there is no experimental evidence of such fact. This combined molecular scale structural and dynamical study proves the non ergodicity of hydrogels. Since the dynamics of the polymer show Gaussian dynamics which are independent of the structure of the polymer chains, it can be safely stated that this polymer dynamics are non ergodic.

5.6 Water Dynamics Using Quasi-Elastic Neutron Scattering

Moving to the water dynamics and how it differs from the bulk to the bound population. And what are the equilibrium amount of water molecules that are perturbed compared to the ones unperturbed. To compare the two populations, we need to first measure neat water. Neat water was measured at 280 K, 290 K and 303K in a previous study on bulk water [65]. Dynamics data for both neat water and the hydrogels were collected from two NS spectrometers, BASIS [66] and CNCS [67]. The spectra from both instruments are stitched together for being analyzed [14]. The stitched inelastic neutron scattering spectra of H_2O at 303 K is shown in Figure 5.8 [65] as a function of q and υ. The dynamic structure factor S(q,E) is again converted into the susceptibility formalism, χ''(q,υ) for the reason explained before.
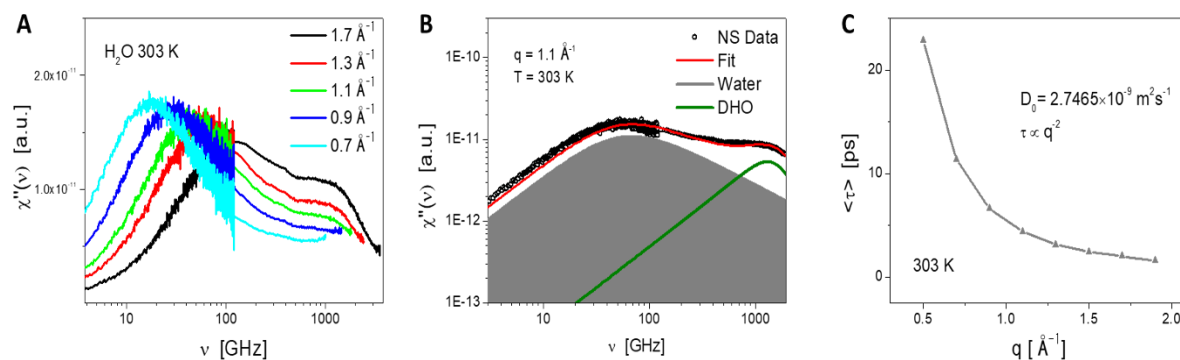
Figure 5.8 Inelastic neutron scattering spectra of H_2O at 303 K.

Spectra of A) H_2O for a range of q-values. A) Illustrates the strong q-dependence of the incoherent scattering feature. B) The model fit of one CD and one DHO functions fitted on water at 303K and 1.1 $Å^{-1}$. C) Coupled translational-rotational relaxation time of water at 303 K. it is clear it has a square dependence with q (diffusive).

Aqueous solutions and hydrogels contain hydrogen rich molecules which in turn means that we are predominantly observing incoherent scattering reflecting self-correlation function of hydrogen atoms in the sample[68]. We are taking the rotational and translational motions of water to be coupled instead of the decoupled formalism used in our previous work on bulk neat water. Teixeira and co-workers have clearly shown the contribution of both translational and rotational motions of water to the NS spectra of neat water[69]. The translational motions were shown to dominate at low q values while the rotational motions influence is seen at high q values. There are also collective vibrational motions seen at higher q values. The decoupling formalism is used for purpose of tracking specific motions of water [65, 69]. But the most realistic description of water molecules is the coupled translational-rotational motions of water, where it is known to be strongly correlated at high q values [70, 71] . therefore, we use a single functional form to obtain water relaxation times using a Cole-Davidson (CD) function, $\{ \chi_{CD}'' = -\mathcal{I}m\{\varDelta_{CD}[1 +$

$i\omega\tau_{CD}]^{-\beta}\}$, where β is a stretching component of 0.7. A damped harmonic oscillator (DHO) [72, 73] is also used to account for the intermolecular collective modes of H-bond bending motions at ~1500 was also used [74, 75].The DHO is given by the relation; $\chi_{DHO}'' = \mathcal{I}m\{\Delta_{DHO}\omega_0^2[\omega^2 - \omega_0^2 - i\omega\Gamma]^{-1}\}$, where ω_0 is the position, Γ is the width, and Δ_{DHO} is the amplitude. It is shown in Figure 5.8 how the model is used on water specifically 290K which is illustrated in Figure 5.8. The coupled translational-rotational relaxation times were extracted from the fit and it was shown that water molecules have a diffusive motion behavior water $\tau \propto q^{-2.0}$. Also, the diffusion coefficient of water at 303 K was calculated from the relaxation times observed $\tau = \frac{1}{D}q^{-2}$ from where the viscosity of the solvent was estimated to be 0.75 mPa.s which is in consistent with the literature and the estimation of the specific viscosity in the previous section. PEG Hydrogels were measured at 303K. The analysis of this data followed the approach in Perticaroli et al.[76] with an addition of one Cole-Davidson function governing the polymer dynamics in the window. The polymer relaxation times extrapolated to the q range in this measurement window shows that the polymer has close dynamics to the probed relaxation times, therefore it is appropriate to take into account the contribution of the polymer to the measured intensity in the quasielastic window, the contribution to incoherent scattering was estimated by the scattering cross section of PEG and the volume fraction in the sample.
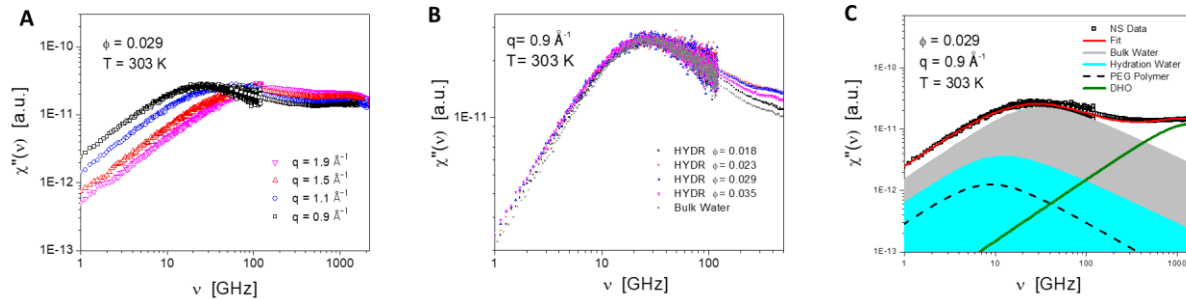
Figure 5.9 Hydration water dynamics in PEG hydrogels.

Typical fit on the spectrum (circles) at q=1.1 Å^{-1}, q=1.3 Å^{-1} and 303 K. Relaxation processes of hydration water, bulk water, and PEG polymer are shown in blue, grey, and orange respectively. DHO for polymer chains and water vibration in green. A) Inelastic neutron scattering spectra of PEG hydrogel $\phi = 0.029$ at 303 K. B) The model fit on PEG hydrogel with $\phi = 0.029$ at 1.1 Å^{-1}. C) The model fit on PEG hydrogel with $\phi = 0.035$ at 1.3 Å^{-1}. It is clear there is an increase in both the PEG polymer contribution and the population of hydrated water for the gel with higher polymer volume fraction.

The water dynamics are addressed as two populations; one bulk water population representing water that is structurally and dynamically unaffected by the solute, and a 'bound' or hydration water population representing water which is dynamically altered by its proximity to the polymer chains. Two Cole Davidson Function were used one for each population of water. The fitting on the gels with $\phi = 0.029$ and $\phi = 0.035$ and q values of 1.1 Å^{-1} and 1.3 Å^{-1} respectively is shown in Figure 5.9.

Relaxation times τ, for hydration and bulk water in the gels along with the polymer relaxation times are reported in Figure 5.10 A as a function of q, along with the retardation factor. Also, Figure 5.10 C shows the perturbed water molecules per monomer of PEG is ranging from 3 to 16 molecules with an average of 8 to 9 across all gels independent on concentration. Comparing this observation with a simulation study on Polyethylene glycol solution[77] where a cutoff of 2 k$_b$T was used to estimate the hydration radius per monomer of PEG which corresponds to 1.5 water

molecules, we observe the lowest number of water molecules perturbed to be around 3 molecules at high q values and an average of 8-9 molecules over the whole q range, this is because we are observing the slow down in dynamics not the water molecules permanently attached to the PEG monomer, this dynamic observation is an average of the motions of water molecules around the PEG monomer for specific length scales (q values). First thing to notice is that water molecules in the bulk are faster than in the bound or hydration population. Also, bulk water shows diffusive behavior $\tau \propto q^{-2.0}$, while bound water shows sub-diffusive behavior $\tau_H \propto q^{-2.25} \sim \tau_H \propto q^{-2.45}$). It is very clear that the perturbed water follows the polymer at high q values (short distances) and has a relaxation time between the bulk and the polymer at low q values (large distances) this shows a clear transition from following polymer dynamics close to the polymer surface all the way to have neat water dynamics at large distances away from the polymer. The amplitude of the two Cole Davidson functions is used to estimate the number of water molecules perturbed per monomer basis according to the equation $N_H = \Delta_{HYDR}(\Delta_{HYDR} + \Delta_{BULK})^{-1}f^{-1}$, where f is the solute mole fraction in the gel. This calculation shows that the ratio of water molecules perturbed in the system is directly proportional to the solute mole fraction, but the water molecules perturbed per monomer are independent on concentration. Where the ratio of increase in the perturbed population is exactly equal to the ratio of increase in polymer mole fraction.
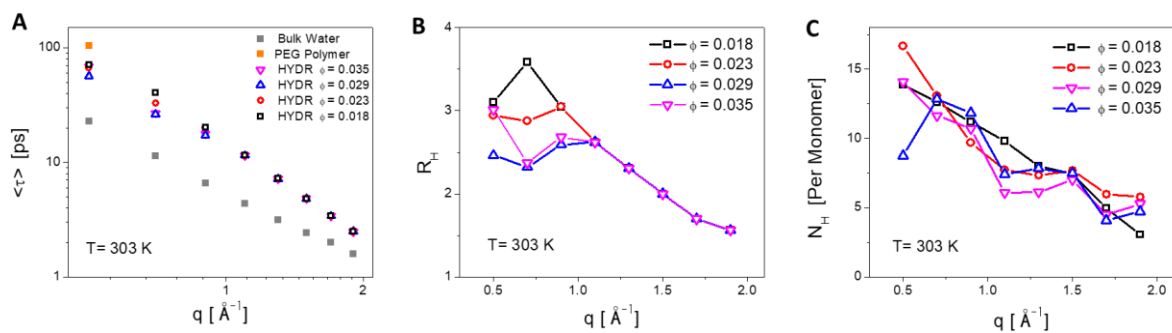
Figure 5.10 PEG Hydrogel dynamics outcome.

A) average relaxation times of hydration (Solid Grey) and bulk (hollow) as a function of q. the bulk water follows a square q dependence while the hydration water does not and is an evidence of sub diffusive behavior. B) retardation factor where at q values below 0.9 Å^{-1}It is clear all the perturbed water is showing a slow down to the polymer's relaxation time. the q dependence is also very weak. This is due to the homogeneity in the topology or structure of the hydrogels. C) the amount of water perturbed per monomer for each gel with an average of 8-9 across all gels.

Figure 5.11 Summary of Dynamics.

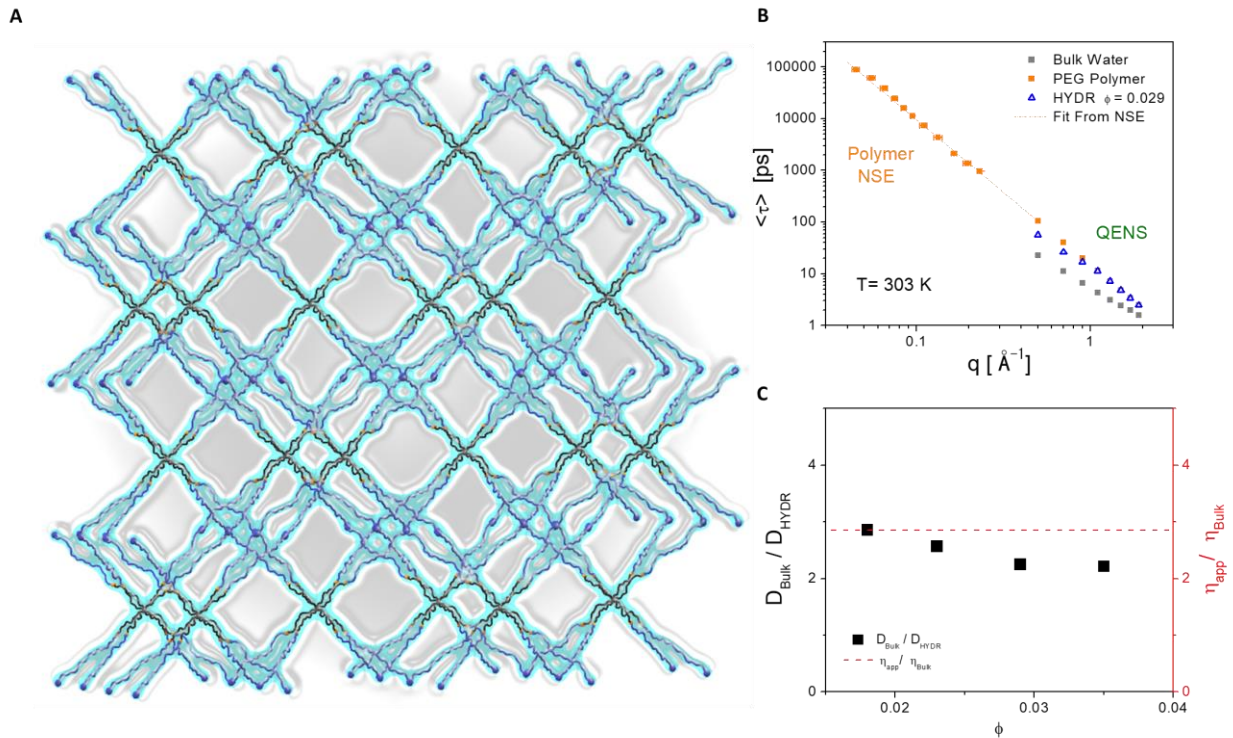A) Relaxation times from QENS and NSE instruments. It is clear that the perturbed water in the hydration layer follows the polymer dynamics. The figure shows the measurements for the gel with the polymer volume fraction of 0.029 at 300K. B) Estimated diffusion coefficient for the perturbed water population compared to bulk populations along with the apparent viscosity compared to bulk viscosity of water at 303K.

This slowdown in the dynamics of water near the polymer surface translates into macroscopic properties or transport and viscoelastic properties of the gels. The observation of the perturbed water dynamics following the polymer's dynamics is shown in Figure 5.11B. We start by calculating the diffusion coefficient of water in the bulk population and in the bound or perturbed population. The diffusion coefficient was calculated for the perturbed water population similarly to previously mentioned for neat water. The ratio of D_{Bulk}/D_{HYDR} shows it is a similar decrease in diffusion coefficient of water molecules which reflects the retardation factor to the water

relaxation time compared to the neat water. it is interesting that the diffusion coefficients are reduced by a factor of 2 similar to the retardation factor of the water molecules in the bound population. The diffusion coefficient in the bound is lower than in the bulk this is because the dynamics of water are perturbed by the presence of polymer chains that reduce the rate at which the water molecules are diffusing. Not only that but also the diffusing behavior becomes sub-diffusive as mentioned before. This hints for an increase in the local viscosity near the PEG polymer surface at the hydration or perturbed layer.

Also, the number of perturbed water molecules increase with increasing concentration this is because more water molecules are in contact with polymer chains in the hydrogel network. It was increased from 7% of water molecules in the gel with lowest concentration to 12.8% of water molecules in the gel with the highest concentration. This means that the ratio of perturbed water molecules increased by around 2 times when the polymer volume fraction was increased by around 2 times. This should be an identification that increasing the polymer volume fraction by a certain factor increase the perturbed water molecules ratio by the exact same factor. It is a key to controlling the amount of desired perturbation to the water molecules in the hydrogel according to the application it is used in. Such control on the dynamics along with specific structural features are keys factors in applications.

Since diffusion is altered this also means the viscosity of the hydrogel changes since a certain percentage of water molecules are diffusing at a lower rate. Since the perturbed water is observed to follow the dynamics of the polymer it is clear that the origin of the apparent viscosity and the contribution of polymer to the viscosity of the PEG hydrogel system is seen from the perturbation of the neat water dynamics near the surface of the polymer this was evaluated in

the NSE section where it was found that the specific viscosity (The contribution of polymer to the solution viscosity) is 1.8.

Since the viscosity is related to diffusion coefficient, they have a similar trend. It is seen in the specific viscosity estimation that the viscosity of the gels increased by a factor of 1.85 which is close to the perturbation and the change in the local diffusion coefficient of the water molecules. this is higher than the observed increase in viscosity in pastor's study which may be due to the different perturbation in the polymer network in the cross-linked PEG hydrogel system where it is reasonable that the gel will have a higher viscosity due to closer contact of water with the polymer network which explains the difference in the viscosity of polymer solutions and gels[77]. If we take the ratio of the apparent viscosity to neat water viscosity at 300K, this value is 2.84 and is clearly shown in Figure 5.11C. It is then a question to raise is how the gels have different viscosities if the increase in local viscosity is similar. The answer is simply that the population that is perturbed and has a diffusion coefficient twice less than the bulk neat water or has a higher viscosity than bulk water is different, the population depends on the amount of polymer present. Whereas mentioned before the percentage of perturbed water molecules varies linearly with the polymer volume fraction. Figure 5.11B summarizes the whole dynamic window of the experiment where we see that the perturbed water follows the polymer dynamics at high q and start to deviate at q values below 0.9 Å^{-1}. The bulk water has dynamics around 2 times faster than the perturbed water. This perturbation is reflected in the diffusion coefficient and the local viscosity near the polymer surface.

Since the population of bulk and bound water are in equilibrium that is driven by entropic competition as explained earlier. The ability of accessing the number of water molecules in each

population is a great advantage for us in explaining the origins of different macroscopic properties of the hydrogels. Since another way of looking at the equilibrium of the two populations is looking at the water activity of the whole aqueous system where water activity is considered as the ratio of water molecules available for hydration. We all know that as explained by Van Hoff model [3] the water activity is related to the osmotic pressure build in the system due to swelling. So, if we can take into consideration the amount of water molecules available for hydration as a measure of the equilibrium or as a measure of the extent to which the polymer-solvent interactions are valuable then we are referring to the degree of swelling because the osmotic pressure is the opposite of swelling where it is the pressure needed to squeeze out a water molecule out of the hydrogel network. The weight fraction of the polymer in the hydrogels used for this dynamic experiment ranges from 0.01 to 0.02 wt% in the swollen state, according to an experimental measurement of water activity this shows [78] that the water activity is above 0.999 for a solution with molecular weight of 7000 similar to our molecular weight between cross-links. By estimating the water molecules that have different water activity than neat water this is very negligible value of less than 1 water molecule per PEG monomer which reflects that PEG is non perturbing to the aqueous system to a degree that changes the water activity. Hence the water molecules are experiencing a slowdown in the dynamics but are still available for hydration. There is an exchange in the two populations which are perturbed by a factor of 2.

If for this work, we consider the water molecules dynamically perturbed by a factor of 2 to be the water molecules assigned for the estimation of the hydrodynamic volume per PEG monomer then simply this volume is estimated by $V_H = V_{PEG} + 8V_{H_2O}$. As appropriate the shape of the PEG monomer is taken to be a cylinder so the Volume is $V_{PEG} = A_{PEG}L_{PEG}$, Where L_{PEG} is the length
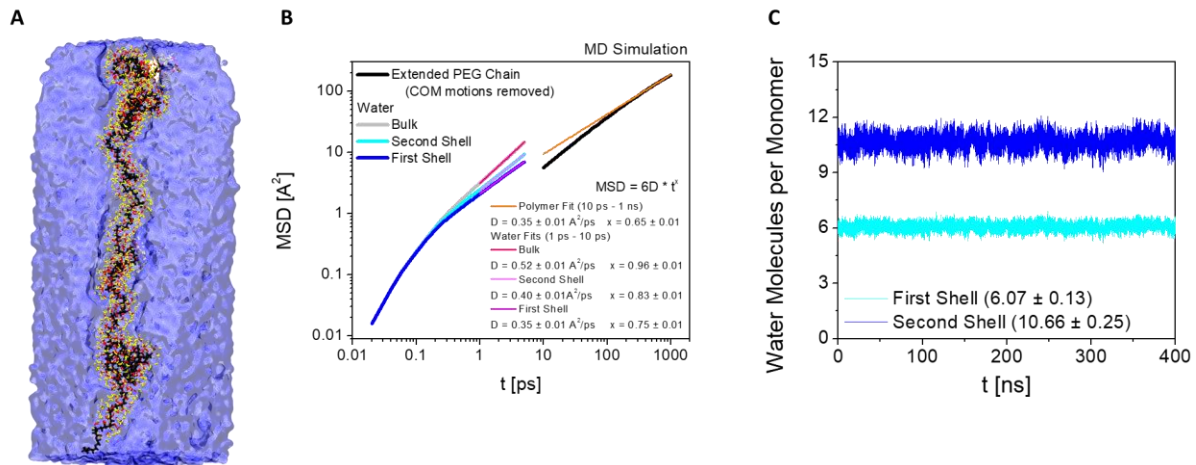
Figure 5.12 MD simulation of extended PEG chain.

(A) MD simulations were performed on a PEG chain which was forced to adopt an extended configuration. The extended chain (black) is shown with the first (red, 3.4 Å cutoff) and second (red, 5 Å cutoff) shells of water highlighted. (B) A parallel analysis of polymer and water dynamics has been performed. The mean square displacement has been computed as a function of correlation time, and a power law fit applied. The bulk water was found to have diffusive motions, while water in the first hydration shell of the polymer chain exhibited slower sub-diffusive motions. The nanosecond scale polymer dynamics resembled the Zimm prediction with a Zimm pre-factor on the order of the sub-diffusion pre-factor calculated for the first hydration shell water population. (C) The number of close contact waters has been computed to compare to the experimentally determined hydration number, N_H, to the simulation defined number of close water contacts. A close agreement between the experimental estimate and number of close contacts in the first shell was observed.

of one PEG monomer known to be 0.35nm [38]. The volume of one PEG monomer calculated from its molar volume is 64.75 $Å^3$. This gives us a radius of 0.2426nm. The volume of water molecule at 300K is calculated from the density to give a volume of 30 $Å^3$. The total estimated hydration volume is 304.75 $Å^3$. So, for the 170 monomers between crosslinks, we take the summation over the whole chain 170 V_H. The estimated hydration radius is $R_H = 3.843$ Å for the polymer of 7500 between crosslinks. Which is reasonably close to the definition of the cutoff

distance from the polymer for the second hydration shell in MD simulations[79] . The MD simulations results is shown in Figure 5.12 .

Molecular dynamics simulations for a PEG molecule with 170 monomers with a restrained end-to-end distance of 160 Å in the Z direction. The system was prepared by CHARMM GUI Polymer Builder[80, 81]. The water box for the simulation has side lengths of 70 Å, 70 Å, and 200 Å for x, y, and z directions, respectively. The estimated volume fraction for both simulations is around 0.01. After equilibration, 400 ns production simulations were run and repeated three times in an NPT ensemble at 300 K and 1 atm. The time step is 2 fs, and frames were saved every 10 ps.

The polymer dynamics were analyzed by calculating the Mean Square Displacement (MSD) for each monomer. To remove the global motion of the polymer chain, the center of mass motion was removed before calculating MSD. The MSDs were then averaged for all monomers. The diffusion in three-dimensional space was modeled as:

$$MSD = 6D * t^{\alpha} \tag{5.10}$$

where D is the generalized diffusion coefficient and α is the anomalous diffusion exponent. D and α were obtained by linear fitting for the log MSD - log t curve in a range from 10 ps to 1 ns.

The water dynamics were analyzed from a subset of the simulation trajectory run with a 1 fs timestep and frames saved every 20 fs for a duration of 10 ns, with other conditions kept the same. These simulations were also repeated three times. The MSD of water molecules were calculated again as a function of time and used to obtain the generalized diffusion coefficient D and anomalous diffusion exponent α. The water dynamics exhibit different dynamical regimes,

with ballistic motions at short times (up to 100 fs) and slower diffusive motions at times greater than 1 ps.

Water was classified into different hydration shells based on its distance to the nearest polymer atom. The first solvent shell is defined to be within 3.4 Å from the polymer, and the second solvent shell in the range of 3.4 Å to 5.0 Å from the polymer. Water molecules that are 8.0 Å farther from the polymer are defined as bulk water. The numbers of water molecules in the first and second hydration shells were counted and averaged on a per monomer basis. The residence time was then calculated by counting the time when a water molecule enters the first solvent shell until it leaves the second shell.

The simulations show approximately 6 water molecules in the first hydration shell and an additional ~10 molecules in the second shell. This puts the experimental of 6-10 molecules of water being perturbed in context. Similarly, Figure 4.12 shows the dynamics of both water and the PEG chain. Here, we see that the MD result supports our model of polymer and water dynamics from the experiments. We see polymer motions following the same power law dependence in terms of their local diffusion. We also see that the water dynamics in the first hydration shell are significantly slowed when compared to bulk and again approach the diffusional time scale of the polymer dynamics.

5.7 Conclusion

As a conclusion we have studied experimentally the perturbation of water molecules in Polyethylene glycol hydrogels at different concentrations. The concentration range was dilute to see any changes in the dynamics of the polymer chains itself, the polymer showed a clear Zimm

model dynamics and no differences in the dynamics were observed over the concentration used although there are clear changes in the structure and flexibility of the Gaussian chain. This study utilized two-dimensional NS data, presented in susceptibility obtained from different instruments. This allowed us to study the dynamics over an extended window. We observed that water molecules are perturbed by about two factors and the amount of water molecules perturbed was directly related to the increase in polymer concentration of the gels. We saw a clear effect on the macroscopic properties and the swelling degree due to the increase in polymer concentration only without any change in the cross-linking density. Around 8 to 9 water molecules were perturbed per monomer of PEG. It was clear and seen that the amount of water molecules perturbed is what really defines the properties of the hydrogels. This is all controlled thermodynamically via competing entropic forces which defines the final bulk structure of the hydrogel. The increase in the apparent viscosity was calculated and this is assigned to the presence of the polymer and perturbing the water dynamics in close to the polymer surface. The fact that the time averaged structure of the chains between cross-links was dependent on the concentration of the polymer and the degree of swelling but there were no changes in the Zimm dynamics outcomes of the polymer dynamics study is a clear prove of non ergodicity in PEG hydrogels.

5.8 Acknowledgments

preparation of the hydrogels for the scattering measurements and from the Ohio State University

from Dr. Xiaolin Cheng Lab for the MD simulations.

References

1. Timasheff, S.N., *Protein-solvent preferential interactions, protein hydration, and the modulation of biochemical reactions by solvent components.* Proceedings of the National Academy of Sciences, 2002. **99**(15): p. 9721-9726.
2. Stokes, R. and R. Robinson, *Interactions in aqueous nonelectrolyte solutions. I. Solute-solvent equilibria.* The Journal of Physical Chemistry, 1966. **70**(7): p. 2126-2131.
3. Gekas, V., et al., *Mass transfer properties of osmotic solutions. I. Water activity and osmotic pressure.* International Journal of Food Properties, 1998. **1**(2): p. 95-112.
4. Harris, J.M., *Poly (ethylene glycol) chemistry: biotechnical and biomedical applications*. 1992: Springer Science & Business Media.
5. Zarzycki, R., Z. Modrzejewska, and K. Nawrotek, *Drug release from hydrogel matrices.* Ecol Chem Eng S, 2010. **17**(2): p. 117-36.
6. Lin, C.-C., A. Raza, and H. Shih, *PEG hydrogels formed by thiol-ene photo-click chemistry and their effect on the formation and recovery of insulin-secreting cell spheroids.* Biomaterials, 2011. **32**(36): p. 9685-9695.
7. Zhu, J., *Bioactive modification of poly (ethylene glycol) hydrogels for tissue engineering.* Biomaterials, 2010. **31**(17): p. 4639-4656.
8. Harris, J.M. and K. Yoshinaga, *Assessment of the Effects of Attaching an Enzyme to Glass by a Poly (ethylene glycol) Tether.* Journal of bioactive and compatible polymers, 1989. **4**(3): p. 281-295.
9. Peppas, N.A., et al., *Hydrogels in biology and medicine: from molecular principles to bionanotechnology.* Advanced materials, 2006. **18**(11): p. 1345-1360.
10. Hoffman, A.S., *Hydrogels for biomedical applications.* Advanced drug delivery reviews, 2012. **64**: p. 18-23.
11. Kim, S.W., Y.H. Bae, and T. Okano, *Hydrogels: swelling, drug loading, and release.* Pharmaceutical research, 1992. **9**(3): p. 283-290.
12. Young, R.J. and P.A. Lovell, *Introduction to polymers*. 2011: CRC press.
13. Deam, R. and S.F. Edwards, *The theory of rubber elasticity.* Philosophical Transactions of the Royal Society of London. Series A, Mathematical and Physical Sciences, 1976. **280**(1296): p. 317-353.
14. Perticaroli, S., et al., *Description of Hydration Water in Protein (GFP) Solution.* Biophysical Journal, 2017. **112**(3): p. 201a.
15. Meilleur, F., K.L. Weiss, and D.A. Myles, *Deuterium labeling for neutron structure-function-dynamics analysis*, in *Micro and Nano Technologies in Bioanalysis*. 2009, Springer. p. 281-292.
16. Conti Nibali, V. and M. Havenith, *New insights into the role of water in biological function: Studying solvated biomolecules using terahertz absorption spectroscopy in conjunction with molecular dynamics simulations.* Journal of the American Chemical Society, 2014. **136**(37): p. 12800-12807.
17. Perticaroli, S., et al., *Dynamics of hydration water in sugars and peptides solutions.* The Journal of Physical Chemistry B, 2013. **117**(25): p. 7729-7736.
18. Sokic, S. and G. Papavasiliou, *Controlled proteolytic cleavage site presentation in biomimetic PEGDA hydrogels enhances neovascularization in vitro.* Tissue Engineering Part A, 2012. **18**(23-24): p. 2477-2486.
19. Rizzi, S.C. and J.A. Hubbell, *Recombinant protein-co-PEG networks as cell-adhesive and proteolytically degradable hydrogel matrixes. Part I: Development and physicochemical characteristics.* Biomacromolecules, 2005. **6**(3): p. 1226-1238.

20.	Metters, A., K. Anseth, and C. Bowman, *Fundamental studies of a novel, biodegradable PEG-b-PLA hydrogel.* Polymer, 2000. **41**(11): p. 3993-4004.

21.	Matsunaga, T., et al., *SANS studies on Tetra-PEG Gel under uniaxial deformation.* Macromolecules, 2011. **44**(5): p. 1203-1210.

22.	Horkay, F., et al., *Osmotic and SANS observations on sodium polyacrylate hydrogels in physiological salt solutions.* Macromolecules, 2000. **33**(22): p. 8329-8333.

23.	Matsunaga, T., et al., *SANS and SLS studies on tetra-arm PEG gels in as-prepared and swollen states.* Macromolecules, 2009. **42**(16): p. 6245-6252.

24.	Lutolf, M. and J. Hubbell, *Synthesis and physicochemical characterization of end-linked poly (ethylene glycol)-co-peptide hydrogels formed by Michael-type addition.* Biomacromolecules, 2003. **4**(3): p. 713-722.

25.	Matsunaga, T., et al., *Structure characterization of tetra-PEG gel by small-angle neutron scattering.* Macromolecules, 2009. **42**(4): p. 1344-1351.

26.	Kim, J., et al., *Characterization of the crosslinking kinetics of multi-arm poly (ethylene glycol) hydrogels formed via Michael-type addition.* Soft matter, 2016. **12**(7): p. 2076-2085.

27.	Flory, P.J., *Principles of polymer chemistry*. 1953: Cornell University Press.

28.	Shibayama, M. and T. Tanaka, *Volume phase transition and related phenomena of polymer gels.* Responsive gels: volume transitions I, 1993: p. 1-62.

29.	Colby, R.H., *Structure and linear viscoelasticity of flexible polymer solutions: comparison of polyelectrolyte and neutral polymer solutions.* Rheologica acta, 2010. **49**(5): p. 425-442.

30.	Linegar, K.L., et al., *Hydrodynamic radius of polyethylene glycol in solution obtained by dynamic light scattering.* Colloid journal, 2010. **72**(2): p. 279-281.

31.	Toepke, M.W., et al., *Characterization of thiol-ene crosslinked PEG hydrogels.* Macromolecular materials and engineering, 2013. **298**(6): p. 699-703.

32.	Bush, B.G., et al., *Mechanical measurements of heterogeneity and length scale effects in PEG-based hydrogels.* Soft Matter, 2015. **11**(36): p. 7191-7200.

33.	Zhao, J., C.Y. Gao, and D. Liu, *The extended Q-range small-angle neutron scattering diffractometer at the SNS.* Journal of Applied Crystallography, 2010. **43**(5): p. 1068-1077.

34.	Butler, P., et al., *SASView for Small Angle Scattering Analysis.* There is no corresponding record for this reference, 2013.

35.	Mendes, E., et al., *Soft order in high-functionality star polymer solutions and gels: A small-angle neutron scattering study.* Macromolecules, 1995. **28**(1): p. 174-179.

36.	De Gennes, P.-G. and P.-G. Gennes, *Scaling concepts in polymer physics*. 1979: Cornell university press.

37.	Higgins, J. and H. Benoit, *Polymers and neutron scattering. Clarendon*. 1994, Oxford.

38.	Cruje, C. and D. Chithrani, *Polyethylene glycol density and length affects nanoparticle uptake by cancer cells.* J. Nanomed. Res, 2014. **1**(00006).

39.	Onuki, A., *Theory of phase transition in polymer gels.* Responsive Gels: Volume Transitions I, 1993: p. 63-121.

40.	Richtering, W. and B.R. Saunders, *Gel architectures and their complexity.* Soft Matter, 2014. **10**(21): p. 3695-3702.

41.	Shao, C., et al., *An integrated self-healable and robust conductive hydrogel for dynamically self-adhesive and highly conformable electronic skin.* Journal of Materials Chemistry C, 2019. **7**(48): p. 15208-15218.

42.	Pusey, P.N. and W. Van Megen, *Phase behaviour of concentrated suspensions of nearly hard colloidal spheres.* Nature, 1986. **320**(6060): p. 340-342.

43.	Gulyuz, U. and O. Okay, *Self-healing polyacrylic acid hydrogels.* Soft Matter, 2013. **9**(43): p. 10287-10293.

44.   Sugimura, A., et al., *Mechanical properties of a polymer network of Tetra-PEG gel.* Polymer journal, 2013. **45**(3): p. 300-306.

45.   Shibayama, M., *Structure-mechanical property relationship of tough hydrogels.* Soft Matter, 2012. **8**(31): p. 8030-8038.

46.   Beaucage, G., et al., *Persistence length of isotactic poly (hydroxy butyrate).* Macromolecules, 1997. **30**(14): p. 4158-4162.

47.   Burchard, W. and K. Kajiwara, *The statistics of stiff chain molecules I. The particle scattering factor.* Proceedings of the Royal Society of London. A. Mathematical and Physical Sciences, 1970. **316**(1525): p. 185-199.

48.   Kratky, O. and G. Porod, *Diffuse small-angle scattering of X-rays in colloid systems.* Journal of colloid science, 1949. **4**(1): p. 35-70.

49.   Benoit, H. and P. Doty, *Light scattering from non-Gaussian chains.* The Journal of Physical Chemistry, 1953. **57**(9): p. 958-963.

50.   Schmidt, P.W., *Small-angle scattering studies of disordered, porous and fractal systems.* Journal of Applied Crystallography, 1991. **24**(5): p. 414-435.

51.   Glatter, O., O. Kratky, and H. Kratky, *Small angle X-ray scattering*. 1982: Academic press.

52.   Yang, C., T. Yin, and Z. Suo, *Polyacrylamide hydrogels. I. Network imperfection.* Journal of the Mechanics and Physics of Solids, 2019. **131**: p. 43-55.

53.   Rubinstein, M. and S. Panyukov, *Elasticity of polymer networks.* Macromolecules, 2002. **35**(17): p. 6670-6686.

54.   Ewen, B. and D. Richter, *Neutron spin echo investigations on the segmental dynamics of polymers in melts, networks and solutions.* Neutron Spin Echo Spectroscopy Viscoelasticity Rheology, 1997: p. 1-129.

55.   Doi, M., S.F. Edwards, and S.F. Edwards, *The theory of polymer dynamics*. Vol. 73. 1988: oxford university press.

56.   Grosberg, A.Y., et al., *Statistical physics of macromolecules.* Computers in Physics, 1995. **9**(2): p. 171-172.

57.   Lisy, V., J. Tothova, and A. Zatovsky, *The Rouse-Zimm-Brinkman theory of the dynamics of polymers in dilute solutions.* arXiv preprint cond-mat/0509398, 2005.

58.   Tchesskaya, T., *A generalized Zimm model: Hydrodynamic screening in polymer solutions.* Journal of Molecular Liquids, 2009. **150**(1-3): p. 77-80.

59.   Richter, D., et al., *Neutron spin echo in polymer systems.* Neutron Spin Echo in Polymer Systems, 2005: p. 1-221.

60.   Poling-Skutvik, R., et al., *Confined dynamics of grafted polymer chains in solutions of linear polymer.* Macromolecules, 2017. **50**(18): p. 7372-7379.

61.   Witte, J., et al., *A comparison of the network structure and inner dynamics of homogeneously and heterogeneously crosslinked PNIPAM microgels with high crosslinker content.* Soft Matter, 2019. **15**(5): p. 1053-1064.

62.   Rubinstein, M. and R.H. Colby, *Polymer physics*. Vol. 23. 2003: Oxford university press New York.

63.   Mazur, P., *Non-ergodicity of phase functions in certain systems.* Physica, 1969. **43**(4): p. 533-545.

64.   Li, X., et al., *Polymer gel with a flexible and highly ordered three-dimensional network synthesized via bond percolation.* Science advances, 2019. **5**(12): p. eaax8647.

65.   Yahya, A., et al., *Molecular origins of bulk viscosity in liquid water.* Physical Chemistry Chemical Physics, 2020. **22**(17): p. 9494-9502.

66.   Mamontov, E. and K.W. Herwig, *A time-of-flight backscattering spectrometer at the Spallation Neutron Source, BASIS.* Review of Scientific Instruments, 2011. **82**(8): p. 085109.

67.   Ehlers, G., et al., *The new cold neutron chopper spectrometer at the Spallation Neutron Source: design and performance.* Review of Scientific Instruments, 2011. **82**(8): p. 085108.

68.   Bée, M., *Quasielastic neutron scattering.* 1988.
69.   Teixeira, M., *Bellissent-Funel, SH Chen, and AJ Dianoux.* Phys. Rev. A, 1985. **31**: p. 1913-1917.
70.   Shen, Y.C. and D.W. Oxtoby, *Density functional theory of crystal growth: Lennard-Jones fluids.* The Journal of chemical physics, 1996. **104**(11): p. 4233-4242.
71.   Liu, L., et al., *Slow dynamics of supercooled water confined in nanoporous silica materials.* Journal of Physics: Condensed Matter, 2004. **16**(45): p. S5403.
72.   Settles, M. and W. Doster, *Anomalous diffusion of adsorbed water: a neutron scattering study of hydrated myoglobin.* Faraday Discussions, 1996. **103**: p. 269-279.
73.   Di Cola, D., et al., *Proton dynamics in supercooled water by molecular dynamics simulations and quasielastic neutron scattering.* The Journal of chemical physics, 1996. **104**(11): p. 4223-4232.
74.   Perticaroli, S., et al., *Broadband depolarized light scattering study of diluted protein aqueous solutions.* The Journal of Physical Chemistry B, 2010. **114**(24): p. 8262-8269.
75.   Perticaroli, S., et al., *Extended frequency range depolarized light scattering study of N-acetyl-leucine-methylamide–water solutions.* Journal of the American Chemical Society, 2011. **133**(31): p. 12063-12068.
76.   Perticaroli, S., et al., *Description of hydration water in protein (green fluorescent protein) solution.* Journal of the American Chemical Society, 2017. **139**(3): p. 1098-1105.
77.   Lee, H., et al., *Molecular dynamics studies of polyethylene oxide and polyethylene glycol: hydrodynamic radius and shape anisotropy.* Biophysical journal, 2008. **95**(4): p. 1590-1599.
78.   Ninni, L., M. Camargo, and A. Meirelles, *Water activity in poly (ethylene glycol) aqueous solutions.* Thermochimica acta, 1999. **328**(1-2): p. 169-176.
79.   https://amberhub.chpc.utah.edu/watershell/.
80.   Jo, S., et al., *CHARMM-GUI: a web-based graphical user interface for CHARMM.* Journal of computational chemistry, 2008. **29**(11): p. 1859-1865.
81.   Choi, Y.K., et al., *CHARMM-GUI Polymer Builder for Modeling and Simulation of Synthetic Polymers.* Journal of chemical theory and computation, 2021. **17**(4): p. 2431-2443.

Chapter 6 :   The Role of Hydrodynamics in the Self Diffusion of Green Fluorescent Protein

6.1 Introduction

Macromolecule's diffusion dependence on concentration play an important role in understanding biological processes. Molecules diffuse within the cell through a crowded media such as the cytoplasm where macromolecules make up to 40% of the available space for diffusion[1]. Studying this macromolecular crowding is required especially on the cell membrane [2], where barriers created by actin filaments hinder the displacement of membrane bound molecules[3, 4]. Also, in mitochondria more than 60% of the space can be assigned to enzymes and proteins[5]. Other crowded examples are the extracellular space between brain cells[6] and red blood cells that filled with hemoglobin with a volume fraction of about 25% [7]. Due to this packed environment, macromolecules will move around obstacles and hence the diffusion rate is reduced compared to infinite dilution diffusion [8]. This may either accelerate or decelerate the rate of reaction rates taking place in the cell. Where, diffusion limited reactions rates are decreased and transition state limited reactions are accelerated[9]. The question of the diffusion mechanism of proteins in such crowded media is a subject of ongoing research [10]. The reduction in the diffusion rate may be assigned to excluded volume effects but the reality is that hydrodynamic interactions is what causes such change while the excluded volume effect on biological reactions rates is a thermodynamic consequence[11]. In this chapter I present experimental evidence that the self-diffusion coefficient of a protein is not equal to the mutual or collective diffusion coefficient, where this is explained by different self and collective frictional factors. The first being dominated by hydrodynamic interactions that explain the reduction in

diffusion coefficient as a function of concentration. The collective diffusion coefficient shows no dependence on concentration while the self-diffusion coefficient shows a decrease even at low concentrations addressed in this study.

The collective diffusion (mutual) coefficient D_c measures the flow resulted from a concentration gradient, while the self-diffusion (tracer) D_s coefficient refers to a flow of a labeled molecule through a solution of uniform concentration. The collective diffusion coefficient is obtained from thermodynamical models combined with the Einstein equation which related the molar mobility to a molecular friction coefficient f_c [12, 13]. This leads to collective diffusion coefficient as a function of both a friction coefficient and osmotic compressibility $K_{os} = \frac{\partial c_p}{\partial \Pi}$. Where, Π is the osmotic pressure and c_p is the molar concentration of the macromolecule. The relationship is shown in the equation below:

$$D_c = \frac{1}{N_A f_c} \left(\frac{\partial \Pi}{\partial c_p} \right)_T \tag{6.1}$$

where N_A is the Avogadro number. The osmotic compressibility acts as a driving force where a low compressibility in the solution will enhance the process of restoring a uniform local concentration. The increase in osmotic pressure is linear with concentration in the case of dilute solutions: $\Pi = RTc_p$ which leads to $D_c = \frac{k_B T}{f_c}$. As concentration increases compressibility decreases, causing faster collective diffusion. On the other side increased particle interactions increase the friction experienced by the macromolecules which acts as a compensation for the osmotic effect which reflects in a concentration independent collective diffusion coefficient. The

self-diffusion coefficient on the other hand is independent of K_{os} and involves only the self-friction coefficient f_s [14].

$$D_s(\tau) = \frac{k_B T}{f_s}$$ (6.2)

The long-time self-diffusion coefficient is what the tracer experiment represents. And the collective diffusion coefficient can be measured using dynamic light scattering. Our purpose here is to show that the collective and self-diffusion coefficients are not equal at non-zero concentration and explain the origin of this observation. Tracer experiments using neutron's sensitivity to isotopic substitution can be used to obtain the self-diffusion coefficient. This will be explained in the experimental section. With this technique we answer the question whether GFP diffusion can be explained by the same theories of colloidal solutions [15, 16]. Where hydrodynamic interactions that are actually mediated by the solvent, play an important role in explaining the diffusion of colloidal particles. Each molecule experiences a hydrodynamic drag in the direction mediated by the neighboring molecules and those hydrodynamic interactions dominate at short times. Whereas direct interactions start evolving during structural relaxation time of the colloids. It is shown that in colloidal solutions the self-diffusion coefficient is not affected by direct interactions and is explained by hydrodynamic interactions while on the other hand collective diffusion is explained by direct interactions[17, 18]. In the following we investigate whether this is correct for GFP solutions at non-zero concentrations.

Macromolecular diffusion which in this case is GFP results in concentration fluctuation which reflects the local density in the solution. Neutron spin echo measures the intermediate scattering

function, $S(q, \tau)$, which is a measure of the intermolecular density fluctuations due to relative protein displacement $r_i - r_j$ [19, 20]:

$$S(q, \tau) = \frac{1}{N} \sum_{ij} \langle exp[-iq.(r_i(\tau = 0) - r_j(\tau))] \rangle \qquad (6.3)$$

where q is the scattering wave vector which is related to the length scale probed through the famous Brag relationship $q = 2\pi/d$. Also τ is the time shift, N is the total number of particles and the brackets $\langle ... \rangle$ is averaging over the initial positions of the particles. With considering the proteins as spherical particles just like in the case of colloidal solutions and without internal degrees of freedom equation (6.3) simplifies to equation (6.4):

$$S(q, \tau) = S(q, 0). \exp[-q^2. D_c. \tau] \qquad (6.4)$$

where the displacement is considered as Gauss distribution with the assumptions made above. S(q,0) donates the static structure factor and D_c is the collective diffusion coefficient that is discussed earlier and goes to D_s when the interparticle interactions are vanished in the case of a static structure factor of 1. Here we are assuming Brownian motion. This means that the collective diffusion coefficient can be found by a simple exponential decay function fit. Following Ackerson [21] , it is also possible to define the hydrodynamic structure factor as $H(q, \tau) = D_c(q, \tau). S(q, 0)/D_0$. Where D_0 is the free particle diffusion coefficient given by:

$$D_0 = \frac{k_B T}{f_0} \qquad (6.5)$$

where f_0 is the protein-solvent friction.

The above approach to find a hydrodynamic factor gives a description of direct and hydrodynamic interactions between protein molecules. This way we will get to know the main origin of reduced mobility and show that it is proposed that not only excluded volume phenomenon. Such computation requires a structure factor, so this is the approach at higher concentrations than what is studied here. For our simple case we will show the deviation from free particle diffusion at infinite dilution D_0.

So as mentioned the self-diffusion coefficient will be evaluated from the tracer experiment which will be explained in the following in more details and the collective diffusion coefficient is found experimentally from dynamic light scattering which gives an experimental approximation of the hydrodynamic radius of the protein.

6.2 Small Angle Neutron Scattering (SANS) and Tracer Experiment

The function of a protein is directly tied to it structure. The structure of protein can be estimated by different methods including NMR, X-ray diffraction and electron[22]. Such experimental techniques lack features which makes neutron scattering more powerful. Such features limitations include the limited small length scales involved, the lack of phase contrast. The main experimental skill used in this work is a tracer sample contrast matched so that the neutron visualizes mostly the self-interactions in the dynamic window of neutron spin echo NSE and to reduce the collective contribution as much as possible. This is achieved upon the isotopic variants of water used. The isotopic sensitivity of neutrons to hydrogen is a powerful tool [23]– with hydrogen (^{1}H) possessing a high incoherent scattering cross section and small negative coherent scattering length; compared to deuterium (^{2}H) which has a small incoherent cross section and a large positive coherent scattering length. The way that these scattering properties manifest into
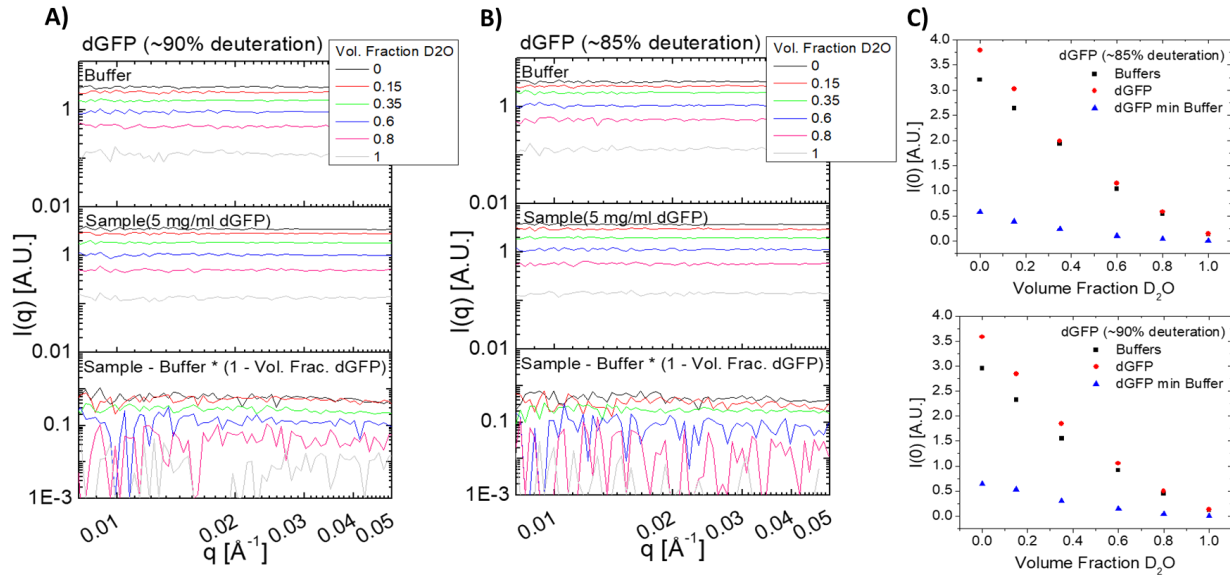
Figure 6.1 Small angle neutron scattering measurements performed on 5 mg/ml GFP in various buffer conditions ranging from 0 to 100%.

Intensity spectra for the buffer and the sample at different buffer conditions. The buffer is subtracted from the sample and scaled by the volume fraction of the protein in the sample. (A) GFP in 90% deuteration (B) GFP in 85% deuteration. (C) Forward scattering I (0) estimated.

scattering experiments differs by the type of neutron scattering measurements being performed.

For the purpose of this work partially deuterated GFP was generated to achieve a contrast match condition as close to 100% D$_2$O as possible. This is confirmed by observing the scattered intensity of natural deuterated GFP at 100% D$_2$O which is reduced to less than 1%. GFP was produced at different culture conditions to optimize contrast. Contrast series measurements were used to finalize the culture conditions that were used in the tracer experiment. The contrast series was performed using shorter measurements at only one low q configuration. This is shown in Figure 6.1.

Small angle neutron scattering was performed on a low concentration of 5 mg/ml GFP in various buffer conditions 0%, 15%, 35%, 60%, 80%, and 100% as shown in Figure 6.1. To estimate the

match point of the deuterated GFP two approaches were used. The first approach considers the forward scattering intensity or the intensity at q=0. The difference between the forward scattering of the sample and the buffer scaled to the volume fraction of the protein in the sample estimated the contribution of the protein to the forward scattering in the sample. As seen in Figure 6.1 the scattered intensity drops predictably with the fraction of D_2O in the sample. indicating contrast is diminished in both deuterated versions of GFP (85% or 90% D_2O culture medium). The second approach used Porod's invariant, q*[24]. This quantity was calculated using an integration range from 0.008 Å^{-1} to 0.04 Å^{-1} and results in a similar observation of steadily decreasing sample contrast at increasing amounts of D_2O in the buffer.

The results of both the approaches are shown in Figure 6.2. The square root of the invariant or I (0) previously obtained are plot against the volume fraction of D_2O in the buffer and a linear fit was used to obtain a null scattering condition for both the cases where the intercept with the x-axis indicated the contrast match point of the deuterated GFP. For the 85% deuterated GFP the match point found is around 0.97 volume fraction of D_2O while for the 90% deuterated GFP the match point was around 100% D_2O. The results were consistent in both the approaches.
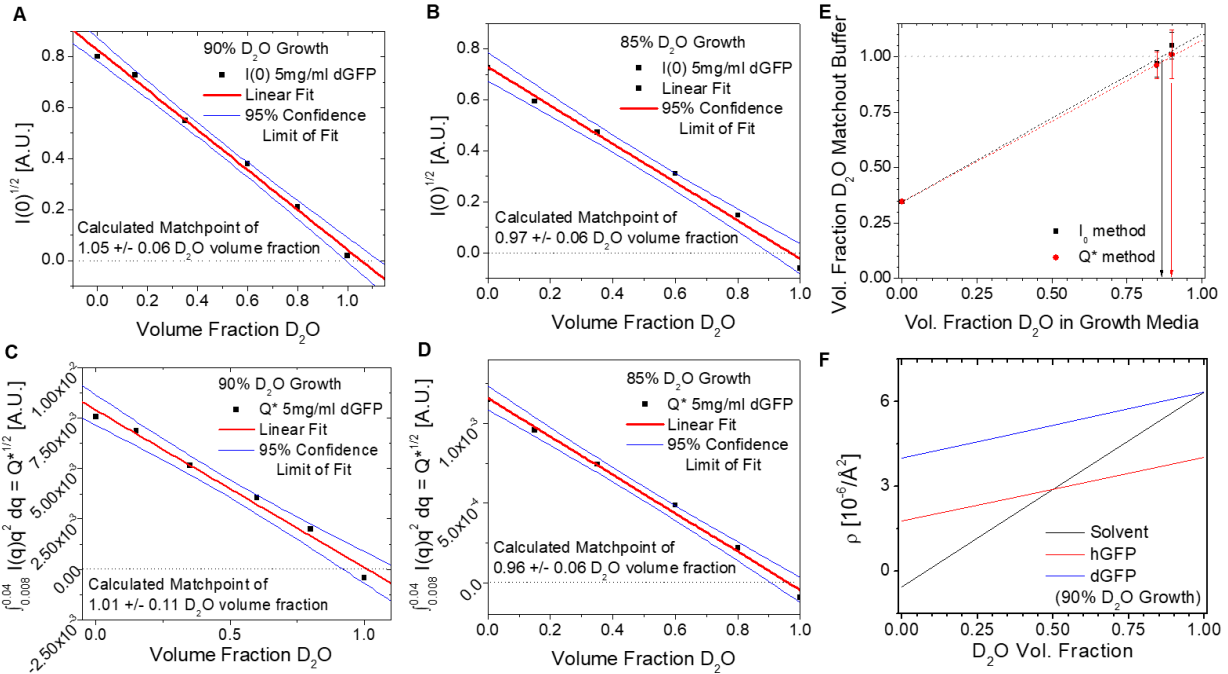
Figure 6.2 Contrast match point analyses for both 85% and 95% deuterated GFP.

(A) Forward scattering approach for 90% growth D_2O. (B) Forward scattering approach for 85% growth D_2O. (C) Porod's invariant approach for 90% growth D_2O. (D) Porod's invariant approach for 85% growth D_2O. (E) Match points for both the method. (F) Scattering length density match point for the 90% D_2O growth GFP.

The growth condition for the study was chosen to be 100% D_2O solvent condition and 95% D_2O growth GFP where the concentration of protein ranged from 5 mg/ml to 25 mg/ml. Table 6.1 shows the samples prepared and the estimated protein volume fractions ϕ_p from dry specific volume of the protein.

Table 6.1 GFP samples prepared and the corresponding volume fractions

Concentration [mg/ml]	ϕ_p [%]
1	0.09
5	0.45
10	0.91
17.5	1.59
25	2.27

Protein solutions were characterized with small angle neutron scattering (SANS). Measurements were carried out at EQ-SANS [25] at the Spallation Neutron Source, Oak Ridge National Laboratory (Tennessee, USA). Over a q-range 0.03-0.45 Å^{-1}. First, it is confirmed that contrast match point is reasonable which is clear in the observed reduced scattering at the 100% D_2O contrast match point of deuterated green fluorescent protein produced in 90% D_2O. This is confirmed also for the 85% growth condition GFP. SANS measurements were also performed at the 35% buffer condition which is the nominal match point for hydrogenated GFP. This is clear in Figure 6.3. Where the results show a clear scattering pattern at 35% D_2O, with the 85% D_2O conditions exhibiting a reduction of the scattered intensity at 35% D_2O buffer. This is expected as there will be more hydrogen in this version of the deuterated protein. Both samples showed drastically reduced scattering at 100% D2O, which is near their match-point.
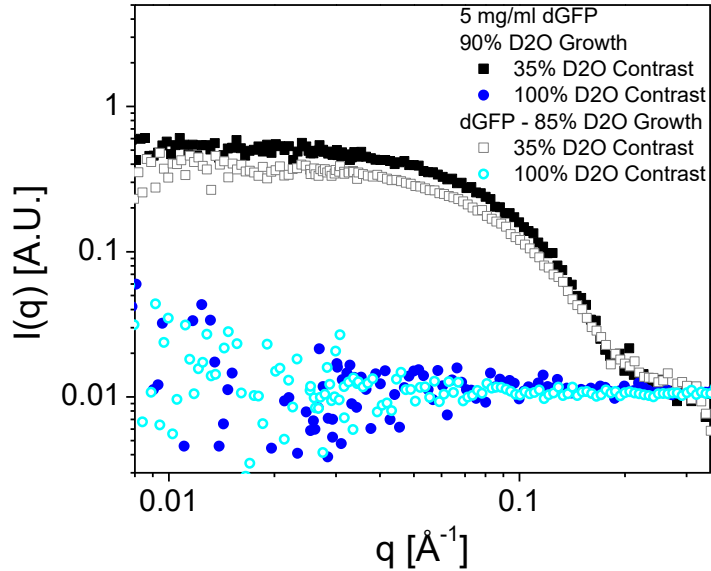
Figure 6.3 Small angle neutron scattering of GFP solutions at different D_2O contrast. Measurements are performed at 290 K.

For structural analysis the spectra of 90% deuterated GFP with a concentration of 5 mg/ml was fitted with SASview suite [26]. The molecular weight was previously estimated by Perticaroli and others to be 29.8 kDa [27]. The spectra were fitted using the elliptical cylinder fit and it resulted in a height of 53.5 ± 1.1 Å with one major radius of 19.6 ± 0.9 Å and a minor radius of 13.6 ± 0.6 Å. This is in good consistency with previous SANS measurements on GFP solution [27]. The results are shown in Figure 6.4.
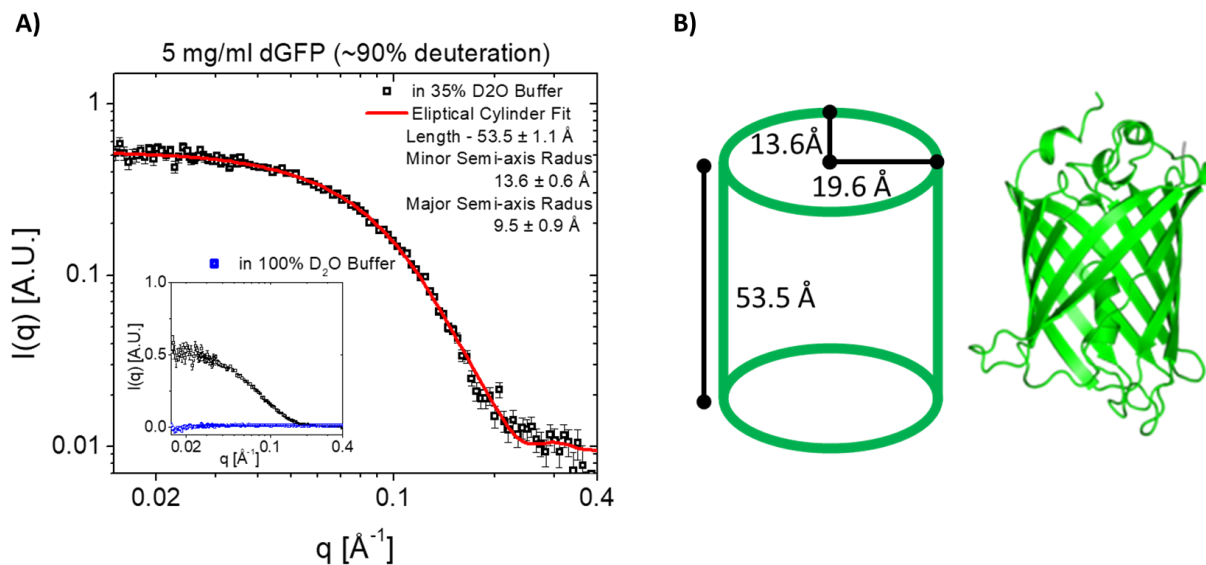
Figure 6.4 Elliptical Cylinder fit on dGFP SANS spectra gives consistent results with previous work [27]. (A) solution scattering from dGFP at 35% buffer was found to be well modeled using elliptical cylinder. (B) dimensions of the elliptical cylinder fitted to GFP.

SANS measurements were also performed on hydrogenated version of GFP which was produced using only natural abundance water. This version presents a strong contrast at the 100% D_2O condition which will be used to see the diffusion at the series of concentrations shown in Table 6.1. So, varying the amount of hydrogenated GFP and deuterated GFP at 100% D_2O is the key tool in the tracer diffusion experiment studied in neutron spin echo measurements. Where in the tracer experiment only 5 mg/ml will be used as hydrogenated GFP while the rest of the concentration will be filled using the deuterated GFP which is not visible to neutrons due to the contrast match at 100 D_2O. This way the collective contribution will be greatly minimized. The samples measured were the concentration shown in Table 6.1. With one set of data using all hydrogenated GFP while the second set uses only 5 mg/ml of the total concentration as hydrogenated GFP visible at 100 D_2O. SANS performed on the samples are shown in
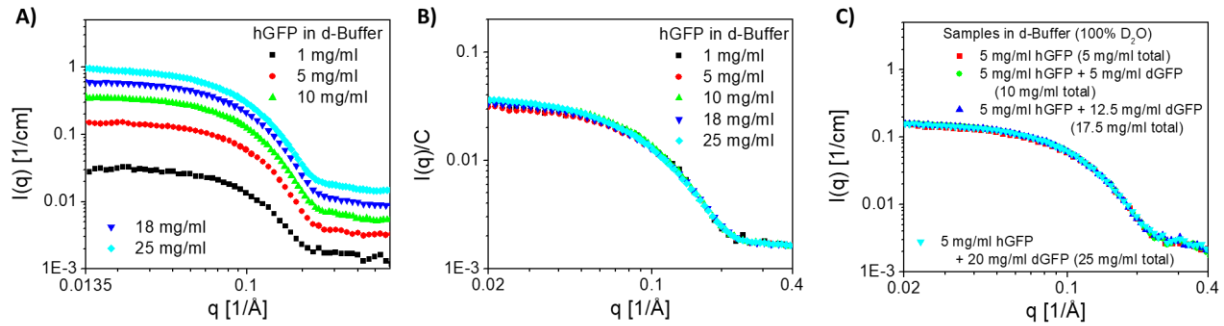
Figure 6.5.

Figure 6.5 SANS measurements at different GFP samples and concentrations.
A) hydrogenated GFP at 100% D_2O, clearly shows increase in the intensity with concentration. B) hydrogenated GFP normalized to concentration. C) Samples used in the tracer experiment clearly shows that the contribution to the intensity is not altered with the increase of deuterated GFP in the sample.

The results clearly show that the intensity of the spectra increases with the amount of hydrogenated GFP used and that deuterated GFP can be used as a crowder without contributing to the intensity of the NSE measurement.

6.3 Obtaining the Self-Diffusion Coefficient using Neutron Spin Echo (NSE)

The mentioned mixture of samples was studied for the diffusion of GFP in solution using neutron spin echo. So, we have utilized Neutron Spin Echo (NSE) to measure GFP dynamics as a function of concentration in two set of data. Both the data are the same concentration range, the only variation is that in the second measurement only 5 mg/ml of GFP was used in the hydrogenated form to be used as a tracer experiment to observe only indirect interactions or self-interactions. Measurements were carried out at the Spallation Neutron Source, Oak Ridge National Laboratory (Tennessee, USA). Over a q-range 0.05-0.16 $Å^{-1}$ covering length scales where only self-interactions are observed at the higher q range. NSE is an ideal method to describe these motions, which occur at 10's to 100's of nanosecond timeframe.
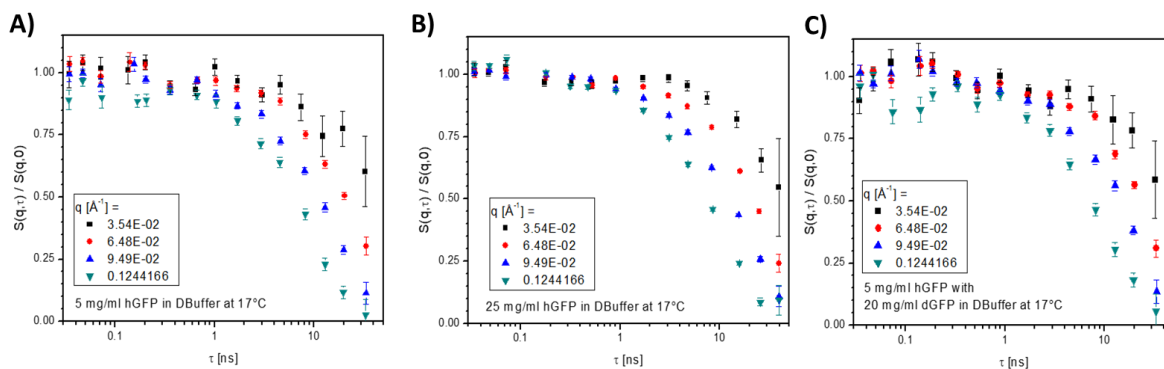
Figure 6.6 Normalized intermediate scattering function of GFP on a log time scale measured with neutron spin echo.

A) 5 mg/ml hGFP B) 25 mg/ml hGFP C) mixture of 5 mg/ml hGFP and 20 mg/ml dGFP. Each sample shows a clear exponential decay with the time constant of the decay deceasing as a function of q.

Figure 6.6 displays the normalized intermediate scattering function $S(q,\tau)/S(q)$ of selected samples. The diffusion coefficient was estimated using equation 6.4. The resultant long time diffusion coefficient is displayed in Figure 6.7. It is clear that the diffusion coefficient increases with decreasing q while above q= 0.09 Å^{-1} a plateau is reached. This is an indication that only self-interactions is observed and an average above q= 0.09 Å^{-1} can be used to estimate the self-diffusion coefficient of GFP. This is taken from the tracer set of experiment where the collective contribution is minimized. We believe that any collective contribution is negligible this is clearly seen in Figure 6.8 where the difference between the 10 mg/ml h-GFP diffusion coefficient and 5 mg/ml h-GFP + 5 mg/ml d-GFP shows no difference. This is an indication that the collective

contribution from the excess 5 mg/ml h-GFP is negligible and hence the tracer experiment shows

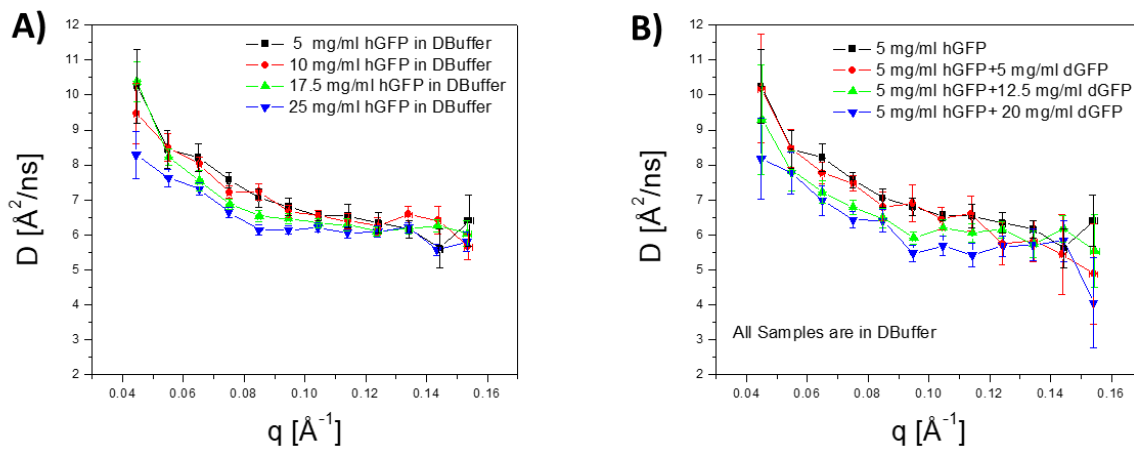solely self-interactions which will be explained by hydrodynamic interactions in the next section.

Figure 6.7 Diffusion coefficients obtained from NSE for all samples.

A) hydrogenated GFP with high contrast at 100% D_2O shows higher diffusion coefficient, this is reasonable due to the higher contribution from the collective interactions in agreement with SANS higher intensity. B) Tracer experiment where it shows lower diffusion coefficient, and the plateau is the self-diffusion coefficient since collective contribution is vanished at high q values.
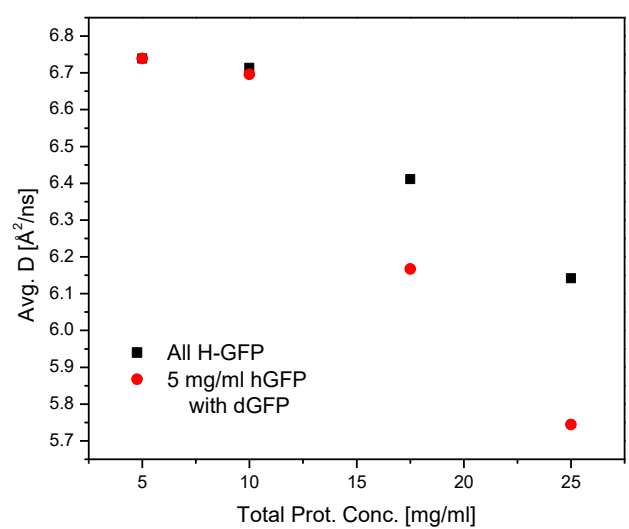

Figure 6.8 Diffusion coefficients obtained from averaging above q= 0.09 $Å^{-1}$.

The tracer diffusion coefficient is the self-diffusion coefficient with minimum contribution from collective interactions. The diffusion coefficient from hydrogenated GFP shows a higher value at higher concentration this is due to higher contribution to the intensity just as observed from SANS and reflects direct interactions that start showing at higher concentrations.

it is also clear that the difference seen in the diffusion coefficient between the tracer and the fully hydrogenated GFP is scaling with concentration difference in h-GFP in the sample. This is not seen at the difference of only 5 h-GFP for the total of 10 mg/ml measurements which make us more confident to assign the diffusion coefficient from the tracer experiment to be solely the self-diffusion coefficient of GFP. The reason for the observed higher diffusion coefficient in the fully hydrogenated GFP even at high q values is due to the increased rotational motions which as mentioned in previous chapters is coupled with the translational motion of the protein.

6.4 Dynamic Light Scattering DLS to Obtain the Diffusion Coefficient at Infinite Dilution

Dynamic light scattering was performed on very dilute samples of 0.6 mg/ml of dGFP and 0.5mg/ml of hGFP to observe the scattered intensity varying with the same time scale as the motions of the solutes in the solution owing to Brownian motion. The excess polarizability by the concentration fluctuation, where the intensity fluctuation can be measured. The characteristic relaxation rate τ_C for the concentration fluctuation is related to the diffusion coefficient $\tau_c = K^2 D_c$ [28], where the scattering field amplitude is proportional to the concentration fluctuation. The free particle diffusion coefficient was found to be 8.915 $\pm$1.8 Å^2 ns^{-1} for the hGFP and 6.72$\pm$ 0.65 Å^2 ns^{-1} for the dGFP. The hydration shell was taken into account for the volume fraction occupied by the protein to estimate the protein volume fraction. This is done by considering the water molecules perturbed in the first and second shell around GFP evaluated in quasielastic previous study. Where it was found that 1706 water molecules are within two hydration shells

around GFP. If we consider, the addition to the protein's volume due to the water molecules moving along with it. We obtain a higher volume fraction through $v_h = v_d + \delta v_s$. Where, v_h is the hydrodynamic specific volume of GFP, v_d is the dry specific volume of GFP, v_s is the specific volume of D$_2$O and δ is the fraction of water contributing to the protein's volume. This yields to an increase in volume fraction of GFP of 2.15 and an estimation of the hydrodynamic radius to be around 2.85 nm with great agreement with literature value of 2.82 nm[29]. The following table shows the adjusted volume fraction of GFP which is necessary to be compared with colloidal particles theories of lager size. Introducing this normalization will reduce the discrepancy observed between theoretical and experimental values of long-time self-diffusion coefficient of colloidal protein solutions. Table 6.2 shows the adjusted polymer volume fractions.

Table 6.2 GFP samples prepared and the corresponding volume fractions including the hydration shell

Concentration [mg/ml]	ϕ_p [%]
1	0.195
5	0.976
10	1.952
17.5	3.416
25	4.879

6.5 Comparison of D_s and D_c

Figure 6.9 shows the normalized $\frac{D_s}{D_0}$ where D_0 the free particle diffusion coefficient at infinite dilution was found in the previous section. The collective diffusion coefficient at this concentration range is basically equal to the free-particle diffusion coefficient and even at higher volume fractions/concentrations it will decrease by a slight factor for the osmotic compensation explained in the first section of this chapter. It is obvious that the self-diffusion diverges with increasing protein volume fraction. Where the collective diffusion coefficient decreases only slightly in a linear dependence, a roughly exponential decrease is observed for the self-diffusion coefficient. The small dependence of the collective or mutual diffusion coefficient is explained by the compensation of osmotic and friction effects. The osmotic compressibility is known to decline in parallel with the tracer or self-diffusion coefficient for similar studies on hemoglobin and myoglobin [30] with a slight difference which reflects the nonequivalence of the self and collective friction factors.
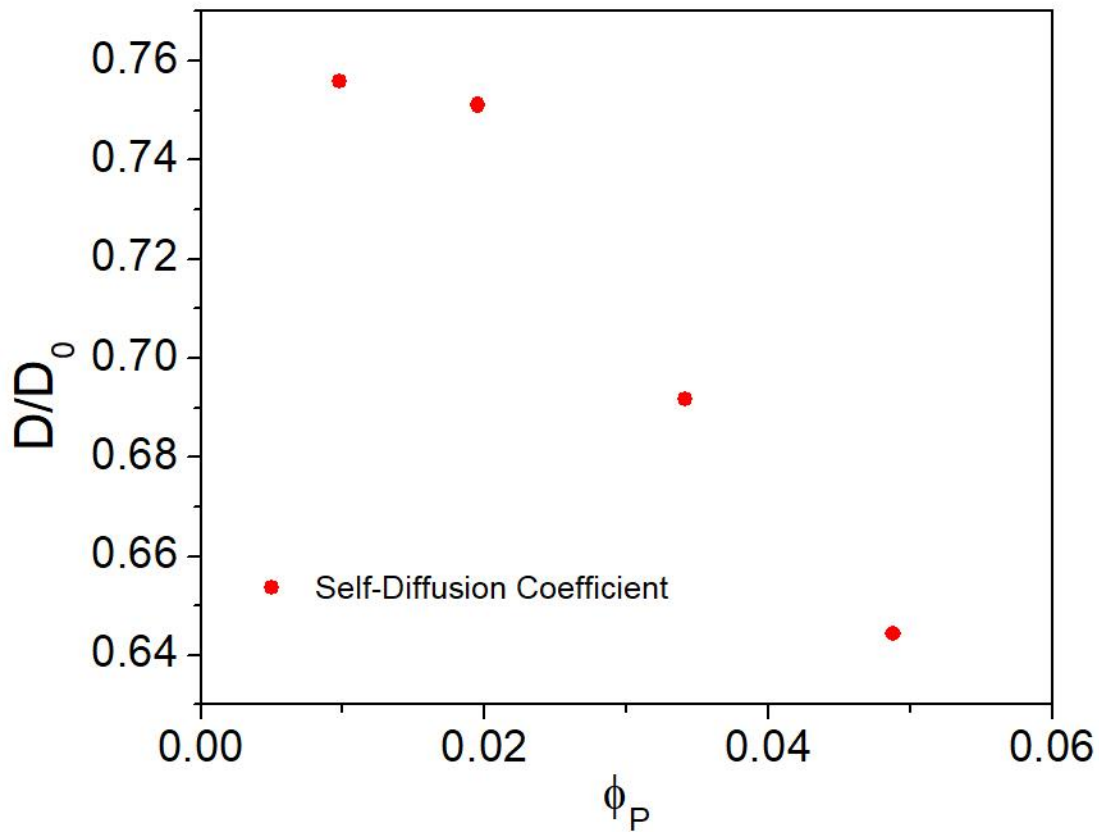
Figure 6.9 Reduction in the self-diffusion coefficient of GFP as a function of volume fraction.

These results are consistent with work done on other proteins like haemoglobin in red blood cells.

The results obtained from the study are shown in Figure 6.10 Collective and Self-Diffusion coefficients for haemoglobin in red blood cells [34]. . In each case there is a linear decrease in the collective diffusion coefficient as concentration increases and the decrease is much less than that found in measurements for tracer diffusion which reflects the self-diffusion coefficient [31-33]. It is clear that even at low concentrations D_s shows a deviation from D_0 which is an indication of the long-range interactions known as the hydrodynamic interactions. At this low concentration we are
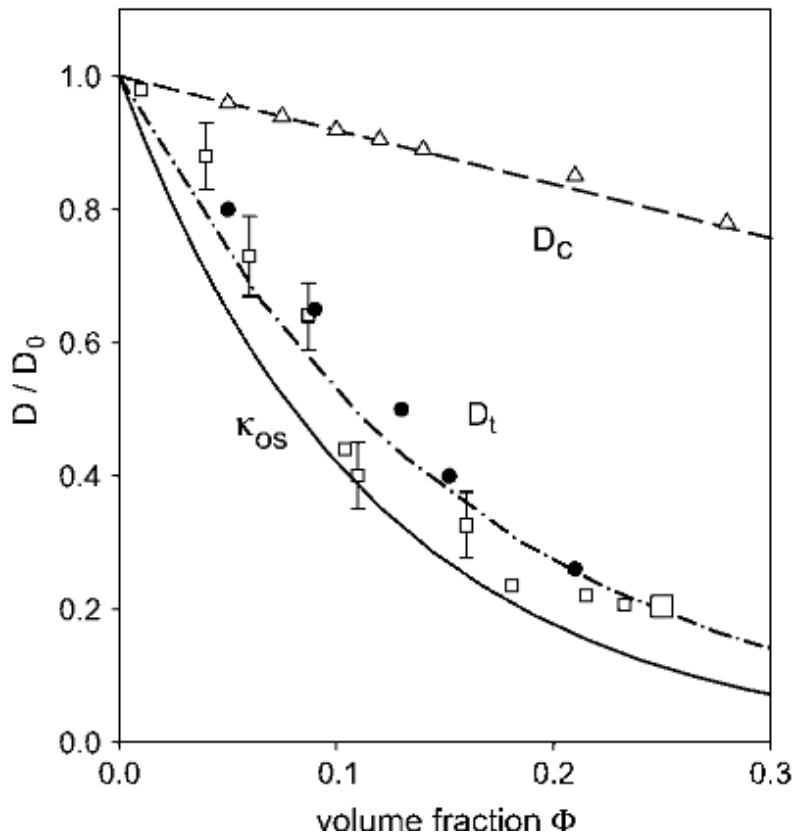
Figure 6.10 Collective and Self-Diffusion coefficients for haemoglobin in red blood cells [34].

also expecting minimum direct interactions. At higher concentrations which is used to study the environment in cytoplasm and human cells where it is crowded by a volume fraction of around 30-40% [9, 35, 36]we are expected to see even further deviation and reduction in self-diffusion coefficient which is assigned to hydrodynamic interactions [37] which is well explained by the colloidal Brownian motion dynamics with hydrodynamic interactions [38]. The collective diffusion shows a much less deviation from D_0 due to the compensation by osmotic pressure and higher concentrations. In the tracer experiment all other molecules act as obstacles which is a good comparison with the reduction of the diffusion coefficient of globular proteins in living cells [39-41] which not only reduces the rate of diffusion but also been proved to induce a sub diffusive

behavior seen at small times to diffusive behavior seen at larger times[42, 43]. Protein being

structurally different from nano colloids where proteins are defined as macromolecules with non

spherical shape and nonhomogeneous topology. Therefor it is a challenge to colloid theory [44].

But it has been proven that considering a protein as a sphere with equivalent radius in simulations

results in reasonable approximation to its diffusion coefficient[39]. The dynamics of a colloidal

suspension is explained by diffusion which occurs at different time scales with corresponding

different regime of diffusion [38]. In real systems where direct interactions give rise to additional

time scales, hydrodynamic interactions are seen on time scales τ_{HI} greater than the diffusive

time scale of the dissolved particles τ_P where it depends on the colloidal volume fraction and the

solvent density where this is the short time diffusive regime. On higher time scales of τ_I where

structural relaxation time where direct interactions are seen and found to affect the long-time

center of mass diffusion. This clearly suits well in explaining the reduction in the self-diffusion

coefficient where we know we are only seeing self-interaction where the structure factor is equal

to 1 and collective interactions are vanished at high q values above the structure factor maximum

peak. One main consideration to be addressed when explaining proteins using colloidal theory is

mapping the protein on an effective sphere [45]. The resultant actual radius has to be larger than

R (the radius of equivalent sphere) due to hydration shell surrounding the protein that increase

the size of the protein. When we took into account the hydration shell water molecules to be

contributing to the volume fraction of the protein the experimental reduction in the self-diffusion

coefficient agreed very well with the normalized self-diffusion coefficient of non charged

colloids[16]. Where, hydrodynamic interactions is the main origin in explaining the dynamics of

concentrated hard sphere suspensions for the whole time range where local hydrodynamic

interactions dominate at short time and non local hydrodynamic interactions arise at longer times and direct interactions are dramatically reduced by hydrodynamic interactions[16, 46]. This clears the concept of reduced mobility in crowded solutions.

6.6 Conclusion

We have clearly demonstrated the different dependence of the collective and self-diffusion coefficient of GFP on concentration. Which can be explained by concepts developed for colloidal suspensions. The main consideration to be addressed here is the difference in effective volume fractions which was normalized by taking into consideration the volume of water molecules in the hydration shell. The conclusion reached here that the reduction in the self-diffusion coefficient of GFP is explained by hydrodynamic interactions just like the case of non charged spherical colloidal suspensions. This conclusion is based on the fact of the greater reduction in the tracer diffusion coefficient where direct interactions are believed to be neglected and the fact that this is more in the dilute regime and direct interactions are not developed and only long-range interactions are dominating (hydrodynamic interactions). On the other hand, the collective diffusion coefficient where it is known to be controlled by direct interactions is nearly independent on concentration which is explained by the osmotic compensation. This is constant value of D_c is also seen in hard sphere colloids at short times where hydrodynamic interactions dominate. This concluded that the collective diffusion coefficient is controlled by direct interactions while the self-diffusion coefficient is controlled by long range hydrodynamic interactions.

References

1. Schnell, S. and T. Turner, *Reaction kinetics in intracellular environments with macromolecular crowding: simulations and rate laws.* Progress in biophysics and molecular biology, 2004. **85**(2-3): p. 235-260.

2. Grasberger, B., et al., *Interaction between proteins localized in membranes.* Proceedings of the National Academy of Sciences, 1986. **83**(17): p. 6258-6262.

3. Medalia, O., et al., *Macromolecular architecture in eukaryotic cells visualized by cryoelectron tomography.* Science, 2002. **298**(5596): p. 1209-1213.

4. Krapf, D., *Mechanisms underlying anomalous diffusion in the plasma membrane.* Current topics in membranes, 2015. **75**: p. 167-207.

5. Verkman, A.S., *Solute and macromolecule diffusion in cellular aqueous compartments.* Trends in biochemical sciences, 2002. **27**(1): p. 27-33.

6. Hrabe, J., S. Hrabětová, and K. Segeth, *A model of effective diffusion and tortuosity in the extracellular space of the brain.* Biophysical journal, 2004. **87**(3): p. 1606-1617.

7. Krueger, S. and R. Nossal, *SANS studies of interacting hemoglobin in intact erythrocytes.* Biophysical journal, 1988. **53**(1): p. 97-105.

8. Meinecke, L., *Multiscale modeling of diffusion in a crowded environment.* Bulletin of mathematical biology, 2017. **79**(11): p. 2672-2695.

9. Ellis, R.J., *Macromolecular crowding: an important but neglected aspect of the intracellular environment.* Current opinion in structural biology, 2001. **11**(1): p. 114-119.

10. Ellis, R.J., *Macromolecular crowding: obvious but underappreciated.* Trends in biochemical sciences, 2001. **26**(10): p. 597-604.

11. Hall, D. and A.P. Minton, *Macromolecular crowding: qualitative and semiquantitative successes, quantitative challenges.* Biochimica et Biophysica Acta (BBA)-Proteins and Proteomics, 2003. **1649**(2): p. 127-139.

12. Edward, J.T., *Molecular volumes and the Stokes-Einstein equation.* Journal of chemical education, 1970. **47**(4): p. 261.

13. Schmitz, K.S., *Introduction to dynamic light scattering by macromolecules*. 2012: Elsevier.

14. Leaist, D. and L. Hui, *Intradiffusion coefficients and integral mutual diffusion coefficients of dilute associating solutes are identical: caffeine in water.* Journal of physical chemistry, 1990. **94**(24): p. 8741-8744.

15. Beenakker, C. and P. Mazur, *Diffusion of spheres in a concentrated suspension II.* Physica A: Statistical Mechanics and its Applications, 1984. **126**(3): p. 349-370.

16. Tokuyama, M. and I. Oppenheim, *Dynamics of hard-sphere suspensions.* Physical Review E, 1994. **50**(1): p. R16.

17. Segre, P. and P.N. Pusey, *Dynamics and scaling in hard-sphere colloidal suspensions.* Physica A: Statistical Mechanics and its Applications, 1997. **235**(1-2): p. 9-18.

18. Van Blaaderen, A., et al., *Long-time self-diffusion of spherical colloidal particles measured with fluorescence recovery after photobleaching.* The Journal of chemical physics, 1992. **96**(6): p. 4591-4603.

19. Dhont, J.K., *An introduction to dynamics of colloids*. 1996: Elsevier.

20. Fitter, J., T. Gutberlet, and J. Katsaras, *Neutron scattering in biology: techniques and applications*. 2006: Springer Science & Business Media.

21. Ackerson, B.J., *Correlations for interacting Brownian particles.* The Journal of Chemical Physics, 1976. **64**(1): p. 242-246.

22.   Wiencek, J., *New strategies for protein crystal growth.* Annual review of biomedical engineering, 1999. **1**(1): p. 505-534.

23.   Meilleur, F., K.L. Weiss, and D.A. Myles, *Deuterium labeling for neutron structure-function-dynamics analysis*, in *Micro and Nano Technologies in Bioanalysis*. 2009, Springer. p. 281-292.

24.   Glatter, O., O. Kratky, and H. Kratky, *Small angle X-ray scattering*. 1982: Academic press.

25.   Zhao, J., C.Y. Gao, and D. Liu, *The extended Q-range small-angle neutron scattering diffractometer at the SNS.* Journal of Applied Crystallography, 2010. **43**(5): p. 1068-1077.

26.   Butler, P., et al., *SASView for Small Angle Scattering Analysis.* There is no corresponding record for this reference, 2013.

27.   Perticaroli, S., et al., *Description of hydration water in protein (green fluorescent protein) solution.* Journal of the American Chemical Society, 2017. **139**(3): p. 1098-1105.

28.   Langowski, J., W. Kremer, and U. Kapp, *[21] Dynamic light scattering for study of solution conformation and dynamics of superhelical DNA*, in *Methods in enzymology*. 1992, Elsevier. p. 430-448.

29.   https://bionumbers.hms.harvard.edu/bionumber.aspx?s=n&v=0&id=104396.

30.   Hall, R.S. and C.S. Johnson Jr, *Experimental evidence that mutual and tracer diffusion coefficients for hemoglobin are not equal.* The Journal of Chemical Physics, 1980. **72**(7): p. 4251-4253.

31.   Jones, C.R., C.S. Jhonson Jr, and J.T. Penniston, *Photon correlation spectroscopy of hemoglobin: Diffusion of Oxy-HbA and Oxy-HbS.* Biopolymers: Original Research on Biomolecules, 1978. **17**(6): p. 1581-1593.

32.   Alpert, S.S. and G. Banks, *The concentration dependence of the hemoglobin mutual diffusion coefficient.* Biophysical chemistry, 1976. **4**(3): p. 287-296.

33.   Veldkamp, W.B. and J.R. Votano, *Effects of intermolecular interaction on protein diffusion in solution.* The Journal of Physical Chemistry, 1976. **80**(25): p. 2794-2801.

34.   Doster, W. and S. Longeville, *Microscopic diffusion and hydrodynamic interactions of hemoglobin in red blood cells.* Biophysical journal, 2007. **93**(4): p. 1360-1368.

35.   Wong, I., et al., *Anomalous diffusion probes microstructure dynamics of entangled F-actin networks.* Physical review letters, 2004. **92**(17): p. 178101.

36.   Zimmerman, S.B. and A.P. Minton, *Macromolecular crowding: biochemical, biophysical, and physiological consequences.* Annual review of biophysics and biomolecular structure, 1993. **22**(1): p. 27-65.

37.   Roosen-Runge, F., et al., *Protein self-diffusion in crowded solutions.* Proceedings of the National Academy of Sciences, 2011. **108**(29): p. 11815-11820.

38.   Ermak, D.L. and J.A. McCammon, *Brownian dynamics with hydrodynamic interactions.* The Journal of chemical physics, 1978. **69**(4): p. 1352-1360.

39.   Ando, T. and J. Skolnick, *Crowding and hydrodynamic interactions likely dominate in vivo macromolecular motion.* Proceedings of the National Academy of Sciences, 2010. **107**(43): p. 18457-18462.

40.   Wojcieszyn, J.W., et al., *Diffusion of injected macromolecules within the cytoplasm of living cells.* Proceedings of the National Academy of Sciences, 1981. **78**(7): p. 4407-4410.

41.   Arrio-Dupont, M., et al., *Translational diffusion of globular proteins in the cytoplasm of cultured muscle cells.* Biophysical journal, 2000. **78**(2): p. 901-907.

42.   Banks, D.S. and C. Fradin, *Anomalous diffusion of proteins due to molecular crowding.* Biophysical journal, 2005. **89**(5): p. 2960-2971.

43.   Saxton, M.J., *Anomalous diffusion due to obstacles: a Monte Carlo study.* Biophysical journal, 1994. **66**(2): p. 394-401.

44.   Piazza, R., *Protein interactions and association: an open challenge for colloid science.* Current opinion in colloid & interface science, 2004. **8**(6): p. 515-522.

45.   Jennings, B. and K. Parslow, *Particle size measurement: the equivalent spherical diameter.* Proceedings of the Royal Society of London. A. Mathematical and Physical Sciences, 1988. **419**(1856): p. 137-149.

46.   Strating, P*., Brownian dynamics simulation of a hard-sphere suspension.* Physical Review E, 1999. **59**(2): p. 2175.

Chapter 7 : Conclusions and Other Neutron Scattering Work

7.1 Conclusions and summary of findings

My dissertation resulted to many valuable findings and estimations, serves as a full data base for research with aqueous solutions. This work focused on both the solvent and the solute from structural and dynamical prospective. Neutron scattering was the main tool I used in estimating important properties of the systems I studied.

The following is a summary of my specific findings:

1) I have successfully experimentally illustrated using neutron and light scattering methods the timescale of bulk viscosity in liquid water at a temperature range of 280-303K and provided a description of the associated molecular relaxation. This can be summarized in few main points as:

   ➢ The timescale observed for bulk viscosity is on the order of 1-2ps.

   ➢ A connection between rotational motions on the length scale of the first sharp diffraction peak for neutrons and the viscous response to volume change was illustrated.

   ➢ A clear comparison to the molecular motions associated with the shear viscous response is shown. Where the motions associated with the bulk viscous response are 2-3 times slower.

   ➢ The dynamics of bulk water were studied on three different temperatures 280,290 and 303K.

- ➤ Properties like the speed of sound, bulk modulus, and bulk viscosity in H_2O and D_2O were estimated at a range of temperature of (7-50 ℃).

- ➤ It was shown that bulk viscous response is associated with local density fluctuations while shear viscous response is most closely associated with changes in water network connectivity.

2) I have successfully prepared a multi-arm PEG hydrogel and studied its structure in detail along with the water dynamics in the system as two populations: bulk and hydration water. The change in apparent viscosity due to the presence of polymer was estimated. Main findings are:

- ➤ A multi arm PEG hydrogel network was prepared from a 4 arm-PEG thiol and an 8 arm PEG Norbornene from a range of initial polymer volume fractions of (0.036-0.286) and a full swelling study was done in both water and PBS.

- ➤ Shear Modulus, Longitudinal Modulus and the Young Modulus were estimated for both in water and PBS.

- ➤ The mesh sizes and polymer volume fraction at fully swollen equilibrium were estimated. The mesh size ranged from 7 to 2.4 nm.

- ➤ The persistence length of the polymer chain was found to decrease with increasing polymer volume fraction.

- ➤ The dynamics of the polymer were found to follow the Zimm dynamics for dilute polymer solutions.

➢ The water dynamics were classified into two different population and the corresponding diffusive behavior were illustrated.

➢ The change in apparent viscosity due to the polymer was calculated using a unitless specific viscosity parameter and it was found to be 1.85. This is assigned to the increase in immobility of the hydration water population.

➢ A unique experimental prove of non-ergodicity in hydrogels was established.

➢ The number of water molecules perturbed per PEG monomer was found to be 8 to 9 water molecules and the amount of perturbation was found to be around 2.

➢ MD simulations with collaborators was obtained to reinforce my findings.

3) I have studied the dynamics of Green Fluorescent Protein solution in a tracer experiment to observe the reduction in self-diffusion coefficient and explain in it in colloidal theories where hydrodynamic interactions control the self-diffusion coefficient. This work had interesting results and findings:

➢ The structure of GFP was found to be well explained by an elliptical cylinder model and results in a height of 53.5 Angstroms and a major radius of 19.6 Angstroms and a minor radius of 13.6 Angstroms.

➢ A tracer experimental approach was successfully done where isotopic sensitivity of neutrons was used to have a contrast match GFP solution invisible to the neutrons.

- The diffusion coefficient of GFP was estimated as a function of protein volume fraction and this was normalized to a hydrodynamic radius using perturbed water molecules in the first two hydration shells. A hydrodynamic radius of 2.85 nm was found with great agreement with literature.

- The reduction in self-diffusion coefficient was explained by the hydrodynamic interactions theories from colloidal solutions.

- The free-particle diffusion coefficient at infinite dilution was found using dynamic light scattering.

This work clearly showed the importance of studying the hydration/perturbed population of the solution where it plays an important role in explaining the increase in apparent viscosity due to the solute-solvent interactions. The immobility of water molecules around solutes results in increased viscosity. The perturbed water molecules contribute to the hydrodynamic volume of the solute. The PEG hydrogels project is being left with a full description of the dynamics and the structural parameters required in applications of PEG hydrogels. The GFP project serves as a prove for the influence of hydrodynamic interactions on the diffusivity of the solute. The size of the protein used in the study and the volume fractions suit well for a future study of solute diffusion with the PEG hydrogel network studied where the mesh sizes serve as a good channel for the diffusion of GFP in it where it can be used as a model of solute diffusion in such network.

7.2 Future work

My suggestions as to the future of this project would be on the applications of a such well-studied system of PEG hydrogels. Where it can be used as a system to study protein diffusion in the

system. I believe GFP can be used as a good protein to check the diffusivity of a solute in the well-studied PEG hydrogel system in this dissertation. Where a combination of the fifth and sixth chapters of this dissertation serve as a database for all the analysis needed. I believe we will observe a diffusion coefficient dependent on the apparent viscosity found in this dissertation. Both neutron spin echo NSE and SANS can be used to see the diffusion coefficient of GFP in the hydrogel. It will be useful to observe whether the diffusion coefficient will always be dependent on the apparent viscosity or will there be a cross over from a diffusion coefficient dependent on the apparent viscosity to a diffusion coefficient where the protein experiences hydrodynamic interactions with the polymer at length scales beyond the mesh sizes. My other suggestion is to study the GFP protein solution at higher volume fractions to be able to extract a hydrodynamic factor.

7.3 Other work

During my PhD studies I have had the opportunity to participate in several other projects which have resulted in or will result in peer reviewed publication. While these are not germane to my proposed thesis work, they do represent work at the University of Cincinnati during my doctoral studies.

- Lipid Rafts: Buffers of Cell Membranes Physical Properties [1]:

  Lipid rafts are considered as platforms for proteins in cells. In this work another role of lipids rafts was proposed and demonstrated by means of molecular simulations and neutron scattering. It was found that lipid rafts can stabilize the physical properties of the membrane with changes in temperature.
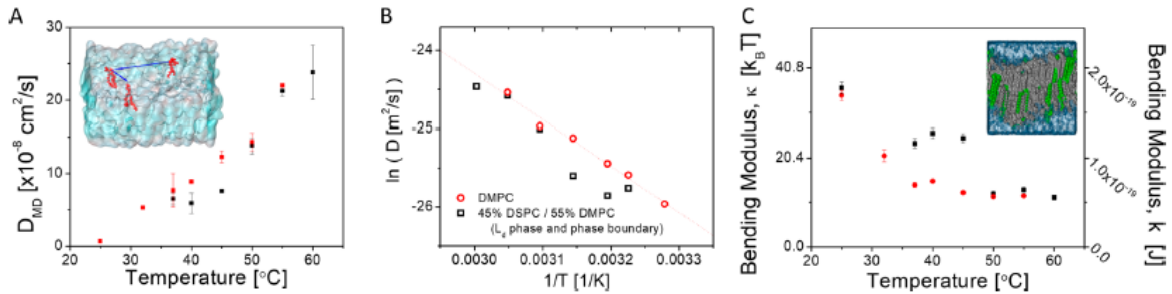
Figure 7.1 Lateral diffusion coefficient and bending modulus obtained from MD Simulations for DMPC and DMPC/DSPC mixtures representing the fluid boundary composition.
(A) a plateau in the lateral diffusion coefficient between 35 and 45 °C. **(B)** An Arrhenius plot demonstrates the effect of compositional changes. **(C)** The bending modulus exhibits a decrease with temperature while it shows a plateau for the temperature range of coexistence.

The idea rises from the fact that the membrane composition itself controls the viscous and mechanical properties of the bilayer of the membrane. Due to different melting points of the lipids in the membrane, the composition is dependent on temperature depending on the movement of high or low melting points membrane components. So, this allows the lipid rafts to be functioning as buffers for the membrane physical properties by basically varying the changes in the environment through changes in composition. This is seen as a higher melting point lipid portioning to the fluid phase when temperature is increased; this results in higher bending modulus and viscosity. To give an insight of how this buffering phenomena, neutron scattering technique along with molecular dynamics simulations were performed on a phase separated model membrane. The observed outcomes demonstrated the buffering effect seen in both the bending modulus and the lateral diffusion coefficient of the fluid phase when temperature is changed. The work was published, and the results are shown in Figure 7.1 [1]:

The clear plateau in both the lateral diffusion and the bending modulus in the case of phase coexistence is shown in Figure 7.1. This clearly shows the temperature dependent buffering effect of the phase separated lipid bilayers. Our group also performed experimental observation of the lateral diffusion coefficient using neutron spin echo technique as a coherent inelastic neutron scattering to observe the collective motions of the bilayer structure and/or the lipids. The observed experimental quantity is the intermediate scattering function which shows us the fraction of pair correlations in the system still existing after a certain probing time. The expected shape is an exponential decay due to the less correlations still existing at the longer times. The diffusion coefficients were obtained by multiplying the constant extracted from the exponential decay by the square of the length scale probed. The results agree with the simulations and highlight a deviation from the usual Arrhenius behavior at temperature below the coexisting temperature.

- Acetone Diffusion in Nafion [Presented to Collaborators]:

Quasielastic neutron scattering measurements were performed on Acetone by itself and in Nafion and Vanillic acid treated Nafion polymer materials. For liquid acetone, a typical three component fit in the intensity versus energy spectra obtained from BASIS was utilized. It consists of a vanadium spectrum representing the elastic scattering, a quasielastic spectra modeled by a Lorentzian fit, and a flat background was utilized to represent thermal background and fast dynamics beyond BASIS window. A q^2 dependence in the half-width at half max of the Lorentzian function was observed. From the observed linewidths, the full width at half max (FWHM) of the Lorentzian function can be converted to the time domain via Plank's constant, $\hbar$. The diffusion
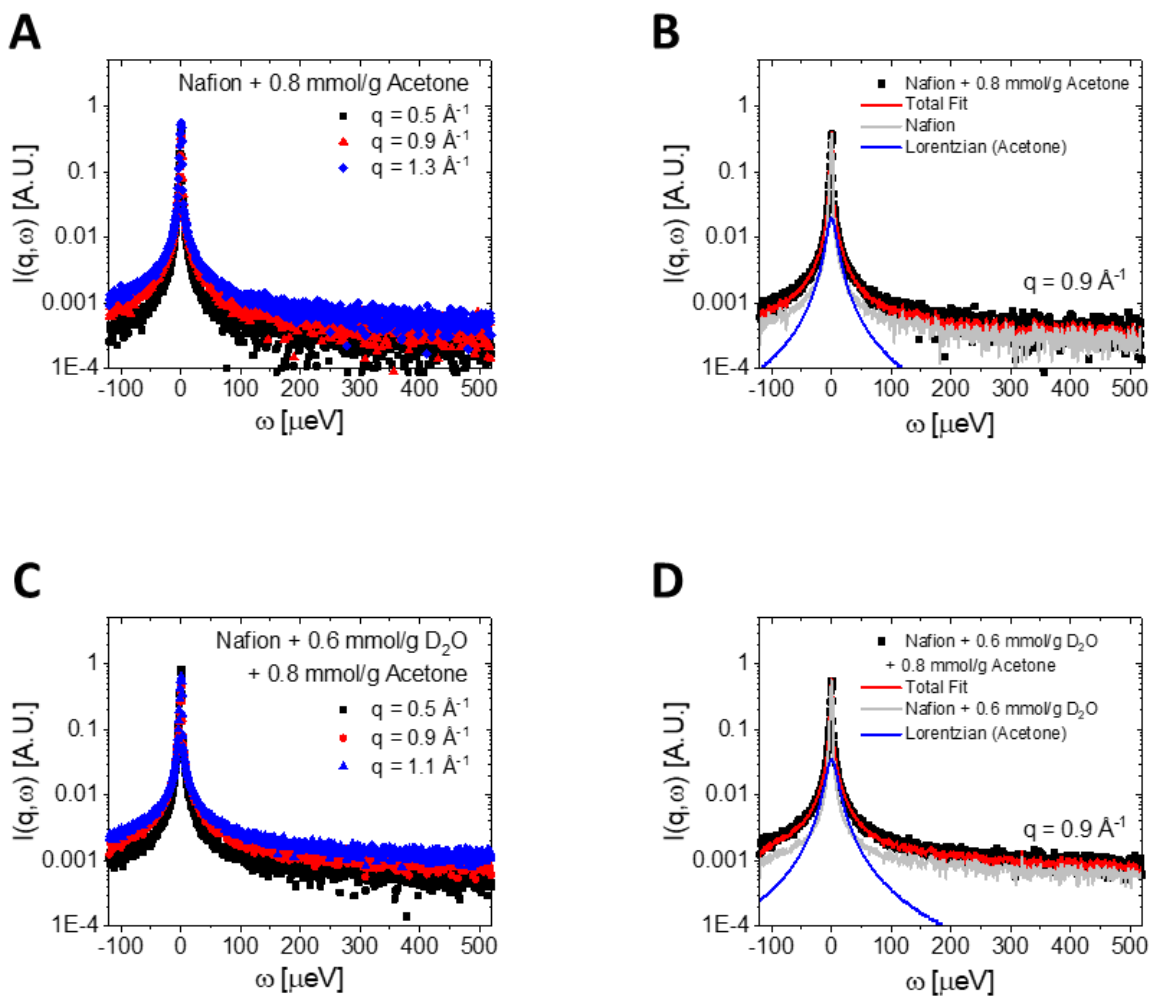
Figure 7.2 QENS spectra of acetone diffusion in nafion materials as a function of scattering wave vector, q and the appropriate fit.

coefficient can be obtained then as a function of scattering wave vector where $D(q) = FWHM(q)/2\hbar q^2$. The acetone dynamics in nafion are treated in the same manner as above. The only consideration here is the elastic dynamics that are accounted by measuring the appropriate nafion spectra without acetone. The analogous use of nafion with vanillic acid spectra was used
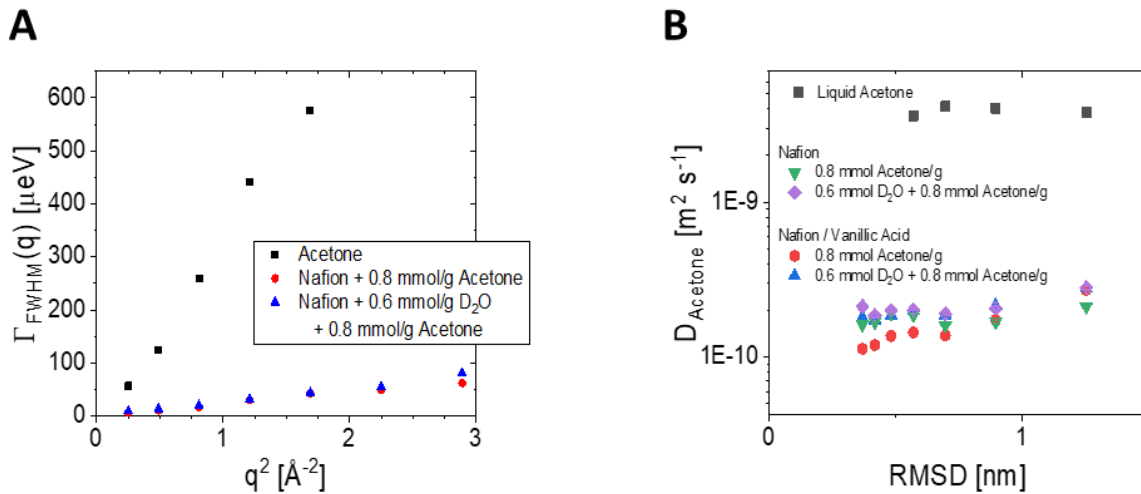
Figure 7.3 (A) The FWHM of the Lorentzian feature describes the diffusive motions of acetone, experiments performed at 296K (B) Acetone diffusion coefficients versus observed length scale of the measurement.

in the fitting of acetone diffusion in those samples. Below is an illustration of the analysis done on acetone in nafion and the final diffusion coefficients evaluated for all the three cases. The broader linewidth of liquid acetone indicates the substantially greater diffusion coefficient in the liquid. The observed acetone diffusion within the Nafion polymer are reduced by over one order of magnitude from the self-diffusion coefficient of acetone in solution. Diffusion coefficients at this short length scale appear to be on the order of 1-2 x 10^{-10} m^2/s. The liquid acetone self-diffusion coefficient is in reasonable agreement with literature. These diffusion terms can be averaged, from which a few trends might be inferred. Firstly, that acetone has a greater diffusion coefficient when water is also present in Nafion, and secondly that acetone appears to have a greater diffusion coefficient when vanillic acid is not present.

- Transition Between Different Diffusion Regimes and Its Relationship with Structural Properties in Nafion by High Field Diffusion NMR in Combination with Small-Angle X-ray and Neutron Scattering [2][Published]:

This work reports a PFG NMR observations of an observed upon increasing water concentration transition from disconnected domains of water channels to fully interconnected water channels. This work allows quantifying the permanence of the domain boundaries, the diffusion of water in Nafion within the domain loaded with both water and acetone, and finally the average size of the domain. In the case of acetone there was no evidence of finite domains where there are resistant to transport at the boundaries; this was observed from the self-diffusion coefficient of acetone. This is not the case with water where there is a clear dependence of the self-diffusivity of water in the case of small water loadings; the diffusion showed time dependence, and this is due to the finite domains existing made up of interconnected channels of water with several micros of size. This is formed in Nafion in the presence of acetone. My contribution to this work was utilizing small angle neutron scattering (SANS) in order to illustrate and explain the relationship between the observed diffusion behaviors and the corresponding structural properties. This structural insight can be accessed by SAXS and SANS on Nafion loaded with acetone. Whereas mentioned in previous chapters and contents the peak position has reciprocal units of length scales. Where here we addressed the length scales of the water channel walls or crystalline regions. SAXS showed for the ionomer/water channels there is a clear parallel increase of the size of the channels and the concentration. While for a constant water concentration there is a significant decrease in the size of the channels with increasing acetone concentration. The same observation was achieved with SANS. For the crystalline region there was no clear

dependence of the peak value and the effective size with water concentration. But there is a notable increase in the peak value with increasing acetone concentration. This dependence is explained by the accumulation of acetone at the perfluoro ether regions at the interface. The swelling of this interface region seemed to decrease the water channel diameter with increasing acetone concentration. This also caused the separation of the crystalline regions further apart from each other. All the measurements suggest that the acetone is located outside of the water channels in the interfacial regions. By now we can tell this is why the diffusion coefficient did not have time dependence when it was observed for water. The location of acetone outside the water channels means that the connectivity of the channels itself will not alter the role of acetone in the diffusion process. The structural analysis using SANS an SAXS also provide an explanation of the increase in the domain size with increasing acetone concentration at a constant water concentration. This is seen as a shrinking process of the water channels which causes the water molecules to collaboratively distribute themselves in regions where little water is present or immobile water molecules are located. This results in a longer water channel with more mobility of the water molecules and reflects in an increased domain of interconnected channels.

7.4 Final statement

The conclusion I have reached after studying specific aqueous solutions is that the water population can be divided into two populations: bulk water and perturbed water. The two populations have different diffusive behavior and relaxation times. This translates into different local viscosities near solute surfaces. Which in the case of hydrogels is important in determining the diffusion coefficient of a solute in the polymer network. Also, I have concluded that the bulk

structure of the hydrogels which is determined by the swelling degree estimated macroscopic properties of the system. I was also able to conclude that the perturbed water follows the dynamics of the polymer chain. In protein solution I concluded that a protein if normalized to a volume fraction including the perturbed water population its self-diffusion coefficient can be modeled and explained by colloidal solution theory where hydrodynamic interactions control the tracer diffusion. Moreover, I was able to define the molecular origin of bulk viscosity of water and compare it to the molecular origin of shear viscosity. which explains why the viscosity of the perturbed water molecules near solutes is altered; this is due to change in the dynamics of the water population and structural reorganization.

References

1.   Nickels, J.D., et al., *Lipid rafts: buffers of cell membrane physical properties.* The Journal of Physical Chemistry B, 2019. **123**(9): p. 2050-2056.
2.   Berens, S.J., et al., *Transition between Different Diffusion Regimes and Its Relationship with Structural Properties in Nafion by High Field Diffusion NMR in Combination with Small-Angle X-ray and Neutron Scattering.* The Journal of Physical Chemistry B, 2020. **124**(40): p. 8943-8950.

Vita

Ahmad Abdulnasir Yahya was born on May 14, 1993, in Bochum, Germany to Nean Adil and Abdulnasir Yahya. He received his General Certificate of Education (an international certificate from Cambridge) from Qurum Private School in May 2011. Ahmad then attended Sultan Qaboos University in Muscat, Oman and received his bachelor's degree in chemical and process engineering in May 2016. While he was at Sultan Qaboos University he served as a cohort representative and participated in teaching and research positions.

In the fall of 2017, Ahmad joined the University of Cincinnati in Ohio, USA to begin his graduate studies in chemical engineering. Under the supervision of Dr. Jonathan Nickels, Ahmad completed his doctoral studies in Fall 2021. In this time, he has written two first author publications and has contributed to others. Ahmad has also obtained his Master of Engineering degree from the University of Cincinnati in the summer of 2018.

Permanent address: Sultan Qaboos University Campus, Street E, Muscat, Oman.

This dissertation was typed by Ahmad A. Yahya